



<https://theses.gla.ac.uk/>

Theses Digitisation:

<https://www.gla.ac.uk/myglasgow/research/enlighten/theses/digitisation/>

This is a digitised version of the original print thesis.

Copyright and moral rights for this work are retained by the author

A copy can be downloaded for personal non-commercial research or study,  
without prior permission or charge

This work cannot be reproduced or quoted extensively from without first  
obtaining permission in writing from the author

The content must not be changed in any way or sold commercially in any  
format or medium without the formal permission of the author

When referring to this work, full bibliographic details including the author,  
title, awarding institution and date of the thesis must be given

Enlighten: Theses

<https://theses.gla.ac.uk/>  
[research-enlighten@glasgow.ac.uk](mailto:research-enlighten@glasgow.ac.uk)

THE MEASUREMENT OF CHOROIDAL BLOOD FLOW USING KRYPTON - 85.

Thesis presented to the University of Glasgow  
for the Degree of Ph.D.

March, 1975

R. Strang, B.Sc.,  
Department of Clinical Physics and Bio-engineering,  
West of Scotland Health Boards,  
11 West Graham Street,  
Glasgow.

ProQuest Number: 10646146

All rights reserved

INFORMATION TO ALL USERS

The quality of this reproduction is dependent upon the quality of the copy submitted.

In the unlikely event that the author did not send a complete manuscript and there are missing pages, these will be noted. Also, if material had to be removed, a note will indicate the deletion.



ProQuest 10646146

Published by ProQuest LLC (2017). Copyright of the Dissertation is held by the Author.

All rights reserved.

This work is protected against unauthorized copying under Title 17, United States Code  
Microform Edition © ProQuest LLC.

ProQuest LLC.  
789 East Eisenhower Parkway  
P.O. Box 1346  
Ann Arbor, MI 48106 – 1346

Thesis  
4235  
Copy 2



C O N T E N T S

	<u>Page</u>
ILLUSTRATIONS	iv
ACKNOWLEDGEMENTS	viii
SUMMARY	x
<u>Chapter 1</u> INTRODUCTION AND REVIEW OF LITERATURES.	
1.1 Introduction.	1.1
1.2 Methods of investigating the ocular circulation.	1.3
1.3 Methods derived from general blood flow techniques.	1.5
1.3.1 Direct measurement.	1.5
1.3.2 Fractionation of the cardiac output.	1.6
1.3.3 Doppler techniques.	1.8
1.3.4 Thermal methods.	1.8
1.3.5 Ocular plethysmography.	1.10
1.3.6 Inert gas clearance.	1.11
1.3.7 $PO_2$ measurement.	1.11
1.4 Discussion.	1.12
<u>Chapter 2</u> THEORY OF THE INERT GAS CLEARANCE METHOD FOR MEASURING BLOOD FLOW.	2.1
<u>Chapter 3</u> RADIOACTIVE INERT GAS CLEARANCE CURVES FROM OCULAR TISSUE.	
3.1 Introduction.	3.1
3.2 Radioisotope.	3.1
3.3 Radiation detectors and associated instrumentation.	3.2
3.4 Experimental animal.	3.3
3.5 Anaesthesia.	3.3
3.6 Experimental method.	3.4
3.7 Krypton - 85 clearance curve.	3.6
3.8 Analysis of washout curve.	3.6
3.9 Results.	3.8
3.10 Discussion.	3.10
<u>Chapter 4</u> DIFFUSION IN OCULAR TISSUE. I. MATHEMATICAL MODEL.	
4.1 4.1.1 Introduction.	4.1
4.1.2 Nomenclature.	4.2
4.2 4.2.1 Derivation of the differential diffusion equation.	4.3
4.2.2 Boundary conditions.	4.4
4.3 4.3.1 The numerical solution of the diffusion equations.	4.5
4.3.2 The finite difference formula.	4.5
4.3.3 The finite difference format of the differential diffusion equation.	4.5
4.3.4 The finite difference format of the boundary conditions.	4.7
4.3.5 Choice of distance increment, $h$ , and time interval, $l$ .	4.8

	<u>Page</u>
<u>Chapter 4</u> (contd.)	
4.4	Comparison between finite difference values and exact values. 4.8
4.5	Rabbit model. 4.10
<u>Chapter 5</u> DIFFUSION IN OCULAR TISSUE. II. RESULTS.	
5.1	Introduction. 5.1
5.2	Partial pressure and concentration profiles. 5.1
5.3	Predicted washout curves. 5.3
5.4	Variation in blood flow term. 5.5
5.5	Prolonged arrival of krypton. 5.7
5.6	Retinal circulation. 5.9
	5.6.1 Introduction. 5.9
	5.6.2 Partial pressure profiles. 5.10
	5.6.3 Predicted washout curves. 5.11
	5.6.4 Variation in blood flow terms. 5.12
	5.6.5 Partial pressure variations. 5.15
	5.6.6 Prolonged arrival of krypton. 5.15
5.7	Discussion. 5.16
<u>Chapter 6</u> MEASUREMENT OF LINEAR ABSORPTION COEFFICIENT, SOLUBILITY, AND DIFFUSION COEFFICIENT.	
6.1	Introduction. 6.1
6.2	Measurement of linear absorption coefficient. 6.1
	6.2.1 Introduction. 6.1
	6.2.2 Method. 6.2
	6.2.3 Results. 6.3
6.3	Measurement of solubility of krypton. 6.3
	6.3.1 Introduction. 6.3
	6.3.2 Method (liquid samples). 6.4
	6.3.3 Method (tissue samples). 6.6
	6.3.4 Results. 6.7
	6.3.5 Discussion. 6.7
6.4	Measurement of diffusion coefficient of krypton. 6.9
	6.4.1 Introduction. 6.9
	6.4.2 Theory. 6.10
	6.4.3 Method. 6.11
	6.4.4 Results. 6.12
	6.4.5 Discussion. 6.13
<u>Chapter 7</u> CARBON DIOXIDE RESPONSE.	
7.1	Introduction. 7.1
7.2	Rabbit experiments. 7.2
	7.2.1 Experimental method. 7.2
	7.2.2 Results. 7.2
7.3	Baboon experiments. 7.3
	7.3.1 Experimental method. 7.3
	7.3.2 Results. 7.5
7.4	Discussion. 7.5
<u>Chapter 8</u> CONCLUSIONS.	
APPENDIX I	
REFERENCES	

I L L U S T R A T I O N S .Chapter 1

- Figure 1.1 Schematic diagram of a section through a human eye.
- Figure 1.2 Schematic diagram of a section through a human eyewall.
- Table 1.1 Ocular blood flow values obtained by direct measurement.
- Table 1.2 Ocular blood flow values obtained by fractionation of the cardiac output.

Chapter 3

- Table 3.1 Physical data of the radioactive inert gases.
- Figure 3.1 Schematic diagram of the radiation detectors.
- Figure 3.2 Diagram of the radioactivity counting equipment.
- Figure 3.3 The arterial supply to the rabbit eye.
- Figure 3.4 Analogue recording of the diminishing radioactivity in the rabbit eye.
- Figure 3.5 Log / linear plot of the radioactivity in the rabbit eye.
- Figure 3.6 Curve stripping technique.
- Figure 3.7 Determination of the initial slope half life.
- Figure 3.8 'Curve stripping' half life versus 'initial slope' half life.
- Table 3.2 Mean values of half life and exponential rate constant.
- Table 3.3 Comparison of normal values of choroidal blood flow.
- Figure 3.9 The variation in choroidal blood flow in one animal throughout the duration of a six hour experiment.
- Figure 3.10 Analogue recording of a washout curve illustrating an arterio-venous shunt.
- Figure 3.11 Analogue recording of the radioactivity following injection of a non-diffusible isotope.

## Chapter 4

- Figure 4.1 Determination of the finite difference formula.
- Figure 4.2 The finite difference rectangular network.
- Figure 4.3 Initial partial pressure distribution used in the comparison between exact and finite difference values.
- Figure 4.4 (A) Variation in the statistical uncertainty of the data points of a washout curve .  
(B) Variation in the percentage difference between the exact values and the finite difference values.
- Figure 4.5 Diffusion model based on the anatomy of the rabbit eye.

## Chapter 5

- Figures 5.1 to 5.4 Predicted distribution of partial pressure and concentration profiles of krypton.
- Figure 5.5 Comparison between a series of predicted curves having different numbers of flow points and an experimental washout curve.
- Figures 5.6 to 5.11 Comparison between predicted curves and experimental washout curves.
- Figure 5.12 Predicted washout curve resulting from diffusion alone.
- Figures 5.13 - 5.19 The effect of prolonged arrival of krypton at the eye on the predicted washout curve.
- Table 5.1 Values of  $T_E$  and  $T_p$  for various values of the exponential rate constant.
- Figure 5.20 Initial uniform distribution of partial pressure of krypton over 3 flow points in the choroid and in the retina.
- Figures 5.21 - 5.23 Predicted distribution of partial pressure profiles of krypton.
- Figure 5.24 Comparison between a predicted washout curve and an experimental washout curve.
- Figure 5.25 Variation in the exponential rate constant of the initial decline of the predicted washout curve with the retinal blood flow term.

- Figures 5.26 & 5.27 Exponential rate constant of the initial decline of the predicted curve versus choroidal blood flow term.
- Figure 5.28 Exponential rate constant of the initial decline of the predicted curve versus the initial partial pressure ratio.
- Figure 5.29 The effect of prolonged arrival of krypton at the eye.
- Table 5.2 Variation in thickness of the sclera, choroid, and retina of the human eye.
- Table 5.3 The effect of variation in eyewall thickness on the exponential rate constant of the initial decline of the predicted curve.

## Chapter 6

- Figure 6.1 Apparatus for the measurement of the linear absorption coefficient.
- Figure 6.2 Detected radioactivity versus absorber thickness. Aluminium.
- Figure 6.3 Detected radioactivity versus absorber thickness. Melinex.
- Figure 6.4 Detected radioactivity (logarithmic scale) versus absorber thickness.
- Figure 6.5 Volume of sample versus weight of sample.
- Figure 6.6 Solubility of krypton in water versus equilibration time.
- Figure 6.7 Solubility of krypton in sclera versus equilibration time.
- Figure 6.8 Solubility of krypton in choroid versus equilibration time.
- Figure 6.9 Solubility of krypton in retina versus equilibration time.
- Figure 6.10 Solubility of krypton in vitreous versus equilibration time.
- Figure 6.11 Solubility of krypton in whole blood versus equilibration time.
- Figure 6.12 Solubility of krypton in plasma versus equilibration time.
- Figure 6.13 Solubility of krypton in erythrocytes versus equilibration time.

- Table 6.1 Ostwald solubility coefficients for krypton at 37°C.
- Table 6.2 Ostwald solubility coefficients - literature values.
- Figure 6.14 Partition coefficient (retina) versus haematocrit.
- Figure 6.15 Apparatus for the measurement of the diffusion coefficient.
- Figure 6.16 Clearance of xenon from empty sample vessel. (1st apparatus).
- Figure 6.17 Clearance of xenon from a retinal sample.
- Figure 6.18 Result of subtraction of residual radioactivity.
- Figure 6.19 Clearance of xenon from empty sample vessel. (2nd apparatus).
- Figure 6.20 Clearance of xenon from a vitreous sample.
- Table 6.3 Final exponential clearance half lives for various thicknesses of vitreous.
- Figure 6.21 Square of the sample thickness (vitreous) versus clearance halving time.
- Table 6.4 Diffusion coefficients.
- Table 6.5 Typical dimensions of the tissue samples employed in the determination of the diffusion coefficients.

## Chapter 7

- Figure 7.1 Choroidal blood flow / perfusion pressure versus  $P_a\text{CO}_2$ . Rabbit.
- Figure 7.2 Percentage change in (A) choroidal and (B) cerebral blood flow in the baboon versus  $P_a\text{CO}_2$ .

A C K N O W L E D G E M E N T S.

I would like to thank Drs. F.C.Gillespie and P.W.Horton, Principal Physicists, Department of Clinical Physics and Bio-engineering, West of Scotland Health Boards, Dr. T.M.Wilson, Senior Lecturer, Tennent Institute of Ophthalmology, University of Glasgow, and Dr. A.M.Harper, Reader in Clinical Physiology, Wellcome Surgical Research Institute, University of Glasgow, for their invaluable help and advice during these studies.

The studies in Chapter 3 were performed in collaboration with Dr. T.M.Wilson. The primate experiments described in Chapter 7 were performed in collaboration with Dr. T.M.Wilson and Mr. E.T.MacKenzie, Research Assistant, Wellcome Surgical Research Institute, University of Glasgow. I would like to thank Mr. N.F.Johnson, Research Assistant, Tennent Institute of Ophthalmology, University of Glasgow, for surgical assistance in the studies described in Chapter 6.

I would also like to thank Professor W.S.Foulds, Tennent Institute of Ophthalmology, University of Glasgow, and Professor J.M.A.Lenihan, Regional Physicist, Department of Clinical Physics and Bio-engineering, West of Scotland Health Boards, for their continued support.

This study was supported by a grant from the M.R.C. to Professor W.S.Foulds.

S U M M A R Y.

Chapter 1 contains a brief description of the anatomy of the eye followed by a review of the methods used previously to measure ocular blood flow.

The theory of the inert gas clearance method for measuring blood flow in homogeneously perfused tissues is discussed in Chapter 2.

A series of experiments designed to measure control values of choroidal blood flow in rabbits using krypton-85 is described in Chapter 3.

The clearance of krypton from rabbit ocular tissue is complex. An explanation of the complex nature of the clearance curve was obtained by studying the diffusion of krypton in ocular tissue. Initially a diffusion model whose structure was based on the anatomy of the rabbit eye was developed (Chapter 4). Predicted clearance curves, obtained from this model, indicated that the half life of the initial exponential decline of the clearance curve was a measure of choroidal blood flow and that the subsequent decline in radioactivity was dependent on the diffusion of krypton in ocular tissue. A model based on the anatomy of the baboon eye was also developed.

In Chapter 6 the results of measurements of the linear absorption coefficient, solubilities and diffusion coefficients of krypton in the different ocular tissues are presented. These are necessary for the numerical evaluation of the model.

In Chapter 7 the method has been applied to examine the effect of increased arterial carbon dioxide tension on the

choroidal blood flow in rabbits and baboons. The response of the choroidal blood flow in rabbits was variable. In the baboon there was a 3.5% increase in choroidal blood flow per mmHg rise in  $P_aCO_2$ .

Chapter 8 is a general discussion of the work presented in this thesis and its value.

## Chapter 1

### Introduction and Review of Literature

#### 1.1 Introduction

The eye is approximately spherical. It houses an optical apparatus which produces an inverted reduced image of the outside world on a layer of nerve cells. (figure 1.1). The optical apparatus consists of two refracting elements; (a) the cornea, and (b) the lens. A variable aperture is provided by a contractile membranous partition called the iris. Posteriorly the eyewall consists of three distinct tissue structures surrounding the gel-like vitreous (figure 1.2).

The outermost structure, the sclera, consists of relatively avascular fibrous tissue forming the 'white of the eye'. This fibrous structure protects the more delicate inner structures and when distended by the intraocular pressure gives the eyeball its shape.

The innermost structure, the retina, developed embryologically from brain tissue, consists of layers of different cellular types. The outermost layer contains the photoreceptor cells (the rods and cones). Within this layer light is converted into a neural signal.

Separating the metabolically active retina from the avascular fibrous sclera is the third structure, the choroid. This consists almost entirely of blood vessels of various sizes which give rise to a bed of large capillaries, the choriocapillaris, which is separated from the cells of the retinal pigment epithelium by Bruch's membrane.

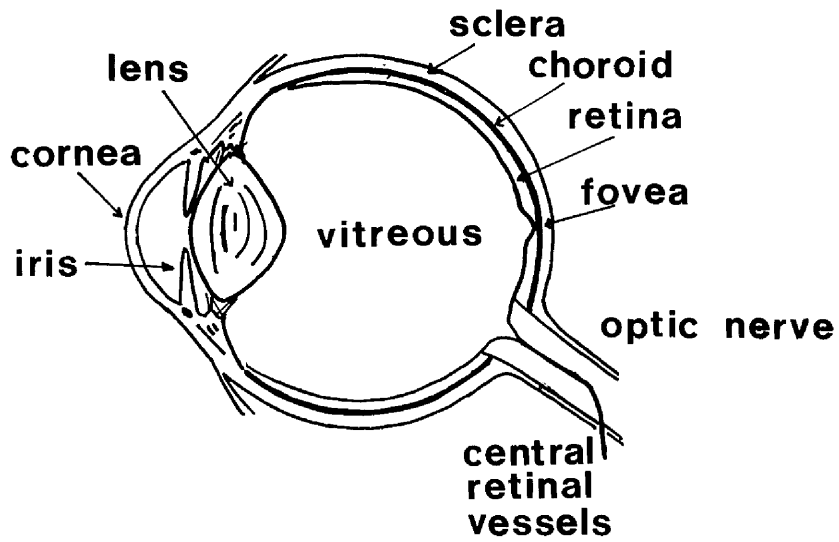


Figure 1.1 Schematic diagram of a section through a human eye.

VITREOUS

RETINA

CHOROID

SCLERA

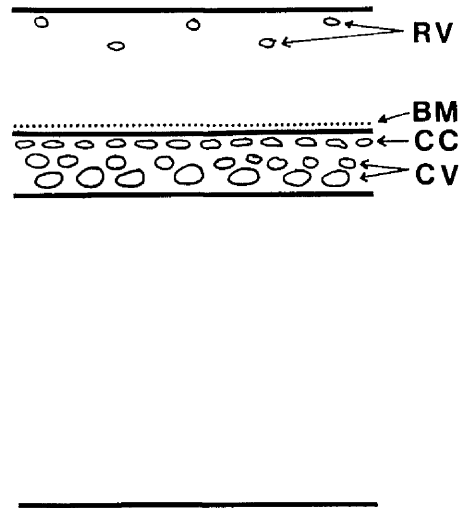


Figure 1.2 Schematic diagram of a section through a human eyewall.

The retina in the primate is sustained by two distinct circulations. The inner layers of the retina are sustained by the retinal circulation. The retinal vessels which radiate from the optic disc penetrate at most the innermost third of the retina. They are supplied by the central retinal artery which enters the eye through the optic nerve (figure 1.1, 1.2). The outermost layers of the retina are sustained by the choriocapillaris. Thus two thirds of the primate retina are sustained by vessels which do not penetrate the retina.

Since the introduction of the ophthalmoscope by Helmholtz in 1851, it has been possible to examine visually the retinal vessels. The advent of fluorescein angiography (Novotny, and Alvis, 1961) allowed the retinal circulation to be closely studied in normal and diseased states such as glaucoma and diabetic retinopathy.

Ophthalmoscopy and fluorescein angiography have shown the importance of the ocular circulation in the maintenance of a functional eye. They have also allowed the effects of altering various physiological parameters such as intraocular pressure, carbon dioxide and oxygen levels in arterial blood, to be studied. However, these techniques give no information about the choroidal circulation since this is normally screened from visual examination by the retinal pigment epithelium. This thesis describes a practical and reliable method for measuring and studying the functional characteristics of choroidal blood flow.



In the last few decades several methods have been developed for measuring blood flow in various organs and tissues. Many of these methods have been applied to the measurement of ocular blood flow. This thesis describes the application of the inert gas clearance method to the measurement of choroidal blood flow in experimental animals.

## 1.2 Methods of Investigating Ocular Circulation

The techniques employed in investigating ocular circulation may be divided into two groups:

- (a) Methods specific to the eye.
- (b) Methods developed from techniques used in other regions of the body.

### Methods specific to the eye

Most of the techniques for investigating the ocular circulation in this category depend on the fact that the retinal vessels, unlike the vessels of other organs of the body, are clearly visible to the investigator. This has allowed the diameters of retinal vessels to be measured under a variety of clinical and experimental conditions, for example, the effects of the following have been investigated;

- (a) arterial carbon dioxide and oxygen tensions. (Green, 1961; Frayser, and Hickam, 1964; 1965; Frayser, Saltzman, Anderson, Hickam, and Sieker, 1967)
- (b) ocular hypertension. (Dobree, 1956; Dollery, Henkind, Kohner, and Paterson, 1968).

The introduction of fluorescein dye to enhance the appearance of the retinal vessels has allowed the retinal circulation to be studied in normal and diseased states (Dollery, Hodge, and Engel, 1962; Dollery, Henkind, Paterson, Ramalho and Hill, 1966; Kohner, 1969; Oosterhuis, and Gortzak-Moorstein, 1970). Recently developments have been made in fluorescein angiography which have allowed further quantitative measurements of retinal blood flow and dye transit times to be made. These developments include:

- (a) the use of cine-photography (Flocks, Miller and Chao, 1959; Dollery, Henkind, Kohner, and Paterson, 1968).
- (b) the use of densitometric techniques.

Various workers have obtained relative values of retinal blood flow from dye-dilution curves of fluorescing human retinal vessels (Trokkel, 1964b; Hickam, and Freyser, 1965; Oosterhuis, Bakker, and Van Berge, 1970; Winkelman, Zappia, and Gay, 1971). Tsacopoulos and David (1973) have obtained dye-dilution curves from primate eyes and from these were able to derive relative values for retinal blood flow. Ben-Sira and Riva (1973) obtained dye-dilution curves from individual retinal vessels on the human fundus. Trokkel (1964a; 1965a; 1965b) derived a value of 1680 ml/100 gm/min. for the choroidal blood flow in albino rabbits from dye-dilution curves obtained by the passage of Evan's blue dye through the choroidal vessels.

Other investigators have used infrared absorption angiography with indocyanine green dye to give better visualisation of the choroidal vessels (Kogure, David, Yamanouchi, and Choromokos, 1970; Flower, 1972; Flower and Hochheimer, 1973).

One other technique belonging to this category is the scleral window technique of Wudka and Leopold (1956). In this technique the larger vessels of the choroid are visualised by observation through transparent dehydrated sclera. These workers used this technique to investigate the effect of various autonomic drugs on the calibre of the choroidal vessels.

### 1.3 Methods Derived from General Blood Flow Techniques

The more general methods of measuring ocular blood flow are based on:

- (1) Direct Measurement
- (2) Fractionation of the cardiac output
- (3) Doppler methods
- (4) Thermal methods
- (5) Ocular plethysmography
- (6) Inert gas clearance
- (7)  $PO_2$  measurement

#### 1.3.1 Direct Measurement

In 1912 Hill and Flack investigated the effect of increased intraocular pressure on blood flow from an excised vortex vein in experimental animals. Meesman (1930), Fischer (1930), Sondermann (1932), and Linner (1952) by collecting the blood from an opened vortex vein obtained values for ocular blood flow in rabbits.

Bill (1962a) showed that above an intraocular pressure of 10-15 mmHg quantitative determinations of uveal blood flow in

rabbits could be obtained by measuring the flow through a single vortex vein and multiplying the result by the number of vortex veins. Similarly he showed that for cats cannulation of the superior anterior ciliary vein could give an estimate of blood flow through the uvea (Bill, 1962b).

Cohan and Cohan (1963a, 1963b) cannulated a ciliary vein in dogs to estimate ocular blood flow. However, they reported that the technique raised both the pressure in the ciliary vein and the intraocular pressure. Elgin (1964) also with dogs cannulated an anterior superior ciliary vein and after ligation of the vortex veins obtained an estimate for total uveal blood flow.

Nakamura and Goulstine (1973) used a bubble flow-meter to measure changes in vortex vein flow in rabbits as the intraocular pressure was increased.

Table 1.1 summarises the quantitative results obtained by direct measurement of ocular venous blood flow.

### 1.3.2 Fractionation of the Cardiac Output

In 1956 Sapirstein pointed out that any marker which diffuses freely into tissue would, following intravenous administration, be distributed initially to the various organs in proportion to their blood supply. Essentially, each tissue may be regarded as a filter. For a certain time the venous drainage of the marker will be negligible. During this time the fractional distribution of the marker among the organs will correspond to the fractional distribution of the cardiac output.

**Table 1.1** Ocular blood flow values obtained by direct measurement

AUTHOR	ANIMAL	BLOOD FLOW (ml/min.)	
		Whole Eye	Anterior Ciliary Vein
Fischer (1930)	Rabbit	1.3	-
Heesman (1930)	Rabbit	1.9	-
Sondermann (1932)	Rabbit	1.1	-
Linner (1952)	Rabbit	1.8	-
Cohan and Cohan (1963a)	Dog	-	0.87
Cohan and Cohan (1963b)	Dog	-	0.84
Elgin (1964)	Dog	-	0.78
Nakamura and Goulstine (1973)	Rabbit	1.8	-

Sapirstein (1956, 1958) used radioactive potassium to determine the blood flow to various organs in rats (excluding the eye). His results for most organs were in good agreement with those obtained by other workers. However, a notable exception was the brain. He surmised that this was due to the fact that the brain is highly perfused and hence the assumption that early venous drainage of the marker could be ignored was no longer valid.

Levene (1957) used radioactive potassium to determine total ocular blood flow in albino rabbits. However, he observed a considerable scatter in his results and concluded that this method was also subject to the difficulty encountered by Sapirstein in the cerebral circulation.

Flohr (1968) and Flohr and Kaufmann (1971) attempted to overcome the problem of venous drainage by injecting iodine (I-131) labelled macro-aggregated albumin which they assumed would be distributed according to the distribution of the cardiac output and would become lodged in the capillaries long enough to allow enucleation of the eye and hence allow accurate determination of the fraction of radioactivity initially trapped in the eye.

Recently several groups of workers have used carbonised radioactive microspheres instead of macro-aggregated albumin in a variety of studies (O'Day, Fish, Aronson, Pollycove, and Coon, 1971; Alm, and Bill, 1972b; 1973; Alm, Bill, and Young, 1973; Weiter, Schachar, and Ernest, 1973a, 1973b; Schachar, Weiter, and Ernest, 1973; Aronson, Howes, Fish, Pollycove, and O'Day, 1974).

Table 1.2 summarises the values of the ocular blood flow obtained by the above investigators using the principle of the fractionation of the cardiac output.

Table 1.2 Ocular blood flow values obtained by fractionation of the cardiac output

AUTHOR	ANIMAL	BLOOD FLOW (ml/min)		
		Whole Eye	Choroid	Retina
Levene (1957)	Rabbit	1.7	-	-
Flohr and Kaufmann (1971)	Cat	1.1	-	-
O'Day et al (1971)	Rabbit	-	0.84	0.025
	Monkey	-	1.36	0.049
Alm and Bill (1972)	Cat	-	0.734*	0.015*
Alm and Bill (1973)	Monkey	-	0.607*	0.025*
Alm, Bill and Young (1973)	Monkey	-	0.677*	0.034*
Weiter, Schacher and Ernest (1973)	Cat	-	2.04	-
Aronson et al	Rabbit	1.3		

### 1.3.3. Doppler Techniques

The majority of methods using the Doppler principle to measure blood flow utilize the transmission properties of ultrasound in tissue. The Doppler techniques are based upon the fact that when a beam of ultrasound is reflected from moving blood cells it will have its frequency changed; the change in frequency being proportional to the velocity of the moving blood cells.

Suzuki and Satomura (1959) first described an ultrasonic Doppler flow detector for the measurement of ocular blood flow. Various workers (Goldberg, and Sarin, 1967; Maroon, Pieroni, and Campbell, 1969; and Coleman, 1971) have studied changes in ultrasonic frequency using transducers placed on the eyelid. Schlegel and Lawrence (1969) employed an ultrasonic Doppler flowmeter to measure changes in blood flow in an exposed vortex vein in rabbits as the intraocular pressure was increased. In a similar investigation Tokoro (1972) employed a miniature Doppler transducer to measure blood velocity in the ciliary body of rabbits.

Riva, Ross and Benedek (1972) used a laser beam and from the Doppler principle determined the velocity spectrum in a retinal artery of a rabbit.

The Doppler techniques, whilst allowing continuous measurement, do not readily provide absolute measurements of blood velocity or blood flow.

### 1.3.4. Thermal Methods

Two basic techniques involving thermocouples have been used for measuring ocular blood flow. In the method due to Gibbs (1963), two junctions of a thermocouple are placed on the

sclera. One junction is heated electrically. This results in a temperature difference between the two junctions. The temperature of the heated junction is influenced by the rate at which heat is carried away from it. This rate depends largely on the blood flow in the underlying tissue.

This method has been used to study uveal and ciliary blood flow in rabbits (Bill, 1960; 1962c; 1962d; 1963; Niesel, 1962; and Rodenhauser, 1963); uveal blood flow in cats (Seidel, Rodenhauser, Hagihara, and Hensel, 1960; Rodenhauser, 1963) and in man (Rodenhauser, 1960; 1969).

A second thermocouple method was developed by Cole and Rumble (1970a) for measuring relative changes in blood flow through the rabbit iris. In this approach the circulating blood is considered to be the heat source. The temperature immediately in front of the iris adjusts such that the heat gained from the iris vessels is equal to the heat lost to the environment. Knowledge of this last factor allows changes in temperature immediately in front of the iris to be correlated with changes in iris blood flow. Using this technique Cole and Rumble investigated the effects of catecholamines on the iris circulation (Cole, and Rumble, 1970a) and also determined the changes in iris blood flow arising from stimulation of the cervical sympathetic nerve (Cole, and Rumble, 1970b).

The techniques described above, involving thermocouples, enable continuous measurements of flow to be made. However, only relative measurements are obtained.

### 1.3.5. Ocular Plethysmography

Originally plethysmography was used to give an index of blood flow, usually in an extremity, by measuring the change in volume occurring in the extremity following occlusion of the venous return.

The techniques of ocular plethysmography provide relative values of ocular blood flow by measuring the changes in a particular parameter arising from the arterial pulsation of the ocular circulation. Several different parameters have been used. Bishop and Nyboer (1962) in dogs and man, and Taylor and Allison (1964) in man have related changes in the electrical impedance during arterial pulsation to mean blood flow. Lawrence and Schlegel (1966) in rabbits, and Bynke (1968) in rabbits and man have correlated the magnitude and frequency of fluctuations in intraocular pressure with the arterial pulse rate by placing a pressure transducer on the eyelid.

The most commonly employed form of ocular plethysmography is photoelectric plethysmography. This is an extension of the technique developed by Broadfoot, Gloster, and Greaves (1961) on fundus reflectometry. In this technique retinal blood flow is determined from the variations in the intensity of light from a constant external source reflected from the fundus.

Matsuo, Kogure, and Takahashi (1966); Kogure, Asatani, Togashi, and Yaginohashi (1971), and Christensen, Polalski, Wong, and Weisman (1971) have used this method in a series of experimental investigations in dogs. Gloster

(1969); Oosterhuis, Bakker, and Van Den Berge (1970); and Asatani (1970); have obtained photoelectric photysmograms from the human eye.

Plethysmographic techniques have the same principal disadvantages as the Doppler techniques. They suffer from problems of absolute calibration, either in terms of blood volume or blood flow.

#### 1.3.6. Inert Gas Clearance Technique

Pilkerton, Bulle and O'Rourke (1964) employed the nitrous oxide method of Kety and Schmidt (1945) to measure ocular blood flow in dogs. Friedman, Kopald and Smith (1964) measured choroidal blood flow in rabbits and other animals using radioactive krypton. These techniques are based on the Fick principle which relates the rate of removal of an inert diffusible substance from an organ to the blood supply to that organ. This thesis describes the measurement of choroidal blood flow in experimental animals using the radioactive inert gas clearance technique. The theory of this method will be discussed in detail in Chapter two.

#### 1.3.7. PO<sub>2</sub> Measurement

Alm and Bill (1972a) correlated changes in oxygen tension of the vitreous in close proximity to the retina with changes in retinal blood flow. They investigated the effect of changes in intraocular pressure and arterial oxygen tension on the retinal blood flow in cats (Alm and Bill, 1972a). Alm (1972)

also used the method to study the effect of various vasoactive drugs on retinal blood flow.

This technique, like many of those previously described, suffers from the difficulty of obtaining absolute values of blood flow. It has the added disadvantage that it cannot be used in any situation in which oxygen utilisation in tissue is likely to be altered.

#### 1.4 Discussion

The methods employed to investigate the ocular circulation, described in this chapter, all have inherent advantages and disadvantages.

In general, the methods specific to the eye, fundus photography and fluorescein angiography give only qualitative information about circulation, and then only the retinal circulation. Historically these techniques have been important for stimulating interest in the ocular circulation and clinically they remain an important tool for the ophthalmologist in diagnosing many ocular abnormalities.

The use of radioactive microspheres for measuring ocular blood flow probably overcomes the earlier difficulties encountered by Levene. However, no author has published data on the concentration of microspheres in the ocular veins to test whether or not the assumption that all microspheres entering the eye were trapped in the ocular capillaries is true. This technique allows measurement of choroidal, retinal and ciliary blood flow. Its main disadvantage is that for most species only one determination of flow can be made without

significantly altering the blood flow.

The techniques of plethysmography, ultrasonics, temperature measurements, and the  $PO_2$  measurement of Alm and Bill have similar advantages and disadvantages. They all give continuous measurements but are difficult to calibrate in terms of absolute blood flow.

The radioactive inert gas clearance method has proved to be the most important general method for obtaining repeated measurements of absolute blood flow in organs and tissues. Although the eye does not exhibit the homogeneity assumed to exist in the application of the inert gas clearance method it will be shown in subsequent chapters that despite this inhomogeneity the inert gas clearance method can be employed to give repeated measurements of absolute blood flow through the choroid.

Chapter 2

Theory of the Inert Gas Clearance Method for Measuring Blood Flow

Inert gas clearance techniques for measuring blood flow depend upon the Fick principle which was first enunciated by Fick in 1870. The principle is a special case of the more general principle of the conservation of matter. It states that:-

"For any substance carried by the blood to an organ or region, then within the time interval  $\Delta t$ , the quantity brought in,  $Q_a$ , must be equal to the quantity disposed of, either by accumulation,  $\Delta Q_i$ , or by conversion within the region,  $Q_m$ , or by transport out of the organ or region through all possible routes of exit,  $Q_e$ ."

Mathematically the Fick principle states that

$$\frac{Q_a}{\Delta t} = \frac{\Delta Q_i}{\Delta t} + \frac{Q_m}{\Delta t} + \frac{Q_e}{\Delta t} \quad (2-1)$$

where the symbols are defined as above.

If the following conditions are satisfied

- (1) metabolism of the substance in the organ or region is zero, i.e.  $Q_m = 0$ ,
- (2) the blood flow is the only significant path of supply and removal of the substance, and
- (3) the arterial and venous blood flows are equal and constant ( $F$ , ml/sec.)

then, equation (2-1) reduces at any instant to

$$\frac{dQ_i}{dt} = F(C_a - C_v) \quad (2-2)$$

where  $Q_i$  = total quantity of substance in the organ, including its contained blood (g),

$C_a$  = arterial concentration of the substance (g/ml),

$C_v$  = venous concentration of the substance (g/ml),

$$\text{and } \frac{\Delta Q_i}{\Delta t} = F C_a, \quad \frac{\Delta Q_e}{\Delta t} = F C_v.$$

Under certain conditions equation (2-2) may be used to measure blood flow without determining  $Q_i$  directly. After a sufficient time,  $u$ , a state of virtual equalisation will have become established between the mean concentration in the organ or region,  $C_r$ , and that in the venous blood which drains it.

Then,

$$C_r(u) = \frac{Q_i(u)}{V_r} = C_v \cdot \lambda \quad (2-3)$$

where  $V_r$  = the volume of the organ or region (ml), and

$\lambda$  = the tissue-blood partition coefficient for the substance, that is the ratio of the solubility of the substance in 1 gram of tissue to its solubility in 1 ml of blood.

Integrating equation (2-2) with respect to time gives

$$\int_0^u \frac{dQ_i}{dt} dt = \int_0^u F \cdot (C_a - C_v) dt$$

i.e.  $Q_i(u) = F \int_0^u (C_a - C_v) dt$

Substituting for  $Q_i(u)$  from equation (2-3) gives

$$\frac{F}{V_r} = \frac{C_v(u) \cdot \lambda}{\int_0^u (C_a - C_v) dt} \quad (2-4)$$

This equation is valid for measuring blood flow through a homogeneous organ or region using an inert highly diffusible substance. It was first derived by Kety and Schmidt (1945) for measuring cerebral blood flow using nitrous oxide as the inert

diffusible substance. As Kety pointed out (Kety, 1951) certain conditions are required before equation (2-4) is applicable to measuring blood flow. It must be possible to obtain representative venous blood from the region under study with minimal contamination from other regions, and the time,  $u$ , required for equilibration must not be impractically long. This technique was also applied successfully to measure coronary circulation (Bing, Hammond, Handelsman, Powers, Spencer, Eckenhoff, Goodale, Hafkenschiel, and Kety, 1949) and renal circulation (Conn, Wood and Schmidt, 1953).

Lassen and his co-workers (Lassen and Munck, 1955; Lassen, 1959; Lassen and Ingvar, 1961) modified the basic Kety-Schmidt technique by replacing nitrous oxide as the inert marker by the radioactive inert gases, krypton-85 and xenon-133. With these radioactive gases it is possible to measure their rate of clearance from tissue by external counting, thus obviating the need to obtain arterial and venous samples. This development simplified the method and allowed it to be applied to many other organs including the eye.

In this technique the expression relating the blood flow to the measured quantities is derived from equation (2-2). Dividing both sides of equation (2-2) by  $V_r$  (the volume of the organ or region) gives

$$\frac{dQ_i}{V_r \cdot dt} = \frac{dc_i}{dt} = \frac{F}{V_r} \cdot (C_a - C_v) \quad (2-5)$$

Jones (1950) and Evans, Busuttill, Gillespie and Unsworth (1974) have shown that in most tissues the exchange of substances of small molecular weight between capillary and tissue is not limited by the process of diffusion.

Thus over all time:

$$C_v = \frac{C_i}{\lambda} \quad (2-6)$$

Substituting into equation (2-5) yields

$$\frac{dC_i}{dt} = \frac{F}{\lambda \cdot V_r} (\lambda C_a - C_i)$$

i.e. 
$$\frac{dC_i}{dt} = k \cdot (\lambda C_a - C_i) \quad (2-7)$$

where 
$$k = \frac{F}{\lambda \cdot V_r} \quad (2-8)$$

Integrating equation (2-7) gives:-

$$\int_0^T \frac{dC_i(t)}{dt} dt = \int_0^T k \cdot (\lambda C_a(t) - C_i(t)) dt$$

This has the following solutions

(1) when  $C_a$  is constant

$$C_i(T) = \lambda \cdot C_a (1 - e^{-kT}) \quad (2-9)$$

(2) when  $C_a = 0$

$$C_i(T) = C_i(0) \cdot e^{-kT} \quad (2-10)$$

(3) when  $C_a$  is variable but equal to zero at time zero, i.e.  $C_a(0) = 0$

$$C_i(T) = \lambda \cdot k \cdot e^{-kT} \int_0^T C_a(t) e^{kt} dt \quad (2-11)$$

Equation (2-10) has become the basis for the measurement of capillary blood flow by the clearance of a radioactive inert substance introduced directly into the tissue.

One method of introducing the inert substance into the tissue is to administer it as a bolus into the arterial supply to the organ under study. Once the inert substance reaches the capillaries it diffuses almost instantaneously out of the blood into the surrounding tissue. After the injection has ceased, fresh blood, containing no inert gas, will pass through the capillaries. The inert substance in the tissue will equilibrate with the blood and be carried by the blood flow out of the organ. Approximately ninety-five per cent of the inert gases krypton and xenon are eliminated in each passage through healthy lungs (Chidsey, Fritts, Hardewig, Richards and Courmand, 1959). Thus, if the inert gas is introduced into the arterial supply to the organ negligible recirculation of the inert gas to the organ occurs.

By placing a suitable radiation detector over the organ or tissue under study it is possible to monitor the amount of inert gas in the tissue.

As the inert gas is removed by the blood flow the radioactivity will decrease according to equation (2-10). Equation (2-10) states:-

$$C_i(T) = C_i(0) \cdot e^{-kT}$$

Taking the logarithm of both sides

$$\log\left(\frac{C_i(T)}{C_i(0)}\right) = -kT \quad (2-13)$$

Thus, provided the conditions outlined above apply, a graph of the logarithm of the radioactivity measured by the detector against time on a linear scale (hereafter referred to as a log/linear plot) should be linear. By re-arranging equation (2-8) the blood flow can be

determined from the slope,  $k$ , of the log/linear plot.

Equation (2-8) states:

$$k = \frac{F}{\lambda \cdot V_r}$$

Re-arranging and replacing  $V_r$  by  $W/\rho$  gives

$$F = \frac{\lambda \cdot k \cdot W}{\rho}$$

$$\text{i.e. } F = \frac{0.693 \cdot \lambda \cdot W}{T_{1/2} \cdot \rho} \quad (2-15)$$

where  $F$  = blood flow (ml/100g/min.),

$\lambda$  = tissue/blood partition coefficient,

$V_r$  = volume of tissue (ml),

$k$  = exponential rate constant (mins<sup>-1</sup>),

$$= 0.693/T_{1/2}$$

$T_{1/2}$  = half life, i.e. the time (mins.) taken for the radioactivity to fall to half that of a given value,

$\rho$  = density of tissue (g/ml), and

$W$  = weight of tissue (g).

Thus from a knowledge of the tissue/blood partition coefficient and the density of the tissue it is possible to determine the blood flow. Generally the weight is unknown, and the flow is expressed in units of ml/min/100g of tissue.

$$\text{i.e. Flow} = \frac{0.693 \cdot \lambda \cdot 100}{T_{1/2} \cdot \rho}$$

$$\text{i.e. } F = \frac{69.3 \cdot \lambda}{T_{1/2} \cdot \rho} \quad (2-16)$$

In practice equation (2-16) is the one most commonly used for calculating flow in studies involving radioactive krypton and xenon.

Flow as calculated using methods involving venous sampling (e.g. the nitrous oxide technique) includes blood which passes directly from arterial to venous channels without participating in capillary exchange. The result of inert gas clearance technique excludes flow through arteriovenous shunts and measures only capillary blood flow.

The equations derived to date apply to cases in which clearance of the inert substance from tissue is monoexponential and refer to homogeneous tissue. In the brain there are two distinct tissues, white and grey matter, with widely differing perfusion rates. The clearance curve of a  $\gamma$ -emitting inert gas (xenon-133) from the brain is biexponential. Each exponential rate constant is assumed to be of the form of equation (2-8).

Generally, the radioactivity measured by the detector is assumed to consist of a summation of terms each attributable to a homogeneous tissue within the region under study. In the case of the brain:

$$\begin{aligned} C_{\text{TOTAL}}(T) &= C_W(T) + C_G(T) \\ &= C_W(0)e^{-k_W \cdot T} + C_G(0)e^{-k_G \cdot T} \end{aligned}$$

where the subscripts W and G refer to white and grey matter respectively. A knowledge of  $k_W$  and  $k_G$  will allow the flows through the white and grey matter to be calculated by applying equation (2-16) to each compartment in turn.

The extension of equation (2-10) from a homogeneous tissue to a heterogeneous tissue consisting of a series of homogeneous compartments is not without limitations. Gillespie (1968) pointed out that multi-exponential analysis of the clearance from non-homogeneous tissue must be interpreted with great care due to the possibility of intercompartmental diffusion of the inert gas affecting the clearance from each compartment. This is particularly important in organs which have both a high and low blood flow. Diffusion will occur from regions of low blood flow to regions of high due to the lower partial pressures of the inert substance in the vicinity of the high blood flow resulting from the faster removal of the substance by the high blood flow.

The eye is not a homogeneous tissue but comprises layers of tissues some of which are perfused by blood and some of which are not. Diffusion of inert tracer between perfused and non-perfused layers occurs and the clearance pattern is very complex. One aim of this thesis is to analyse and interpret this complex pattern of diffusion and clearance in order to determine whether blood flow in the perfused region can be determined by the slope of a portion of the clearance curve.

Chapter 3Radioactive Inert Gas Clearance Curves from Ocular Tissue3.1 Introduction

The studies of Lassen and his coworkers allowed the inert gas clearance method to be applied to a greater range of organs. This chapter describes the application of the technique to the measurement of choroidal blood flow in rabbits and discusses the results obtained from a series of experiments designed to obtain control values of choroidal blood flow.

3.2 Radioisotope

The application of the inert gas clearance technique to the measurement of choroidal blood flow requires three criteria to be met in the choice of radioisotope. The criteria are:

- (1) commercial availability,
- (2) convenient physical half life, and
- (3) suitable radiation emissions to allow measurement of the radioactivity within the eye with minimal interference from extraocular tissue.

The physical properties of the commercially available radioisotopes of the inert gases are shown in table 3.1. Krypton-85 was chosen as the most suitable isotope. It has a long physical half life (10.6 yrs), thus eliminating transport and storage problems encountered with short-lived radioisotopes. It is principally an emitter of beta particles (99.3%) with only 0.7%  $\gamma$  emission. The maximum range in tissue of the beta particles is 2.8 mm. Monitoring of the radioactivity within the eye is therefore possible without interference from external tissue. Xenon-133 with its more penetrating 81 kev  $\gamma$  emission is much less suitable in this respect.

Table 3.1 Physical data of the radioactive inert gases

ISOTOPE	HALF LIFE	EMISSION		EMISSION		
		ENERGY (MEV)	%	ENERGY (MEV)	%	
Argon Ar-37	34.5 d	-	-	0.0026	100	
	Ar-41	100 m	1.20	99.1	1.29	99.1
Krypton Kr-85m	4.4 h	0.82	81	0.305	13	
				0.15	78	
Kr-85	10.6y	0.15	0.7	0.51	0.7	
		0.67	99.3			
Xenon Xe-131m	12 d	-	-	0.164	21	
	Xe-135m	2.3 d	-	-	0.23	13.5
	Xe-133	5.3 d	0.34	99	0.081	36.5

### 3.3 Radiation Detectors and Associated Instrumentation

Two radiation detectors were used to monitor the radioactivity within the eye. These were:-

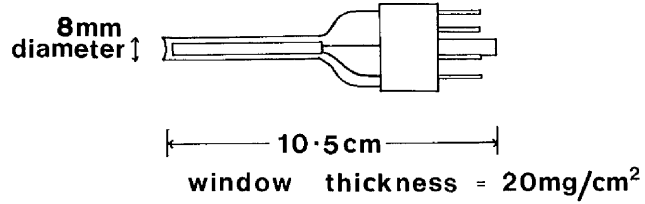
- (a) Silicon solid state planar detector (developed by Dr. F.L. Allsworth, Atomic Energy Research Establishment, Harwell).
- (b) Geiger-Müller tube (20th Century Electronics, type MB4II).

A schematic diagram of these detectors is shown in figure 3.1.

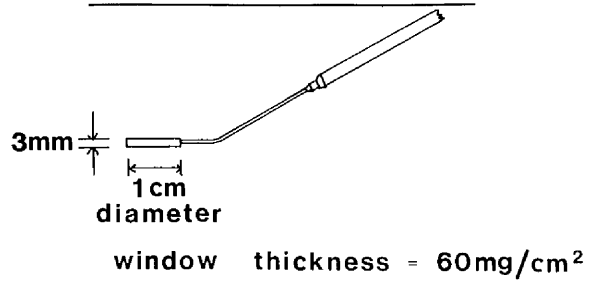
The count rate from each detector was processed by an amplifier/pulse height analyser system (Ekco type M5050F) linked to ratemeters (Ekco type M5183A) to give digital and analogue recordings of the change in radioactivity (fig. 3.2a,b). No significant differences in the shape of the inert gas clearance curves obtained from ocular tissue were noticed between the two detectors.

Solid state detectors have been used in many different situations where their shape and small size have proved an advantage over more conventional beta detectors (Grängsjö, Ulfendahl and Wolgast, 1966; Wolgast, 1968; Abson, Allsworth and Salmon, 1968; Yamamoto, Phillips, Hodge and Feindel, 1971; Lauber and Wolgast 1972; Wolgast and Lauber 1972). The shape and size of the solid state detector was particularly advantageous in the external monitoring of the radioactivity within the eye, since less operative interference was required in siting the detector next to the sclera. Unfortunately, the solid state detector proved to have a shorter life time than expected. Approximately 80% of the measurements of choroidal blood flow in this control study were obtained using the solid state detector. The remaining 20% and all measurements in subsequent studies were

**A. GEIGER - MULLER TUBE**



**B. SOLID STATE DETECTOR**



· Figure 3.1 Schematic diagram of radiation detectors employed to measure ocular radioactivity.  
(A) Geiger-Muller tube  
(B) Solid state detector.

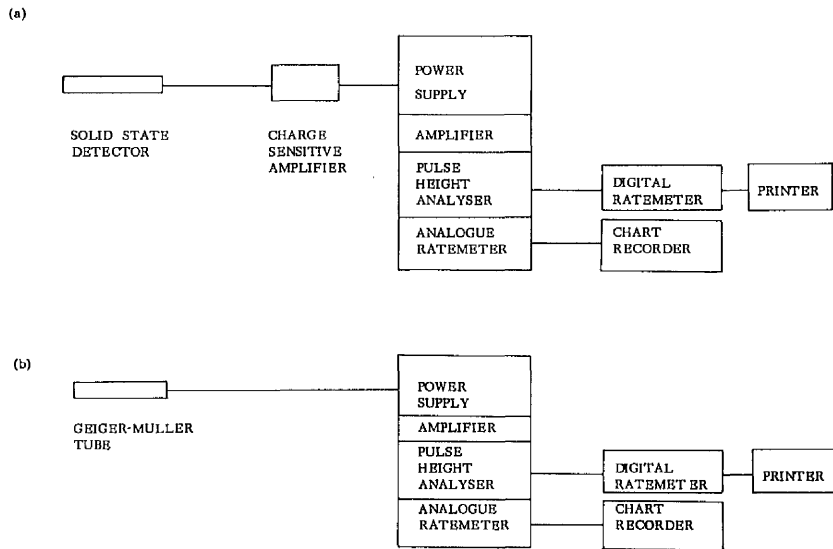


Figure 3.2 Diagram of counting equipment for  
 (a) Geiger-Muller tube  
 (b) Solid state detector.

obtained using a Geiger-Müller tube.

#### 3.4 Experimental Animal

Thirty albino and four Dutch pigmented rabbits were used in an initial series of experiments designed to study the feasibility of measuring choroidal blood flow using the inert gas clearance technique. Rabbits were selected for study because their retinæ are almost completely maintained by the choroidal circulation. The retinal blood vessels are restricted to a small region extending from the optic nerve head. (David, 1929). Thus by suitable positioning of the radiation detector on the sclera it is possible, using krypton -85, only to view those parts of the eye served by the choroidal circulation.

Figure 3.3 shows the anatomy of the ocular arterial supply in the rabbit. Rabbits differ from primates in that the ophthalmic artery is supplied by the external carotid artery and not the internal carotid artery. The ophthalmic artery gives rise to the ciliary artery from which branch some of the short posterior ciliary arteries which supply the choroidal circulation. The single retinal artery which gives rise to the retinal circulation is a branch of a short posterior ciliary artery. It penetrates the optic nerve close to the entrance to the globe.

#### 3.5 Anaesthesia

After initial premedication with phencyclidine (6-8mg) anaesthesia was induced and maintained with a mixture of halothane, nitrous oxide and oxygen on open circuit. Tracheostomy was performed on all animals. The expired air was vented to the outside atmosphere.

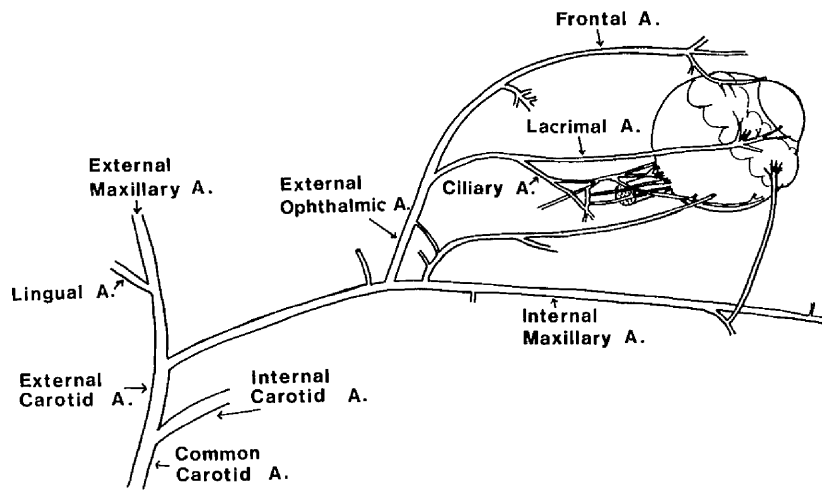


Figure 3.3 The arterial supply to the rabbit eye.

In preliminary experiments on nine animals a halothane concentration of 0.5 - 2.5% (from a Fluotec vaporiser Mk.II) was used for the duration of the experiment (minimum period of six hours). However, in these nine animals, degenerate changes were found in the retinal fine structure (Johnson, Wilson and Strang, 1973). These changes were most marked in the visual cells and retinal pigment epithelium. In view of this, the results from these animals were not included.

Administration of 0.5% halothane for periods up to 6 hours produced no ultrastructural changes in the rabbit retina. (Johnson, Strang and Wilson, 1973). This concentration of halothane was used in all subsequent experiments.

### 3.6 Experimental Method

Radioactive krypton was introduced into the arterial supply to the eye via a polythene cannula (O.D. = 0.75 mm) inserted into the lingual artery; the distal end of the artery being tied (see Figure 3.3). This site of catheterisation was chosen to minimise disturbance to the ocular circulation, yet achieve a bolus arrival of the radioisotope at the choriocapillaris.

Systemic arterial blood pressure was monitored continuously by connecting a polythene cannula (O.D. = 1.34 mm) inserted into a femoral artery to a low volume displacement pressure transducer (Bell and Howell type L221) and pen recorder (Devices M2). This cannula also provided a means of collecting arterial blood samples for the measurement of blood gases. Arterial blood  $pH$ ,  $P_a CO_2$ , and  $P_a O_2$  were measured on a micro-Astrup apparatus at each determination of choroidal blood flow. Rectal temperature was monitored continuously.

The intraocular pressure of the eye under investigation was monitored continuously by connecting the anterior chamber with a fine steel cannula to a second low volume pressure transducer and recording system.

Initially this cannula was also connected via a three-way tap to a saline reservoir. The height of the reservoir was adjusted so that the intraocular pressure was maintained at a pressure of 15mmHg.

Although the eye equilibrates within two minutes with the saline reservoir, this arrangement results in the pressure transducer measuring only the pressure head of the saline reservoir. For this reason the reservoir was separated from the measuring system in later experiments by introducing a second steel cannula into the anterior chamber and connecting it to the saline reservoir. With this arrangement it was easier to test the patency of the pressure measurement and control systems.

The conjunctiva was incised circumferentially in the upper nasal quadrant and reflected. The radiation detector (either the solid state detector or the Geiger-Müller tube) was then placed on the sclera so that the centre of the sensitive face coincided with the mid-equatorial region of the eye.

Thirty minutes were allowed to elapse between the end of the preliminary operative procedures and the commencement of measurements. Boluses of approximately 0.2 ml of krypton-85 dissolved in saline (activity approximately 10mCi/ml) were injected into the carotid artery via the lingual artery cannula. The clearance of krypton-85 radioactivity from ocular tissue was monitored with

sequential recording periods of 0.4 second for the first minute and thereafter with a period of ten seconds until the radioactivity within the eye had decreased to background levels. Only then were repeat determinations of choroidal blood flow made.

### 3.7 Krypton-85 Clearance Curve

Figure 3.4 shows the first 25 seconds of a typical analogue recording of the diminishing radioactivity in the eye. It is characterised by a sharp rise in radioactivity following injection. This is followed by momentary equilibrium and then by a period of rapid decline. This decline will be referred to as the 'washout curve'.

Figure 3.5 shows a log/linear plot of the digital information corresponding to the washout curve illustrated in figure 3.4. The curve is characterised by a sharp fall in radioactivity lasting approximately five seconds which is followed by a period of slower decline. The count rate does not reach background levels until 20-30 minutes after injection. This time is dependent upon the peak radioactivity.

### 3.8 Analysis of Washout Curve

Friedman, Kopald, and Smith (1964) initially assumed that the washout curve could be represented as the sum of decreasing exponential components and that the fastest of these components reflected choroidal blood flow. These workers substituted the half life of this component into equation (2-16)

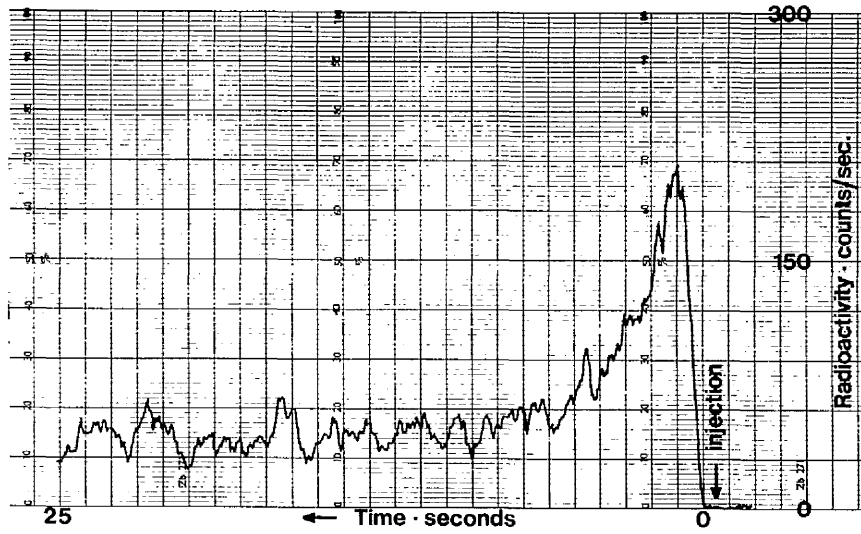


Figure 3.4 Analogue recording of the diminishing radioactivity in the rabbit eye.

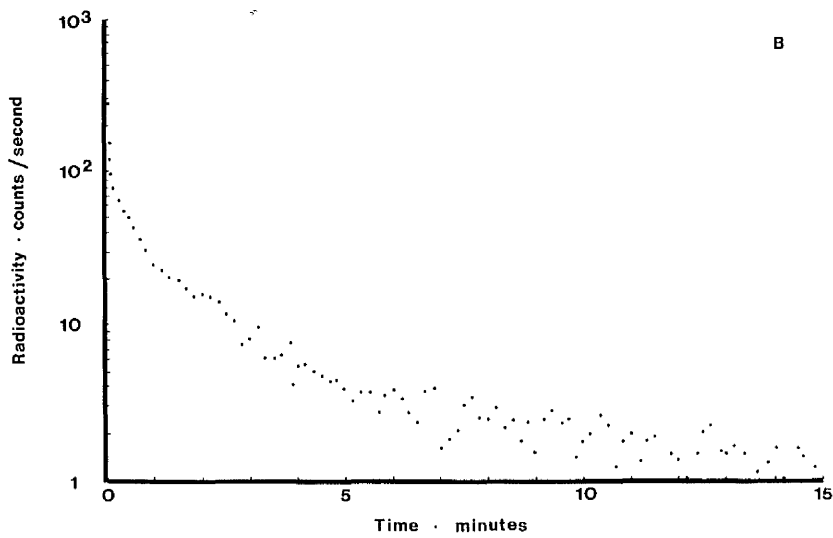
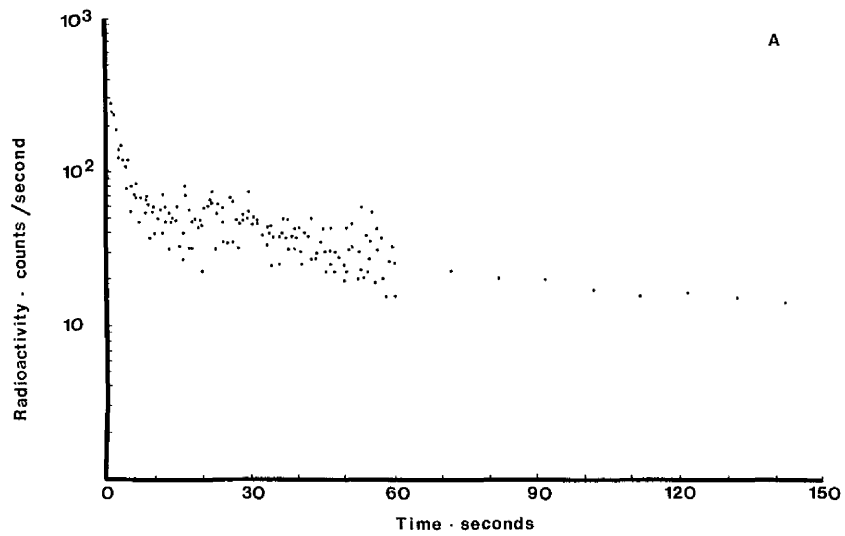


Figure 3.5 Plot of diminishing radioactivity within a rabbit eye (logarithmic scale) against time (linear scale).  
 (A) first 150 seconds      (B) first 15 minutes

$$F = \frac{69.3 \cdot \lambda}{T_{1/2} \cdot \rho} \quad \text{ml/100g/min} \quad 3.7$$

and obtained a value for the choroidal blood flow. In a later paper, Friedman and his co-workers, without explanation, used the half life of the initial decline in radioactivity in equation (2-16) and not the half life of the initial slope of the fastest exponential component obtained by curve stripping (Friedman, and Smith, 1965). It will be shown in Chapter 5 on theoretical grounds that the initial slope of the clearance curve and not the slope of the fastest component is the true indicator of choroidal blood flow.

In order to facilitate comparison between Friedman's data and the data obtained from this study, both 'curve stripping' and 'initial slope' values of choroidal blood flow were determined. Figure 3.6 illustrates the technique of curve stripping used to determine the exponential components of the washout curve. In this technique the data is plotted on log/linear graph paper. The slope of the final linear section of the curve is taken as the exponential rate constant corresponding to the slowest exponential component of the clearance of krypton from the eye (figure 3.6a). This linear section of the curve is extrapolated to time zero (time of peak radioactivity) and subtracted from the original washout curve. This yields a new curve again having a final linear section, the slope of which is taken as the exponential rate constant of the second slowest component of the washout curve. This process of extrapolation and subtraction is repeated until only a single exponential component is left. (figure 3.6 c,d).

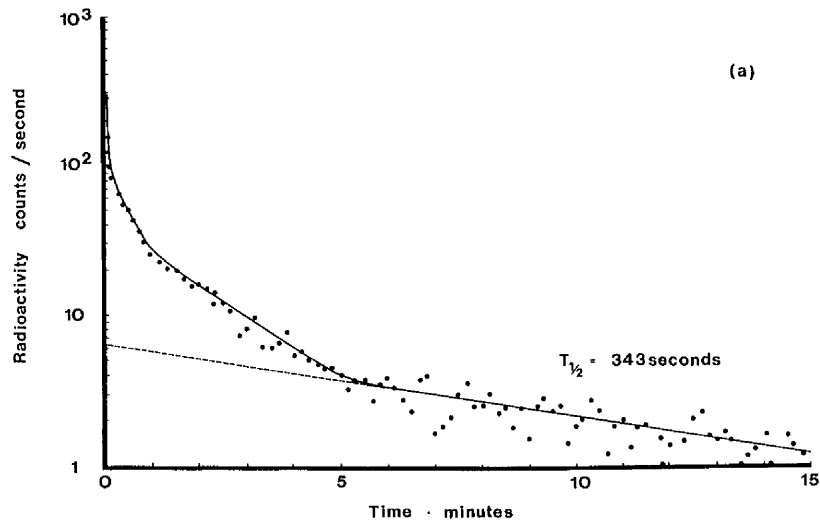


Figure 3.6(a) Curve stripping technique. The late linear part of the curve corresponds to the slowest exponential component. This component is extrapolated and subtracted from the original curve.

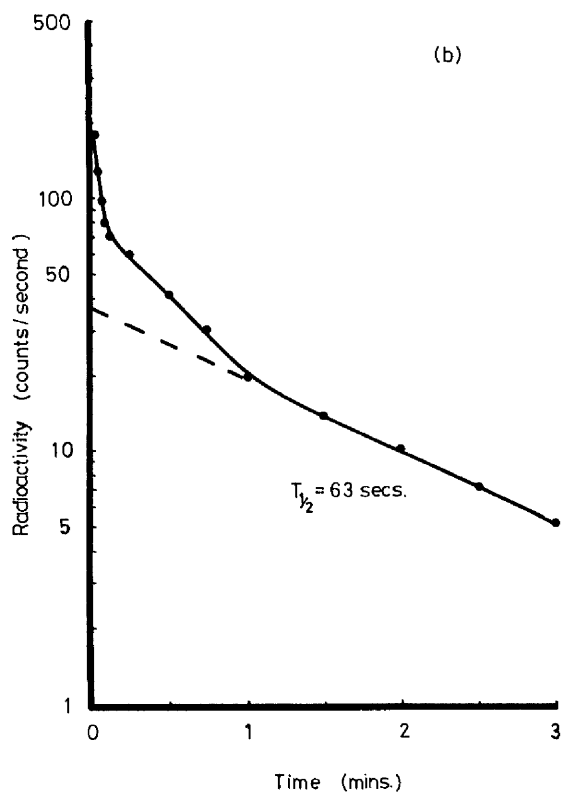


Figure 3.6(b) Curve stripping technique. The result of the first subtracted yields a new curve again having a late linear section which corresponds to the decrease in radioactivity of the next slowest component. This component is extrapolated and subtracted from the new curve.

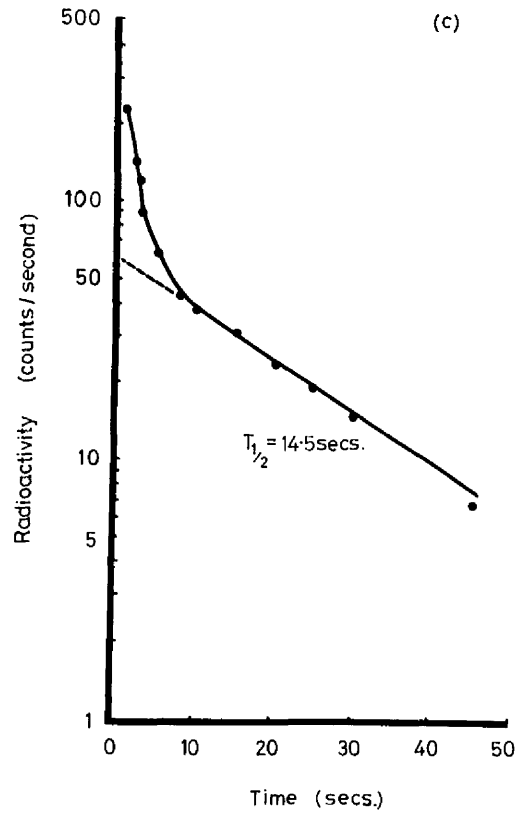


Figure 3.6(c) Curve stripping technique. Result of the second subtraction.

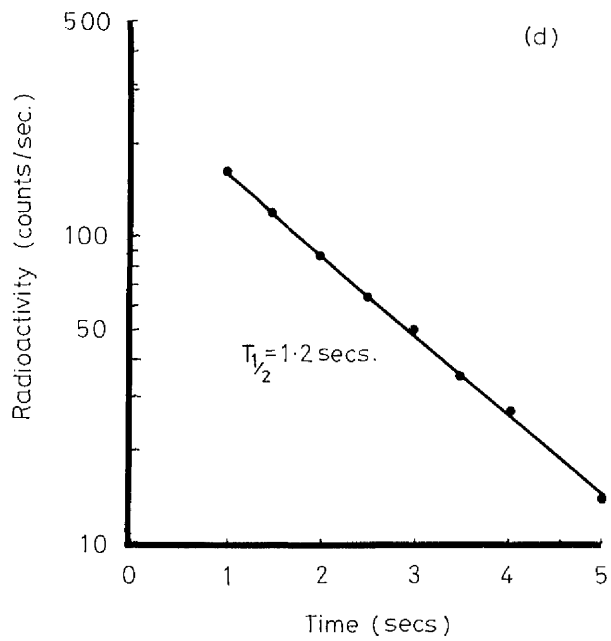


Figure 3.6(d) Curve stripping technique. The third subtraction results in a final linear component. The half life of this component is used to determine the "curve stripping" value of the choroidal blood flow.

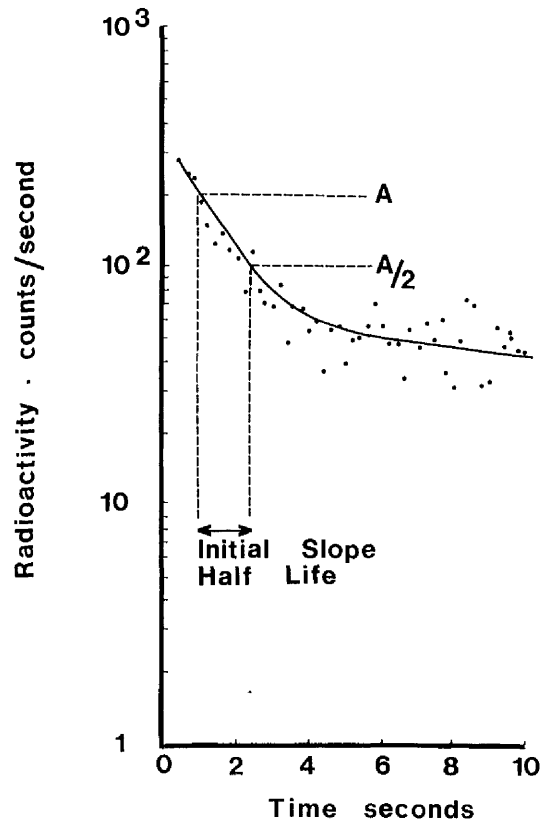


Figure 3.7 The first 10 seconds of a log/linear plot illustrating the determination of the "initial slope" half life.

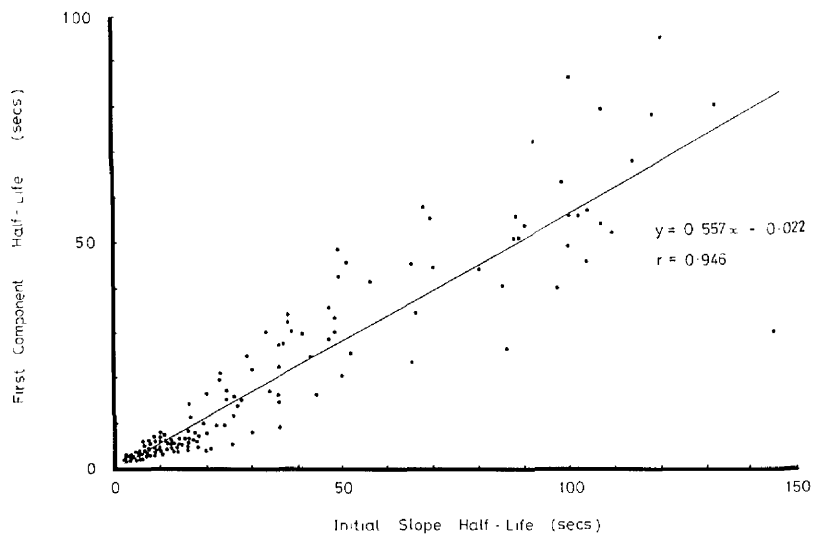


Figure 3.8 "Curve stripping" half life versus corresponding "initial slope" half life.

The half life of this fastest component is then substituted into equation (2-16) to obtain the 'curve stripping' value of choroidal blood flow.

Figure 3.7 shows the first 10 seconds of a log/linear plot of the washout curve and illustrates the method of determining the half life of the initial slope. The process of curve stripping yields a half life for the fastest component which is smaller than the half life of the initial slope, although there is a correlation ( $r = 0.946$ ) between the two values (figure 3.8). The 'curve stripping' value is thus an overestimation of the choroidal blood flow, as will be shown from theoretical considerations in Chapter 5.

### 3.9 Results

In this series of experiments only values derived from washout curves obtained from animals maintained within a narrow range of  $P_a CO_2$ ,  $P_a O_2$  and mean femoral arterial blood pressure (MABP) were regarded as valid in view of the known effects of these on ocular blood flow. (Bettman and Fellows, 1956 ; Bill, 1962c; Trokel, 1965; Anderson, Saltzmann and Frayser, 1967; Friedman, 1970; Alm and Bill, 1972b; Friedman and Chandra, 1972; Tsacopoulos and David, 1973).

These ranges were:-

$P_a CO_2$	32-48 mmHg (mean 40 $\pm$ 1 S.D.)
$P_a O_2$	85-137 mmHg (mean 111 $\pm$ 1 S.D.)
MABP	56-76 mmHg (mean 66 $\pm$ 1 S.D.)

Within these limits a total of 85 measurements on 34 rabbits were obtained. Application of the curve stripping technique resulted in the washout curve being represented as the sum of four exponential components. Mean values of the half lives of the four

components are shown in table 3.2. Friedman and his co-workers originally obtained three components in the washout curve from rabbits using a Geiger-Müller tube (Friedman, Kopald and Smith, 1964). Later they reported that when a solid state detector was used four components could be identified (Friedman and Smith, 1965). They reported that the half life of the first component varied between 2.5 and 5 seconds and that the half lives of the second and third components varied between 1.5 and 30 minutes. The mean value of the half life of the initial slope from this study was  $4.5 \pm 1.6$  seconds (mean  $\pm$  1 S.D.).

The choroidal blood flow was calculated from equation

$$(2-16):- \quad F = \frac{69.3 \cdot \lambda}{T_{1/2} \cdot \rho}$$

where  $F$  = choroidal blood flow (ml/100g/min),

$T_{1/2}^1$  = half life (mins.). (Initial slope or 1st component),

$\rho$  = density of the choroid ( $\text{g cm}^{-3}$ ), and

$\lambda$  = partition coefficient (i.e. the ratio of the solubility of krypton in lg of choroid to its solubility in 1ml of blood).

In all calculations of the choroidal blood flow a value of unity has been taken for the density of the choroid, in accordance with the measurements of Friedman, Kopald and Smith (1964). The partition coefficient was also taken to be unity. This value was used because the choroid consists of approximately 95% blood and the solubility of krypton in exsanguated choroid is approximately half that in whole blood (see Chapter 6).

Applying equation (2-16) to the data from this series of experiments the following values of the choroidal blood flow in rabbits were obtained (mean  $\pm$  1 S.D.).

Table 3.2 Mean values of half-life ( $T_{1/2}^1$ ) and exponential rate constant ( $k$ ), (mean  $\pm$  1.S.D.)

	$T_{1/2}^1(\text{sec})$	$k(\text{sec}^{-1})$
Component 1	2.5 $\pm$ 0.8	0.28 $\pm$ 0.09
Component 2	45 $\pm$ 14	0.012 $\pm$ 0.006
Component 3	180 $\pm$ 105	0.004 $\pm$ 0.003
Component 4	780 $\pm$ 510	0.0009 $\pm$ 0.0005

'Initial slope' choroidal blood flow =  $920 \pm 340$  ml/100g/min.

'Curve stripping' choroidal blood flow =  $1660 \pm 480$  ml/100g/min.

Friedman, Kopald and Smith (1964) obtained 'curve stripping' values of choroidal blood flow in rabbits between 800 and 1600 ml/100g/min. These values are in good agreement with the value obtained in this study.

In all subsequent studies reported in this thesis the value of the choroidal blood flow will be derived from the half-life of the initial slope for theoretical reasons explained in Chapter 5. Such values will be referred to simply as 'the choroidal blood flow'.

### 3.10 Discussion

The use of nitrous oxide and oxygen anaesthesia proved to be unsatisfactory in rabbits. For this reason halothane was introduced into the anaesthetic mixture. Halothane was chosen because it interferes only minimally with autoregulation of the cerebral blood flow in the baboon in response to changes in perfusion pressure (Fitch, 1975). Owen (1971) has shown that urethane anaesthesia greatly inhibits cardiovascular reactivity in cats. The resultant hypotension evident in this study was thought not to be significant owing to the fact that (a) no ultrastructural changes were apparent in the retina after six hours anaesthesia (Johnson, Strang and Wilson, 1973), and (b) the value of the choroidal blood flow obtained in this study is in good agreement with those obtained by other workers in normotensive conditions (see table 5.3).

Table 3.3 Comparison of normal values of choroidal blood flow

METHOD	ANIMAL	CHOROIDAL BLOOD FLOW (ml/min) (ml/100gm/min)	AUTHOR
Reflective densitometry	Albino rabbit	1680	Trokel (1965)
Microspheres	Monkey	1.44	O'Day, Fish, Aronson Pollycove and Coon (1971)
	Rabbit	0.84	
Microspheres	Cat	734 <sup>*1</sup> 1382 <sup>*2</sup>	Alm and Bill (1972)
Microspheres	Monkey	677 <sup>*1</sup>	Alm, Bill and Young (1973)
Microspheres	Cat	1300	Weiter, Schachar, and Ernest (1973)
Inert Gas Clearance	Cat	1200	Friedman et al (1964)
	Rabbit	831-1664	
Inert Gas Clearance	Rabbit	920	Present study

\* 1 mg/min

\* 2 mg/100 gm /min

The variation in choroidal blood flow in one animal throughout the duration of a six hour experiment is shown in figure 3.9. The washout curve corresponding to the 3rd point on the graph with a choroidal blood flow of 320 ml/100g/min. is shown in figure 3.10. In this measurement of blood flow the radioactivity declined initially with a half life of 0.6 second. This is equivalent to the decline observed with the passage of a non-diffusible indicator (Tc -99m labelled human serum albumin) (figure 3.11).

This is indicative that an arterio-venous shunt was present. A-V shunts were present in 6% of the measurements of flow.

Since the rabbit has only a single circulation within the field of view of the detector, the analysis of the washout curve into a series of exponential components has no justification. The half lives of the components obtained in this study are in reasonable agreement with those found by Friedman and his co-workers. At low flow values, four exponential components are not necessarily observed. One possible reason for this is that at low flow values the peak in radioactivity is generally lower and thus the washout curve cannot be monitored for long periods with sufficient statistical accuracy.

Glass and de Garetta (1971) have pointed out that the magnitude of the errors of the various parameters obtained by exponential curve fitting is dependent on:-

- (1) exponent ratios,
- (2) amplitude ratios,
- (3) data accuracy,
- (4) sampling frequency,
- (5) number of data points,
- (6) degree of correlation between the variables,
- (7) initial parameter guesses, and
- (8) curve-fitting method used.

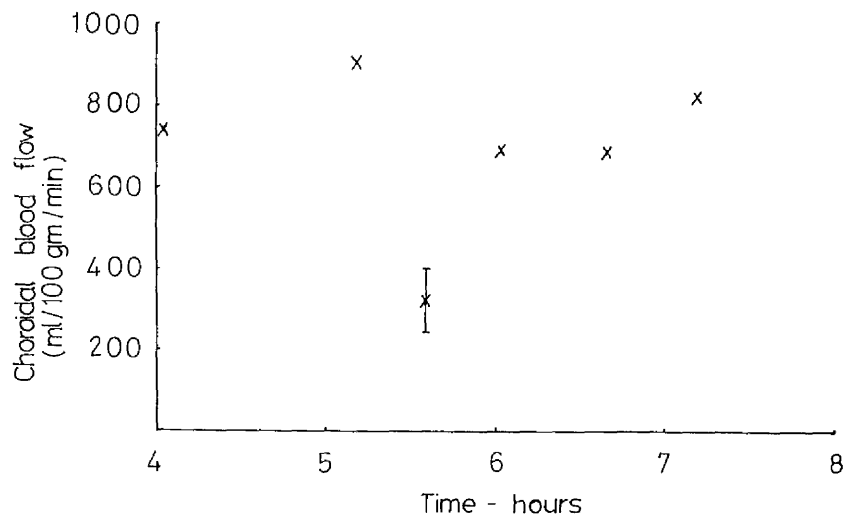


Figure 3.9 The variation in choroidal blood flow in one animal throughout the duration of a six hour experiment. The error bar on the 3rd point is an estimate of the error in the choroidal blood flow at low flow values (see Chapter 5).

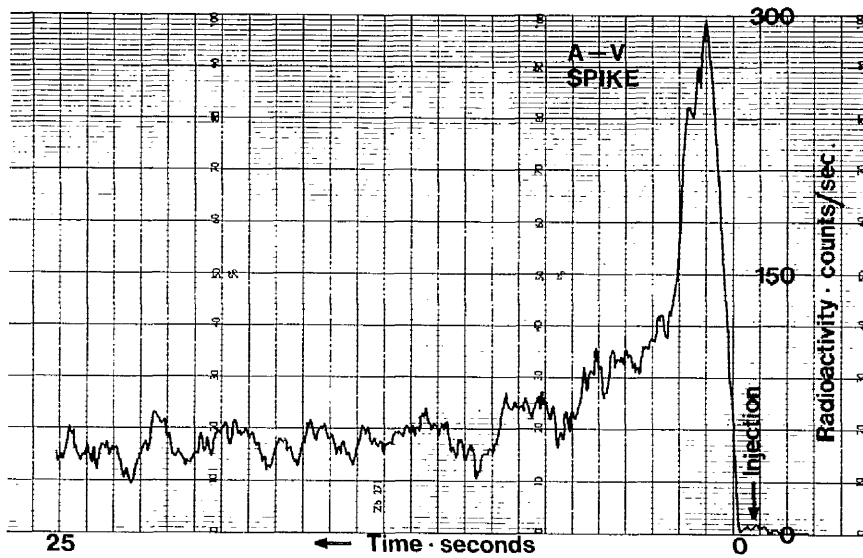


Figure 3.10 Analogue recording of a washout curve illustrating the extremely fast initial decline in radioactivity corresponding to an arterio-venous shunt.

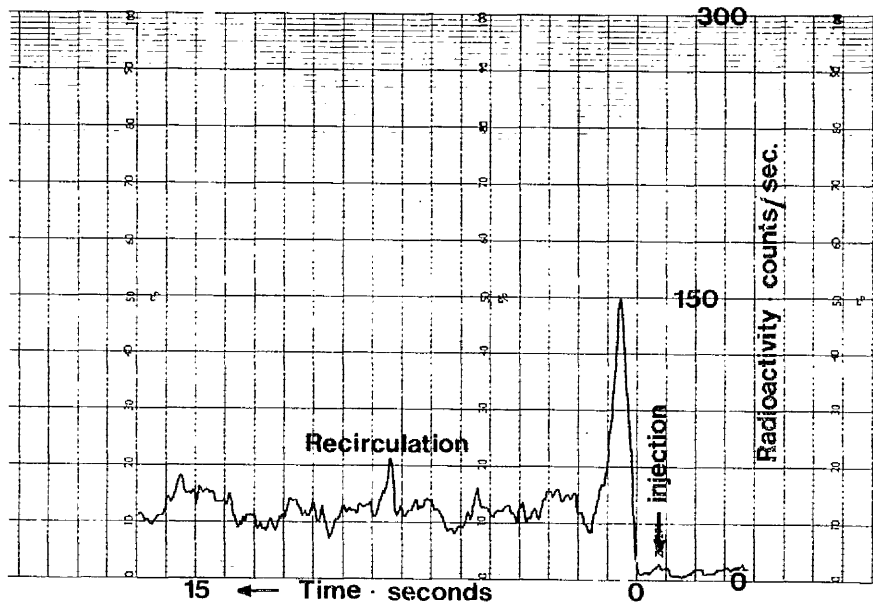


Figure 3.11 Analogue recording of the radioactivity within a rabbit eye following injection of a non-diffusible indicator ( $Tc-99m$  labelled human serum albumin).

From their investigations they concluded that in a biological investigation with less than 60 data points of better than two per cent accuracy, analysis of the data into a number of exponentials greater than three was unlikely to yield useful information.

Rabbits, whilst being ideal in having only a choroidal circulation present, are not suited for prolonged experiments under anaesthesia. The maintenance of a steady blood pressure throughout the duration of a six hour experiment is not without difficulty. However, the presence of the single circulation greatly simplified the initial development of a mathematical model to describe diffusion of krypton in ocular tissue. The explanation of the complex nature of the washout curve in terms of diffusion and the establishment of a relation between the initial slope of the washout curve and the choroidal blood flow will be presented in Chapters 4 and 5.

Chapter 4Diffusion of Krypton in Ocular Tissue 1 Mathematical Model4.1 Introduction

In the previous chapter it was shown that the clearance of radioactive krypton from rabbit ocular tissue is complex and that previously some doubt has existed on the physical nature of the washout curve. The radioactivity measured by the detector placed on the sclera at a given instant is related to the concentration values of krypton summated over the field of view of the detector. In the rabbit krypton arrives at the choriocapillaris and diffuses into the surrounding tissue. As fresh blood passes through the choriocapillaris a fraction of the krypton atoms will equilibrate with the blood and be carried by the blood flow out of the eye, resulting in a decline in radioactivity. However, a significant proportion of the atoms will diffuse out of the choroid into the sclera, retina and vitreous. The diffusion of krypton away from the detector also results in a decline in measured activity due to the increased absorption of the beta particles in tissue.

In this and in the next chapter a mathematical model of diffusion of krypton in ocular tissue will be presented to explain the complex pattern of the washout curve and to investigate the relation between the choroidal blood flow and the decline in activity.

Diffusion is the name given to the process whereby molecules, or atoms, by virtue of their random motion will, on average, move from regions of high partial pressure to regions of low. In this chapter a numerical method of solving the mathematical equations describing the diffusion of a gas within media will be presented for a model whose

structure is based on the anatomy of the rabbit eye. In the next chapter results of the model will be presented, comparison being made between predicted washout curves derived from the model and experimental washout curves obtained from the study described in Chapter 3. Subsequently, the model will be extended to predict the effect of the presence of a retinal circulation on the washout curve.

#### 4.1.2 Nomenclature

The following symbols are used throughout this chapter

$x$  = the spatial coordinate, normal to a reference surface (cm),

$t$  = time (seconds),

$\lambda$  = the solubility of a substance in a given medium,

$c(x,t)$  = the concentration of the diffusing substance in a medium at a point  $x$  cm from some origin at time  $t$  ( $\text{cm}^{-3}$ ),

$p(x,t)$  = the partial pressure of the diffusing substance in a medium,  
 =  $k \cdot \lambda \cdot c(x,t)$  where  $k$  is a constant of proportionality, dependent on the units,

$J(x,t)$  = the flux of diffusing substance ( $\text{cm}^{-2} \text{sec}^{-1}$ ),

= the quantity of substance passing perpendicularly through a reference surface of unit area during unit time,

$D$  = the diffusion coefficient of the diffusing substance in a given medium. It will be assumed throughout that  $D$  is independent of position and partial pressure. ( $\text{cm}^2 \text{sec}^{-1}$ ), and

$Lx$  = the value of  $x$  at the boundary between two media.

The subscripts 1,2,3,....., added to the above symbols indicate that the symbol is applicable to medium 1, medium 2, medium 3,....., respectively.

#### 4.2.1 Derivation of the Differential Diffusion Equation

The analogy between the transfer of heat by conduction due to random molecular motions and the diffusion of substances was first recognised by Fick (1855). He developed the mathematical treatment of diffusion by adopting the equation of heat conduction developed by Fourier in 1822. Fick's first law of diffusion is based on the hypothesis that the rate of transfer of a diffusing substance through a reference surface of unit area of an isotropic medium is proportional to the partial pressure gradient measured normal to the section.

Along one dimension Fick's first law states:

$$J = - D \frac{\partial p}{\partial x} \quad (4-1)$$

The negative sign indicates that diffusion is in the opposite direction to the partial pressure gradient,  $\partial p / \partial x$  i.e. diffusion takes place from regions of high to regions of low partial pressure.

In addition the diffusing particle at the reference surface must obey the laws of conservation of matter

$$\frac{\partial p}{\partial t} + \frac{\partial J}{\partial x} = 0 \quad (4-2)$$

Combining this equation with equation (4-1) results in Fick's 2nd Law:-

$$\frac{\partial p}{\partial t} = D \cdot \frac{\partial^2 p}{\partial x^2} \quad (4-3)$$

Solution of this equation allows the variation in partial pressure (and hence concentration) throughout the medium to be obtained.

### 4.2.2 Boundary Conditions

Where diffusion is occurring in two adjacent media having different diffusion coefficients then within each medium there will be an equation similar to equation (4-3) expressing the diffusion within that medium, viz.:-

(1) for  $x < L_x$

$$\frac{\partial P_1}{\partial t} = D_1 \cdot \frac{\partial^2 P}{\partial x^2} \quad (4-4)$$

(2) for  $x > L_x$

$$\frac{\partial P_2}{\partial t} = D_2 \frac{\partial^2 P}{\partial x^2} \quad (4-5)$$

where  $L_x$  is the value of  $x$  at the boundary between the two media. In obtaining the partial pressure variations from these equations two physical conditions have to be obeyed at the boundary between the media.

(1) The partial pressure is continuous

$$\text{i.e. } P_1 \Big|_{L_x} = P_2 \Big|_{L_x} \quad (4-6)$$

or

$$\lambda_1 C_1 \Big|_{L_x} = \lambda_2 C_2 \Big|_{L_x} \quad (4-7)$$

(2) The flux of particles across the boundary is constant, i.e. the net number of particles leaving medium 1 and entering medium 2 at a given instant is equal to the net number of particles entering medium 2 from medium 1.

$$D_1 \cdot \left( \frac{\partial P_1}{\partial x} \right)_{L_x} = D_2 \cdot \left( \frac{\partial P_2}{\partial x} \right)_{L_x} \quad (4-8)$$

#### 4.3.1 The Numerical Solution of the Diffusion Equations

The exact solution of a system of differential equations by integral transformation is limited to a narrow range of problems. Numerical methods allow approximate solutions to be obtained for a wide range of problems. One of these methods - the finite difference method - was used to obtain values of the partial pressure in the diffusion model described later in this chapter. In this method the derivatives are replaced at discrete points (called nodal points) by expressions which approximate the derivatives at these points.

#### 4.3.2 The Finite Difference Formulae

For a function of one variable, e.g.  $y = f(x)$ , an approximation to the first derivative,  $dy/dx$  can be obtained by replacing the gradient of the tangent to the curve  $y = f(x)$  at  $x = x_i$  by the gradient of the chord joining two adjacent points on the curve at  $x = x_i$  and  $x = x_i + 1$  (see figure 4.1), viz:-

$$\frac{dy}{dx} = \frac{y_{i+1} - y_i}{h} \quad (4-9)$$

$$\text{where } h = x_{i+1} - x_i (= x_i - x_{i-1}) \quad (4-10)$$

In a similar manner an approximation can be obtained for the second derivative, viz:-

$$\frac{d^2y}{dx^2} = \frac{y_{i+1} - 2y_i + y_{i-1}}{h^2} \quad (4-11)$$

#### 4.3.3 The Finite Difference Form of the Differential Diffusion Equation

The finite difference method applied to the one dimensional differential diffusion equation results in solutions being obtained for the partial pressure at nodal points on a rectangular network (see figure 4.2). The abscissa of this network represents the spatial dimension,  $x$ .

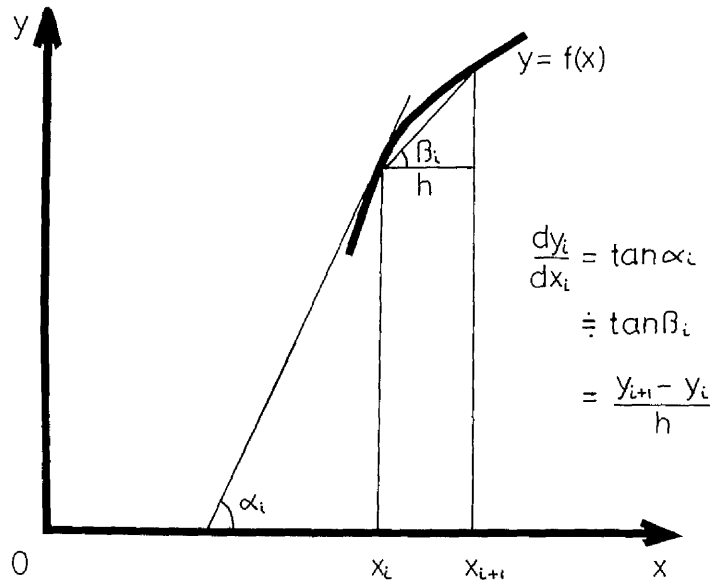


Figure 4.1 Determination of the finite difference relationship.

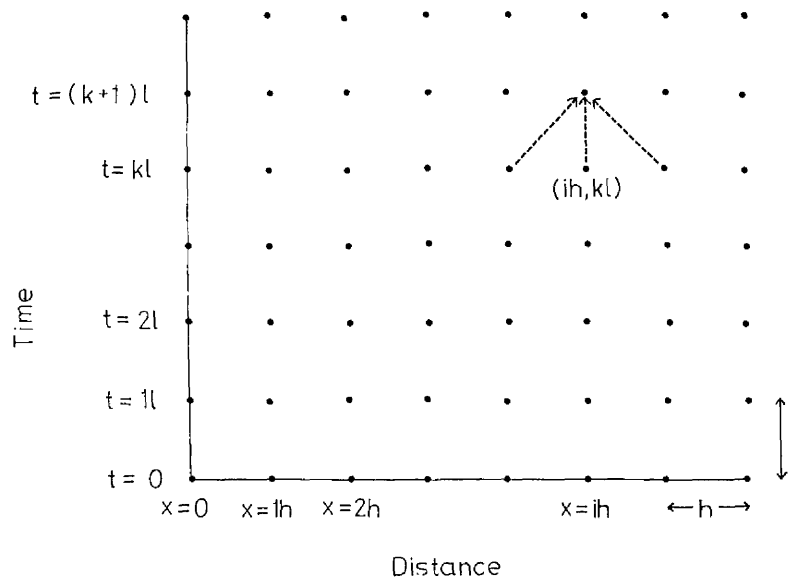


Figure 4.2 The finite difference network. The nodal points are the points of intersection of straight lines parallel to the coordinate axes.

It is divided into equal steps of  $h$  units. The ordinate represents time and it is divided into intervals of  $\ell$  units. The nodal points are the points of intersection of the straight lines parallel to the coordinate axes from  $x = 0, x = h, x = 2h, \dots$  and  $t = 0, t = \ell, t = 2\ell, \dots$ .

Let  $P_{i,k}$  be the actual value of the partial pressure at the point  $x = ih$  at the time  $t = k\ell$  ( $ih, k\ell$ ). The partial derivatives  $\frac{\partial p}{\partial t}$  and  $\frac{\partial^2 p}{\partial x^2}$  at the point  $(ih, k\ell)$  in terms of the finite difference approximations (equations 4-9, and 4-11) are:-

$$\frac{\partial p_{i,k}}{\partial t} = \frac{P_{i,k+1} - P_{i,k}}{\ell} + \epsilon_1 \quad (4-12)$$

$$\text{and } \frac{\partial^2 p_{i,k}}{\partial x^2} = \frac{P_{i+1,k} - 2P_{i,k} + P_{i-1,k}}{h^2} + \epsilon_2 \quad (4-13)$$

where  $\epsilon_1$  and  $\epsilon_2$  are the residual terms tending to zero as  $\ell$  and  $h$  approach zero.

Substituting these relations into equation (4-3) gives:-

$$\frac{P_{i,k+1} - P_{i,k}}{\ell} + \epsilon_1 = D \left( \frac{P_{i+1,k} - 2P_{i,k} + P_{i-1,k}}{h^2} + \epsilon_2 \right)$$

Rearranging

$$P_{i,k+1} = \left( 1 - \frac{2D\ell}{h^2} \right) P_{i,k} + \frac{D\ell}{h^2} (P_{i+1,k} + P_{i-1,k}) + \ell R \quad (4-14)$$

where  $R = D\epsilon_2 - \epsilon_1$

Omitting the residual term,  $\ell R$ , yields the finite difference format of the differential diffusion equation, i.e.

$$P_{i,k+1} = \left(1 - \frac{2QD}{h^2}\right) P_{i,k} + \frac{QD}{h^2} (P_{i+1,k} + P_{i-1,k}) \quad (4-15)$$

where  $P_{i,k}$  is now the approximate value of the partial pressure at the point  $(ih, ik)$ .

This last equation allows the calculation of the values of the partial pressure at the nodal points on the horizontal row  $(k+1)$  from a knowledge of the values of partial pressure on the previous row  $(k)$ . Thus if the initial values (i.e. the values of  $p$  along the x-axis) are known, successive application of equation (4-15) yields the values of the partial pressure at subsequent times.

The value of  $p$  at the two end nodal points on a horizontal row cannot be determined from equation (4-15). In the model described later in this chapter the values of the partial pressure at the end nodal points were obtained by linear extrapolation of the two neighbouring values.

#### 4.3.4 The Finite Difference Format of the Boundary Conditions

The boundary conditions between two media are:-

$$(1) P_1 = P_2 \quad (2) D_1 \left( \frac{\partial P_1}{\partial x} \right)_{L_x} = D_2 \left( \frac{\partial P_2}{\partial x} \right)_{L_x}$$

Inclusion of the first boundary condition is obviously straightforward. The finite difference format of the second boundary condition at a point  $(nh, ik)$  (where  $nh = L_x$  - the value of  $x$  at the boundary) is obtained by substituting the finite difference relation for the partial derivatives, viz:-

$$D_1 \left( \frac{P_{n,k} - P_{n-1,k}}{h} \right) = D_2 \left( \frac{P_{n+1,k} - P_{n,k}}{h} \right)$$

$$\text{i.e. } p_{n,k} = \frac{1}{(D_1 + D_2)} (D_2 \cdot p_{n+1,k} + D_1 \cdot p_{n-1,k}) \quad (4-16)$$

This equation is the finite difference format of the second boundary condition.

Equations (4-15) and (4-16) allow the determination of the partial pressure values for a system comprising of two or more media.

#### 4.3.5. Choice of distance increment, h, and time interval, l,

$$\text{If } p = \frac{eD}{h^2} \quad (4-17)$$

It has been shown (Luikov 1968) that

- (1) the finite difference method remains stable only if  $p \geq 2$ ,
- (2) the largest time step occurs when  $p = 2$ , and
- (3) the larger the value of  $p$ , the closer the approximated value approaches the exact solution.

The choice of the distance step,  $h$ , and the time interval,  $l$ , for any particular situation must satisfy the condition that  $p \geq 2$  for the finite difference method to remain stable. In the model presented later a value of 0.003 cm was used for the distance increment and 0.25 second for the time interval. This gave 'p' values of 2.3, 4.7, 4.5 and 3.0 for the sclera, choroid, retina and vitreous respectively.

#### 4.4 Comparison of Finite Difference and Exact Values

An estimate of the accuracy of the finite difference method was achieved by comparing the finite difference results, under the same conditions of distance increment and time interval as used in the model, with those obtained for an initial condition for which an exact solution of the differential diffusion equation is known. The initial condition

used was

$$\rho(x,0) = N \delta(x-a) \quad (4-18)$$

where  $N =$  a constant

$$\delta(x-a) = \begin{cases} 1 & \text{at } x = a \\ 0 & \text{at } x \neq a \end{cases}$$

For this initial condition the differential diffusion equation has the solution

$$\rho(x,t) = \frac{N}{\sqrt{4\pi Dt}} \cdot \exp\left(-\frac{(x-a)^2}{4Dt}\right) \quad (4-19)$$

The values of  $\rho(x,t)$  obtained from equation (4-19) for  $t = 10$  seconds were used as initial values for the finite difference network (figure 4.3). The value of the diffusion coefficient of krypton in the choroid ( $0.76 \times 10^{-5} \text{ cm}^2 \text{ sec}^{-1}$ ) was used in this comparison. Summated values of the partial pressure over the nodal points were obtained for both the finite difference and the exact values. Figure 4.4 shows the variation in the percentage difference over 15 minutes. The percentage difference was taken as

$$\frac{(\text{Exact value} - \text{finite difference value})}{\text{Exact value}} \times 100$$

The percentage difference varied between 0.0001% at time zero to 0.1% after 15 minutes.

Although these error values only pertain to the particular initial condition, they are at least two orders of magnitude smaller than the statistical uncertainty of the data points of a typical washout curve (figure 4.4). The percentage error of the count rate at a given time on

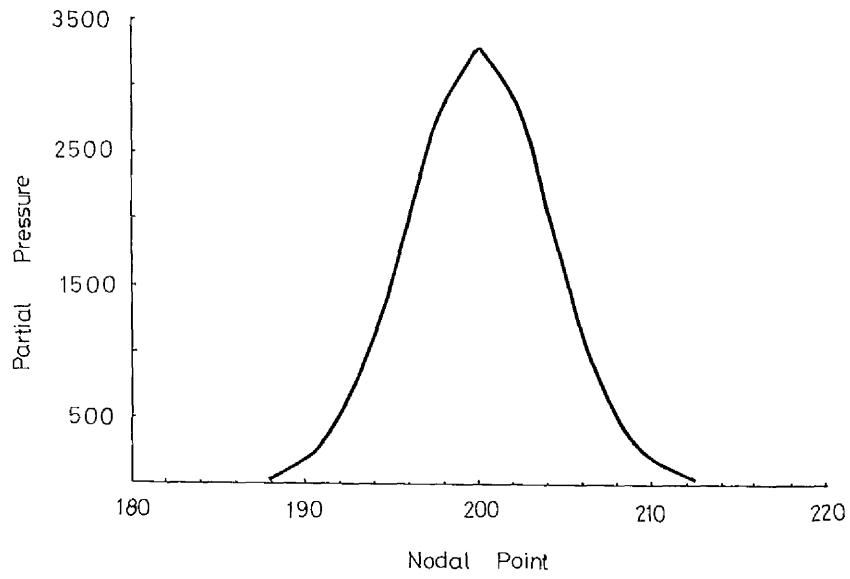


Figure 4.3 Initial partial pressure distribution used in the comparison between exact and finite difference values.

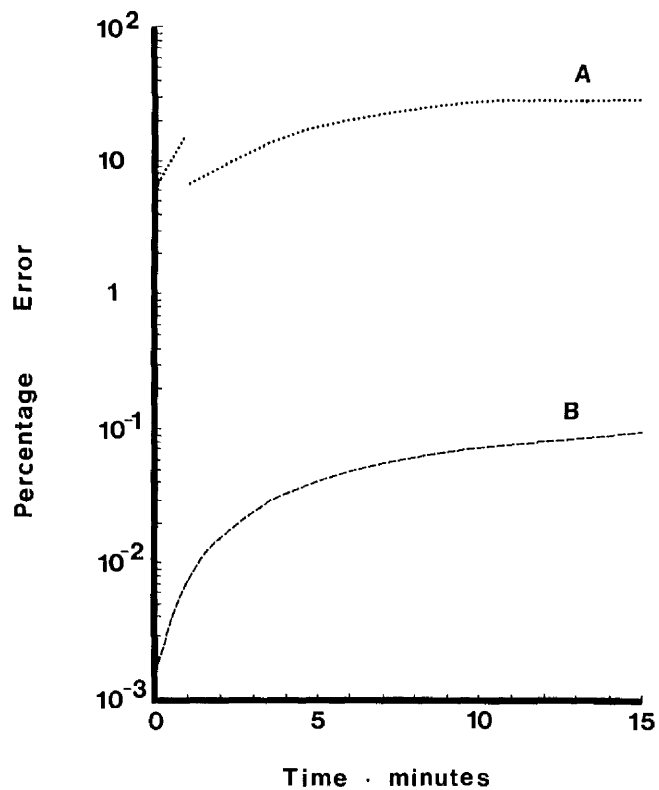


Figure 4.4 (A) Variation in the statistical uncertainty of the data points of a typical washout curve with time.  
 (B) Variation in the percentage difference between the exact values and the finite difference values with time.

the washout curve was calculated from

$$\frac{(\text{Standard deviation of count rate}) \times 100}{\text{count rate}}$$

#### 4.5 Rabbit Model

The radiation intensity measured by the detector placed on the sclera is proportional to the concentrations of krypton summated over the field of view of the detector. Since krypton is mainly an emitter of beta particles the concentration at a given distance from the detector has to be corrected for absorption of the beta particles in tissue. Thus solution of the diffusion equation in terms of concentration of krypton within a volume of ocular tissue at successive times allows the decline in radioactivity with time to be predicted.

The rabbit eye, with its circulation limited to a layer of vessels within the choroid running round the whole eye, allows a very simple model to be used for the study of diffusion within ocular tissue. The model is illustrated in figure 4.5. The spherical geometry of the globe has been replaced by a planar geometry. This is a reasonable approximation since the diameter of the eye (12 mm) is very much greater than the maximum range of krypton-85 beta particles (2.8 mm). The values used for the tissue thickness are also shown in figure 4.5. (Davis, 1929; Prince, 1964). The thicknesses used are those of the equatorial region of the eye. The vitreous was assumed to be semi-infinite.

Within each of the ocular tissues the diffusion of krypton is expressed by the differential diffusion equation

$$\frac{\partial C_i}{\partial t} = D_i \frac{\partial^2 C_i}{\partial x^2}$$

each tissue having its appropriate diffusion coefficient. The values of the diffusion and solubility coefficients are also shown in figure 4.5.

Detector	Sclera			Choroid		Retina		Vitreous			
Nodal pt.	1	3	5	7	9	11	13	15	17	19	21
Thickness (cm)		0.024			0.012		0.015		$\infty$		
Diffusion Coefficient ( $\times 10^{-5} \text{cm}^2 \text{s}^{-1}$ )		1.6			0.76		0.80		1.2		
Solubility		0.027			0.076		0.062		0.059		

Figure 4.5 Diffusion model based on the anatomy of the rabbit eye.

The details of the experimental determination of these values are presented in Chapter 6.

Solutions of the partial pressure of krypton were obtained by computation of the finite-difference relations of the differential diffusion equation and boundary conditions (equations 4-15 and 4-16). The computation was performed by an IBM 370/158 computer. The computer program (see appendix 1) allowed:

- (1) calculation of concentration and partial pressure profiles of krypton throughout the various tissues at various times,
- (2) correction of the concentration values for the absorption of the beta particles in tissue at each nodal point,
- (3) introduction of a term simulating the removal of krypton from the choroid by blood flow, and
- (4) summation of the calculated concentration values (corrected for absorption of the beta particles) over the various tissues at each time interval.

The correction for absorption of the beta particles in tissue was determined experimentally (see Chapter 6) for the Geiger-Müller tube used, by observing the change in count rate with increasing absorber thickness. The count rate declined exponentially with increasing thickness. The exponential rate constant was  $19.9 \text{ cm}^{-1}$ .

The simulation of removal of krypton by the choroidal blood flow was achieved by subtracting a known fraction of the concentration values from the concentration, at a fixed number of nodal points ('flow points') in the choroid.

This fraction,  $k$ , is equivalent to the exponential rate constant in equation 2-14 and will be referred to as the blood flow term.

## Chapter 5

### Diffusion of Krypton in Ocular Tissue II Results

#### 5.1 Introduction

In this chapter the predictions of the model described in the previous chapter will be presented. Initially, the predicted variations in partial pressure and in concentration of krypton in ocular tissue will be described for various values of the blood flow term. This will be followed by a comparison between predicted and experimental washout curves. Subsequently, the effects of variation in the blood flow term, and of prolonged arrival of krypton at the eye will be discussed.

Finally, a model based on the anatomy of the baboon eye will be developed and the effect of a retinal circulation on the washout curve investigated.

#### 5.2 Partial Pressure and Concentration Profiles

Profiles of partial pressure and of concentration of krypton within the ocular tissues were determined at various times after time zero. The choroid was assumed to contain three flow points (nodal points 10, 11, and 12); all other nodal points being non-flow points. A uniform partial pressure throughout the three flow points at time zero was chosen as corresponding to the situation existing at the radioactivity peak of the washout curves. Section 5.3 describes in detail the reasons for the choice of these conditions.

Profiles were obtained for various values of the blood flow term. Figure 5.1a shows the partial pressure profiles at 5, 20, 100 and 500 seconds resulting from diffusion alone, i.e. no blood flow in the choroid to remove krypton from the system. As the krypton alone diffuse

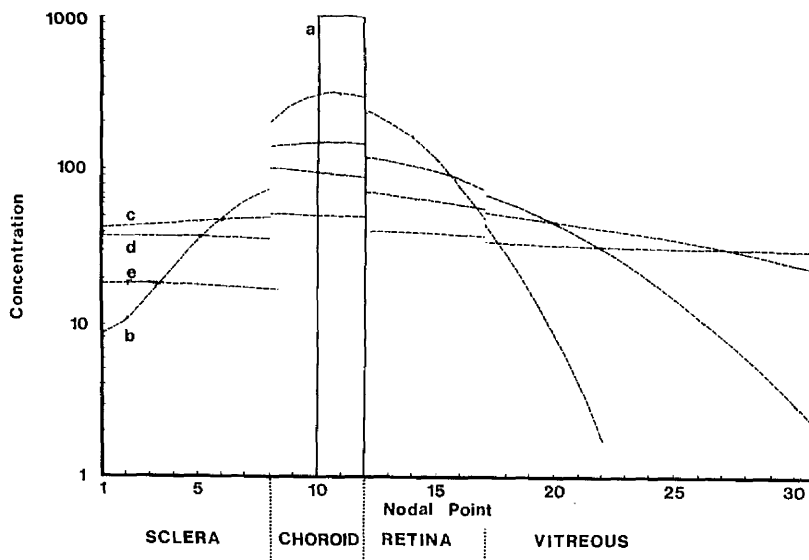
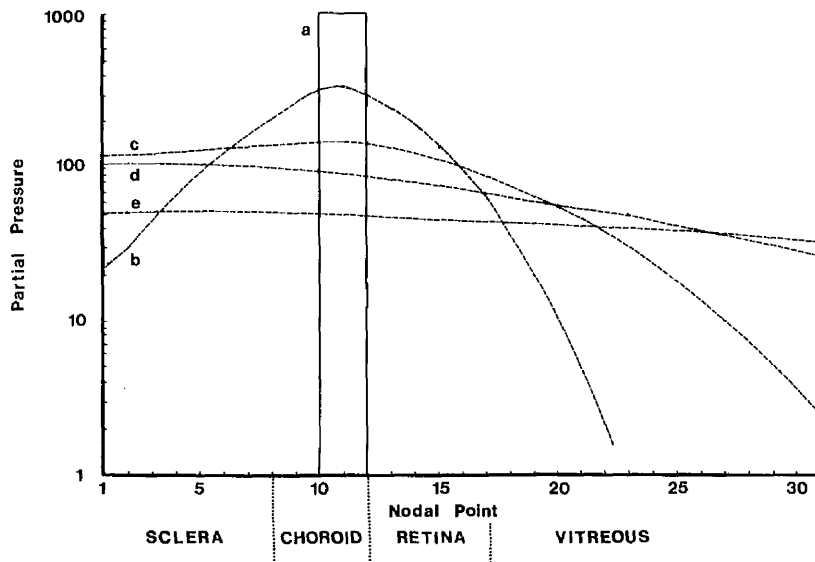


Figure 5.1 Predicted distribution of (A) partial pressure and (B) concentration levels of krypton throughout the ocular tissues resulting from pure diffusion, i.e.  $k=0$ , at (a) zero seconds (initial distribution), (b) 5 seconds, (c) 20 seconds, (d) 100 seconds, and (e) 500 seconds.

from the region of high partial pressure in the choroid into the sclera, retina and vitreous, there is a decrease in the partial pressure levels within the choroid and a corresponding increase in the levels in the other tissues. Thus there is a tendency to equalisation of partial pressure throughout the eye, as would be expected. Figure 5.1b shows the corresponding profiles of the concentration levels of krypton within the various tissues. The concentration profiles have the same basic shape as the partial pressure profiles. The concentration profiles are discontinuous since it is the partial pressure that is continuous across the boundary between tissues with different solubility coefficients and not the concentration. The ratio of the concentration values at the discontinuity at a tissue junction is equal to the inverse ratio of the solubilities.

Figure 5.2a shows the partial pressure profiles at 5, 20, 50 and 100 seconds for the blood flow term,  $k$ , equal to  $0.28 \text{ sec}^{-1}$  (corresponding to a choroidal blood flow of  $1660 \text{ ml}/100\text{g}/\text{min}$ ). Again the profiles indicate the diffusion of krypton from the high partial pressure area in the choroid into the other tissues. However, the removal of krypton by the choroidal blood flow at the three 'flow points' (nodal points 10, 11 and 12) greatly affects the shape of the profiles. At times less than 5 seconds, the partial pressure has a maximum value within the choroid. However, by 20 seconds as a result of (a) diffusion of krypton from the choroid and (b) the removal of krypton at the flow points, the partial pressure within the choroid is lower than that in the surrounding tissue. Thus, preceding 5 seconds there is diffusion of krypton from the choroid into the sclera, retina and vitreous. By 20 seconds, concurrent with the continued diffusion towards the centre of the vitreous, there will be back diffusion from the sclera.

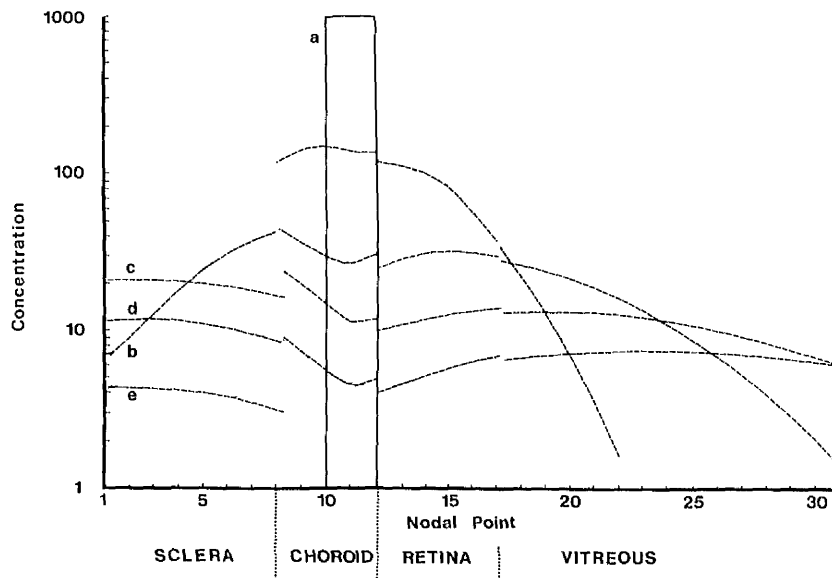
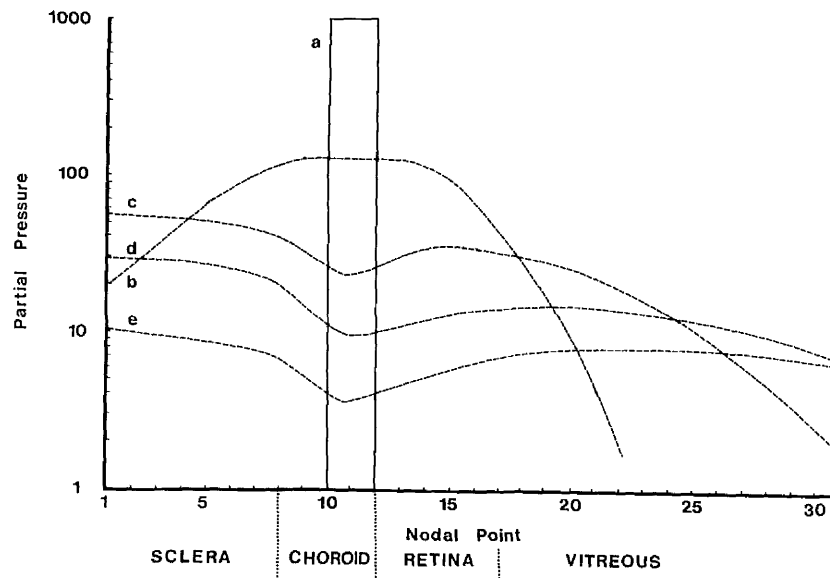


Figure 5.2 Predicted distribution of (A) partial pressure and (B) concentration levels of krypton throughout the ocular tissues for  $k=0.28 \text{ sec}^{-1}$  at (a) zero seconds (initial distribution), (b) 5 seconds, (c) 20 seconds, (d) 50 seconds and (e) 100 seconds.

and retina into the choroid. Figure 5.2a shows the corresponding concentration profiles.

Figures 5.3a,b and 5.4a,b illustrate partial pressure and concentration profiles for a low blood flow term ( $k=0.083 \text{ sec}^{-1}$ , choroidal blood flow = 500ml/100g/min) and for a high blood flow term ( $k = 0.5 \text{ sec}^{-1}$ , choroidal blood flow = 3000 ml/100g/min) respectively. The profiles in these figures illustrate the same basic appearance as those in figure 5.2. In the case of the low blood flow term (figure 5.3) the reduced rate of removal of krypton at the flow points is reflected in the shallowness of the trough in the partial pressure profile within the choroid. The increased removal of krypton occurring with the high blood flow term (figure 5.4) is reflected in the much deeper trough in the partial pressure. In this case the rate of removal of krypton at the flow points is so large that back diffusion into the choroid from the sclera and retina occurs in less than 5 seconds.

### 5.3 Predicted Washout Curves

The radioactivity measured by the detector placed on the sclera is related to the summated concentration values, corrected for absorption of the krypton beta particles, within the field of view of the detector. Predicted washout curves were obtained by repeated summation of the corrected concentration values over all nodal points at time intervals of 0.25 second.

In order to determine the effect of the number of flow points in the choroid, predicted curves were obtained for one flow point (nodal point 12), two flow points (nodal points 11 and 12), three flow points (nodal points 10,11 and 12), four flow points (nodal points 9,10,11 and 12), and five flow points (nodal points 8, 9, 10, 11 and 12) for  $k = 0.28 \text{ sec}^{-1}$ . For all the predicted curves, the

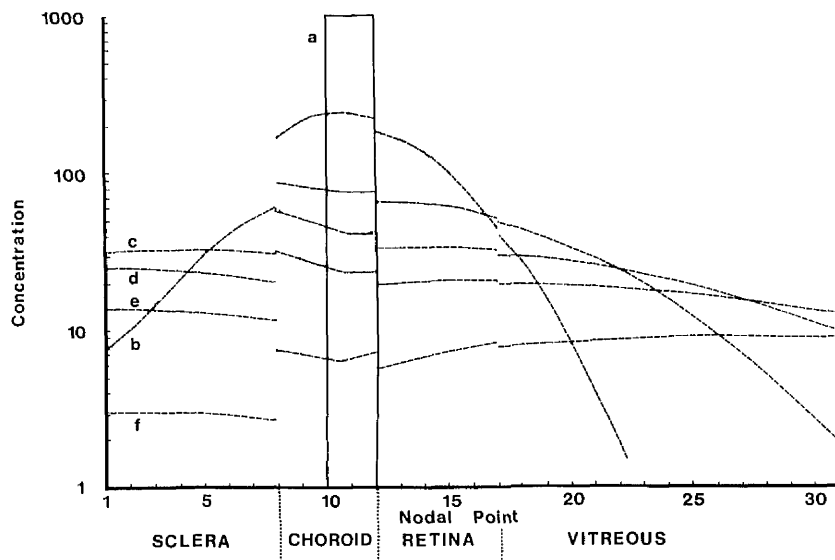
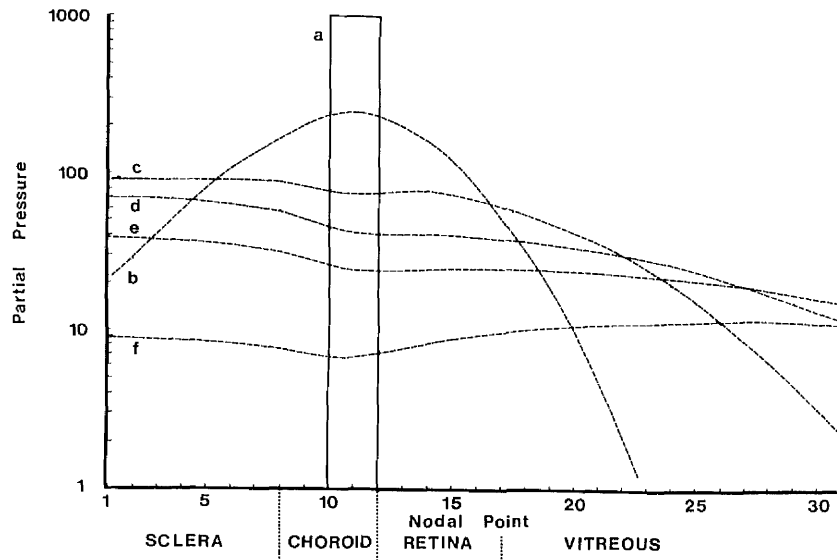


Figure 5.3 Predicted distribution of (A) partial pressure and (B) concentration levels of krypton throughout the ocular tissues for  $k=0.083\text{sec}^{-1}$  at (a) zero seconds (initial distribution), (b) 5 seconds, (c) 20 seconds, (d) 50 seconds, (e) 100 seconds and (f) 250 seconds.

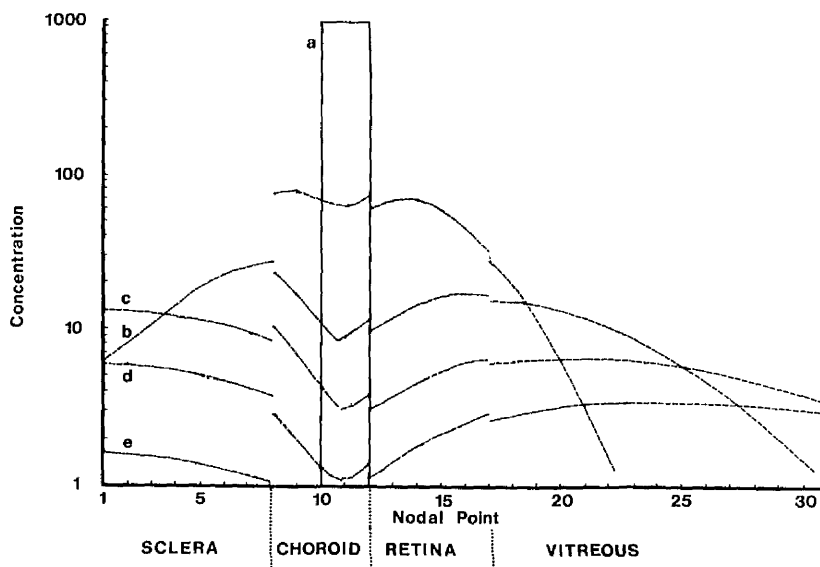
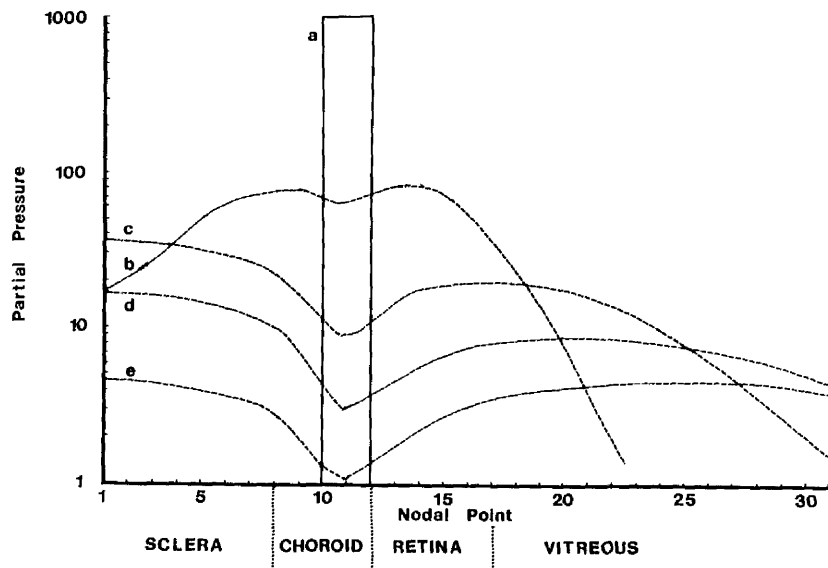


Figure 5.4 Predicted distribution of (A) partial pressure and (B) concentration levels of krypton throughout the ocular tissues for  $k=0.5 \text{ sec}^{-1}$  at (a) zero seconds (initial distribution), (b) 5 seconds, (c) 20 seconds, (d) 50 seconds and (e) 100 seconds.

initial partial pressure levels (at time zero) were taken as constant over the flow points and zero at all other nodal points.

The predicted curves were compared with a corresponding experimental washout curve obtained from the study described in Chapter 3 (figure 5.5a,b). The five predicted curves, corresponding to the different number of flow points, are all characterised by an initial exponential decline. The duration of this initial component of the curve varies between 0.75 second (1 flow point) and 4 seconds (5 flow points). The subsequent decline of the predicted curves varies in magnitude. However, the five curves have a similar shape to that of the experimental washout curve.

The choice of the number of nodal points within the choroid is arbitrary, dependent solely on the conditions described in section 4.3.5 being met. Five nodal points within the choroid were chosen as a compromise between spatial resolution and a practical time interval for iteration. The predicted curves obtained with either one or two flow points, whilst agreeing with the spatial arrangement of the choroidal capillaries, underestimate the duration of the initial exponential component, by comparison with the experimental washout curve. The duration of the initial component of the predicted curves obtained with either three, four or five flow points all agree with the experimental washout curve within statistical accuracy. The predicted curves obtained with either four or five flow points underestimate the count rate at later times (figure 5.5b). The predicted curve with three flow points is in reasonable agreement with the experimental washout curve at all time and for this reason three flow points within the choroid were used in all subsequent studies.

The comparison between the predicted curve with three flow

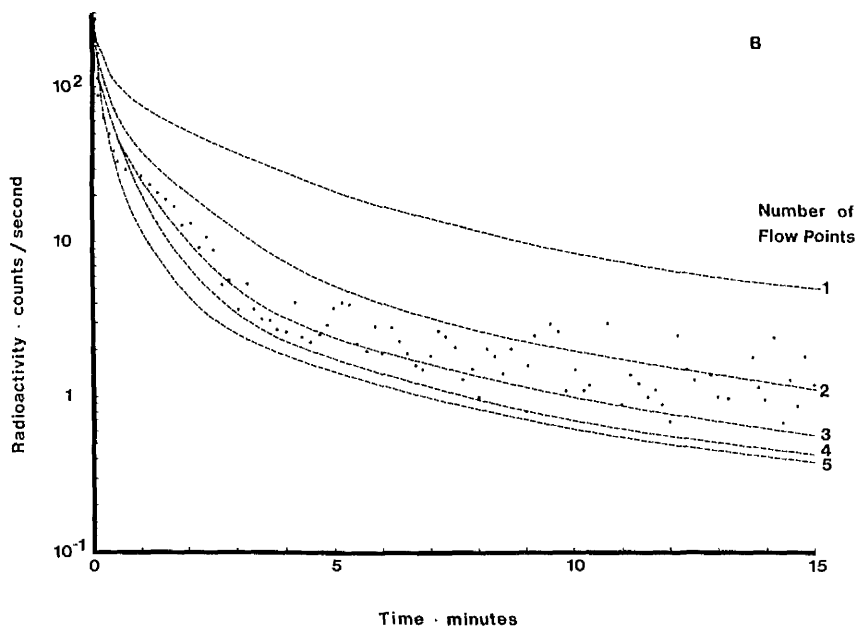
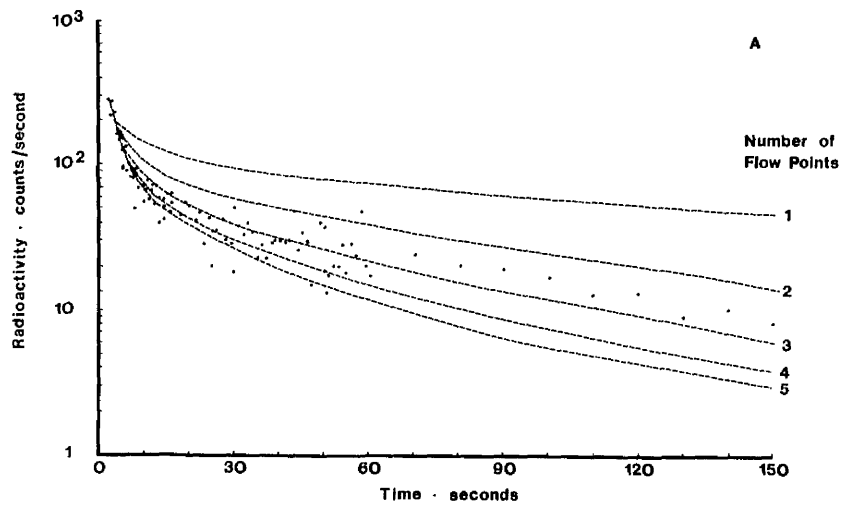


Figure 5.5 Comparison between a series of predicted washout curves having different numbers of flow points ( $k=0.28 \text{ sec}^{-1}$ ) and an experimental washout curve. (A) first 150 seconds (B) first 15 minutes

points and the experimental washout curve is shown more clearly in figure 5.6 a,b. From this comparison the explanation of the complex nature of the washout curve can be obtained. Within the first five seconds the partial pressure is a maximum within the choroid (figure 5.2a) and the removal of krypton by the choroidal blood flow predominates over the diffusion of krypton away from the detector. This is borne out by the fact that the half life of the initial exponential decline of the predicted curve is 2.5 seconds, corresponding to an exponential rate constant of  $0.28 \text{ sec}^{-1}$ . This is equal to the blood flow term introduced into the model, indicating that the half life of the initial slope is a measure of choroidal blood flow. The magnitude of the blood flow is obtained by substituting the half life of the initial slope into equation (2-16).

$$\text{i.e. } F = \frac{69.3 \cdot \lambda}{T_{1/2} \cdot \rho} \quad \text{ml/100g/min.}$$

At times greater than five seconds the maximum of the partial pressure is outwith the choroid. Thus the subsequent decline in radio-activity is due partially to the removal of krypton by the blood flow but also to the diffusion of krypton within the various ocular tissues.

#### 5.4 Variation in Blood Flow Term

In order to determine the range over which the inert gas clearance method accurately measures choroidal blood flow, predicted curves were obtained for values of the blood flow term,  $k$ , within the range  $0 \leq k \leq 0.83$ . These curves were obtained by assuming three flow points in the choroid and assuming that the initial partial pressures at the flow points were the same.

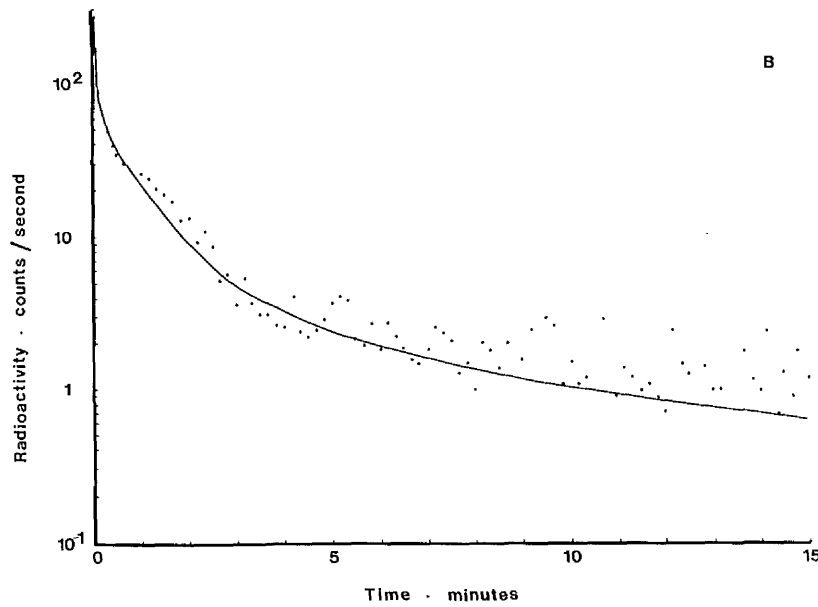
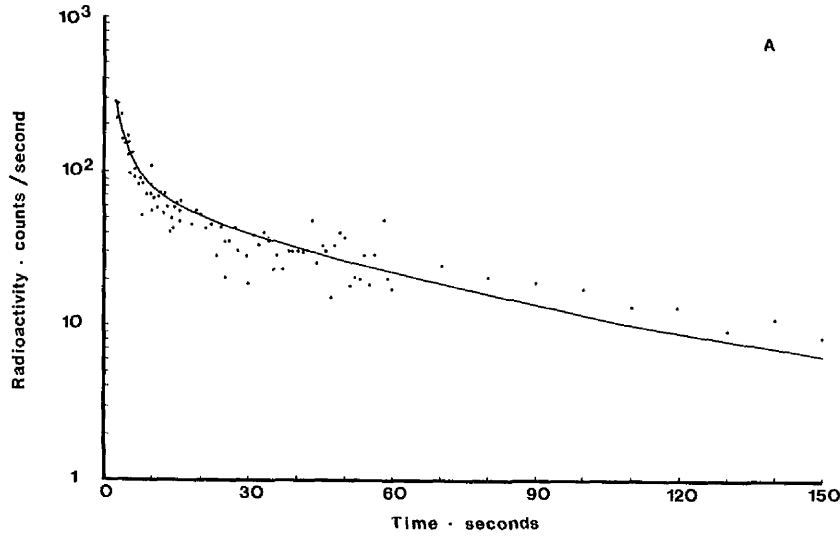


Figure 5.6 Comparison between a predicted washout curve (solid line) with three flow points ( $k=0.28 \text{ sec}^{-1}$ ) and an experimental washout curve (dots).  
 (A) first 150 seconds      (B) first 15 minutes.

The exponential rate constant of the initial decline of the predicted curve was equal to the blood flow term over a range of values of  $k$  between  $0.083$  and  $0.83 \text{ sec}^{-1}$ . This corresponds to a range of choroidal blood flow between  $500$  and  $5000 \text{ ml}/100\text{g}/\text{min}$ . (figure 5.7). Within this range there is good agreement between the predicted curves and the experimental washout curves (figures 5.8, 5.9 and 5.10). The range of choroidal blood flow obtained in the control study (Chapter 3) corresponds to values of  $k$  between  $0.11$  and  $0.24 \text{ sec}^{-1}$ .

For  $k < 0.083 \text{ sec}^{-1}$ , the exponential rate constants of the initial decline of the predicted curves are significantly greater than the corresponding  $k$  values. Thus it would appear that below a choroidal blood flow value of  $500 \text{ ml}/100\text{g}/\text{min}$  (i.e.  $k < 0.083 \text{ sec}^{-1}$ ) the initial slope of the washout curve is not solely dependent on the blood flow but is partially due to diffusion of krypton away from the detector. Figure 5.11 a, b shows the poor correlation between the experimental washout curve with an exponential rate constant of  $0.05 \text{ sec}^{-1}$  ( $T_{1/2}^1 = 14 \text{ secs}$ ) and a predicted washout with  $k = 0.05 \text{ sec}^{-1}$ .

In the situation where only diffusion is occurring (i.e.  $k = 0$ ), the exponential rate constant of the initial decline of the predicted curve is equal to  $0.052 \text{ sec}^{-1}$  (figure 5.12). The decline observed in this situation is due solely to the increase in absorption of the krypton beta particles resulting from the diffusion of krypton out of the choroid into the retina and vitreous which are further from the detector. However, experimental washout curves have been obtained with exponential rate constants less than the theoretical lower limit obtained from the predicted curve with  $k$  equal to zero. One possible explanation of this discrepancy is that in this analysis the arrival of krypton at the choriocapillaris was assumed to be instantaneous. In the

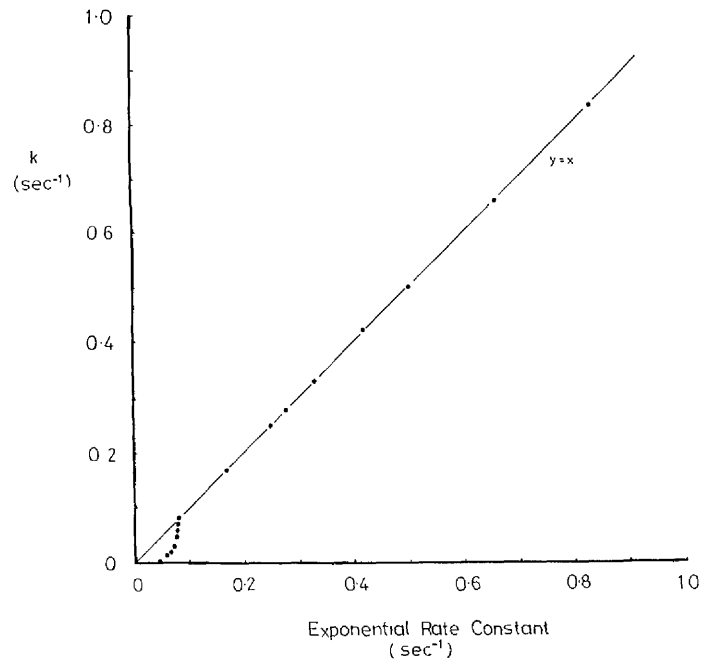


Figure 5.7 Choroidal blood flow term,  $k$ , versus the exponential rate constant of the initial decline of the predicted curve.

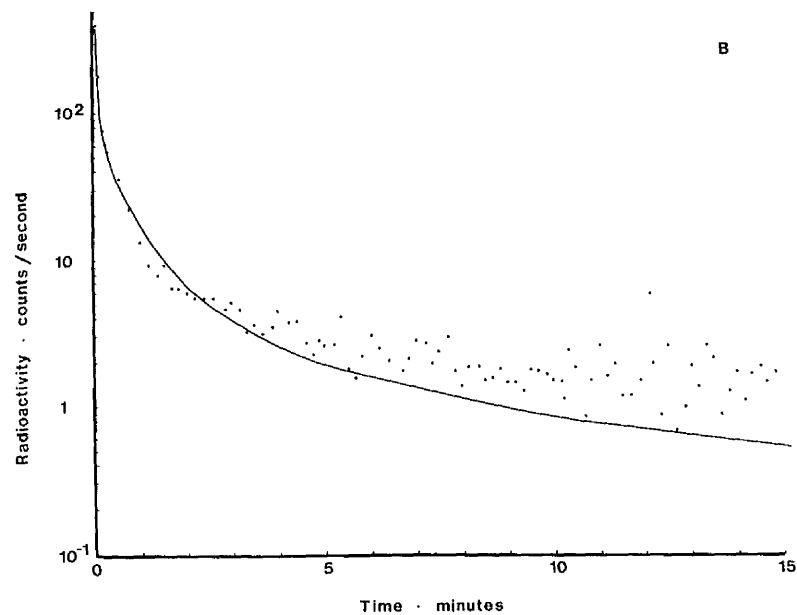
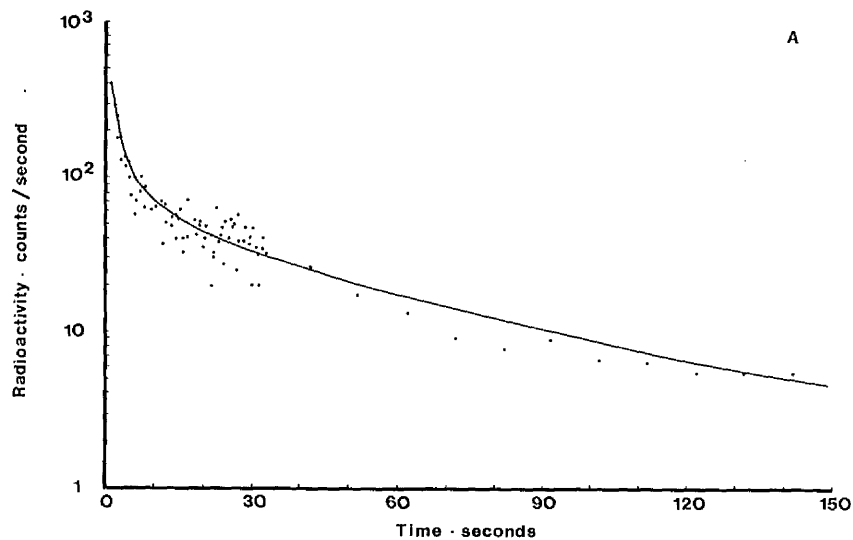


Figure 5.8 Comparison between a predicted washout curve (solid line),  $k=0.41 \text{ sec}^{-1}$ , and a corresponding experimental washout curve (dots).  
 (A) first 150 seconds (B) first 15 minutes.

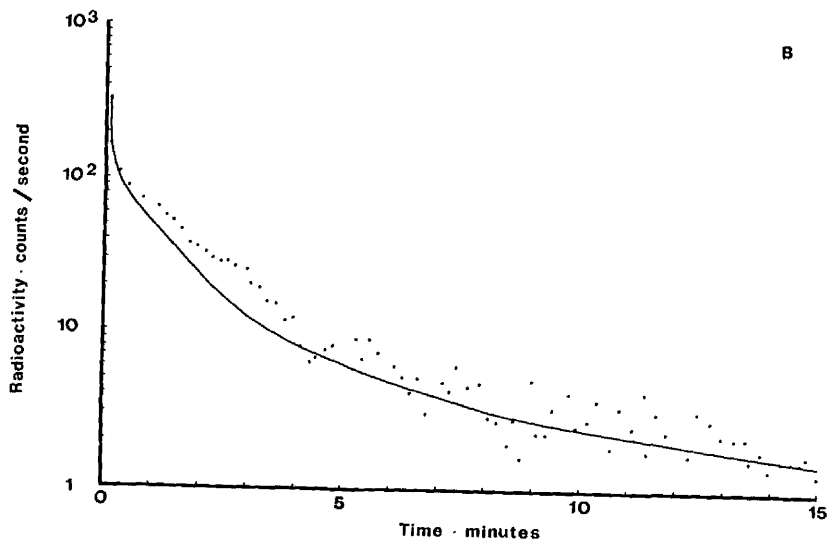
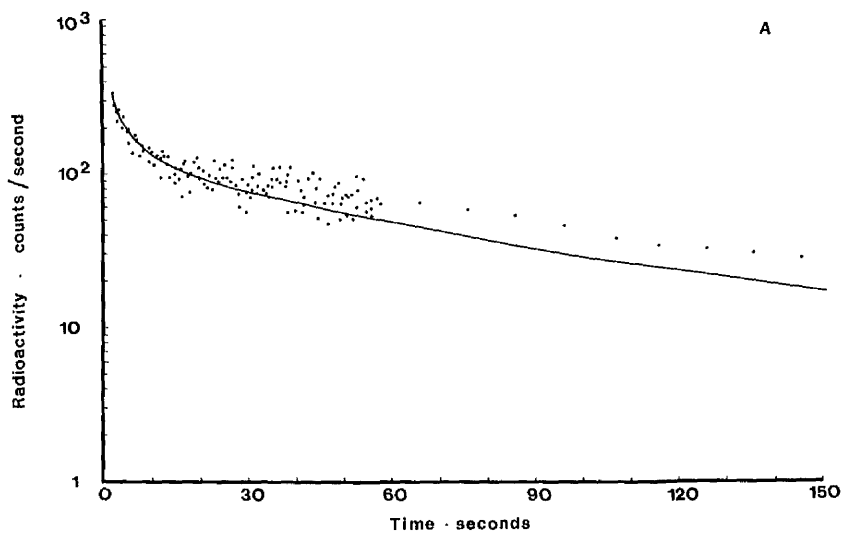


Figure 5.9 Comparison between a predicted washout curve (solid line),  $k=0.17 \text{ sec}^{-1}$ , and a corresponding experimental washout curve (dots).  
 (A) first 150 seconds      (B) first 15 minutes.

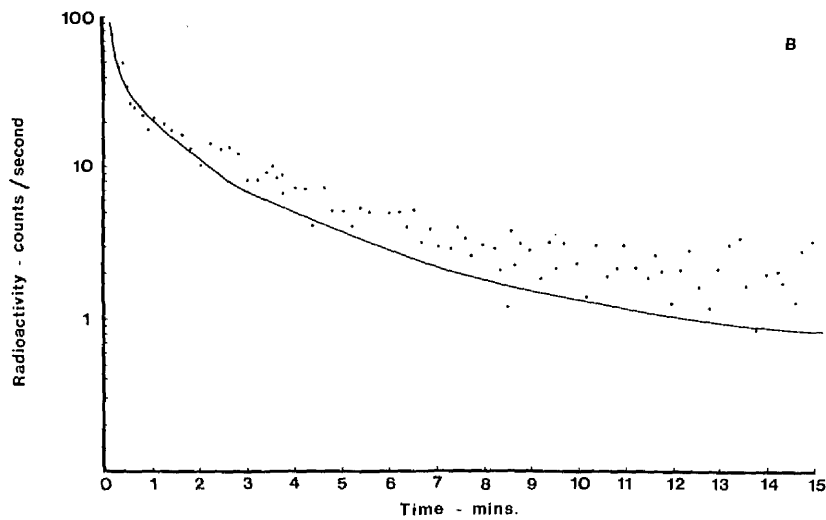
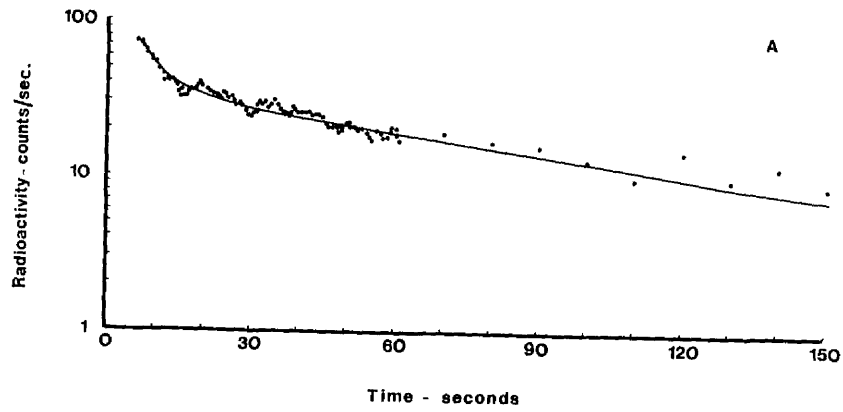


Figure 5.10 Comparison between a predicted washout curve (solid line),  $k=0.083 \text{ sec}^{-1}$ , and a corresponding experimental washout curve (dots).  
 (A) first 150 seconds      (B) first 15 minutes.

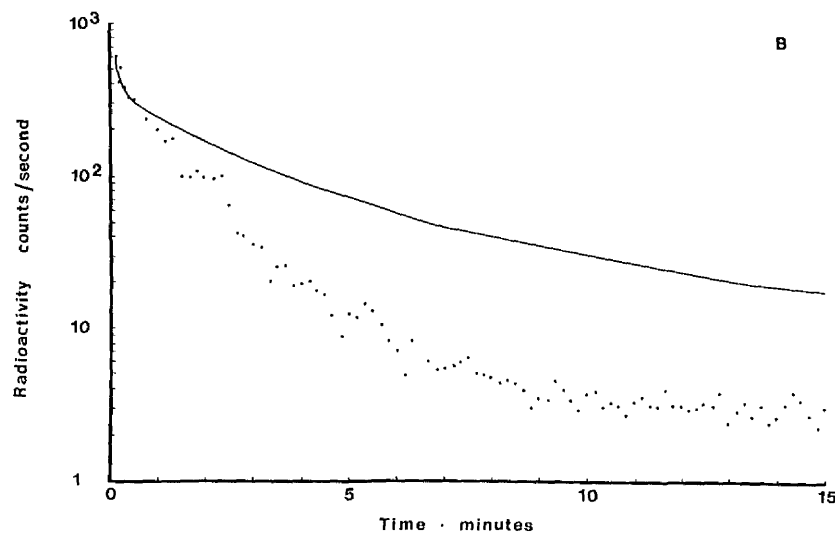
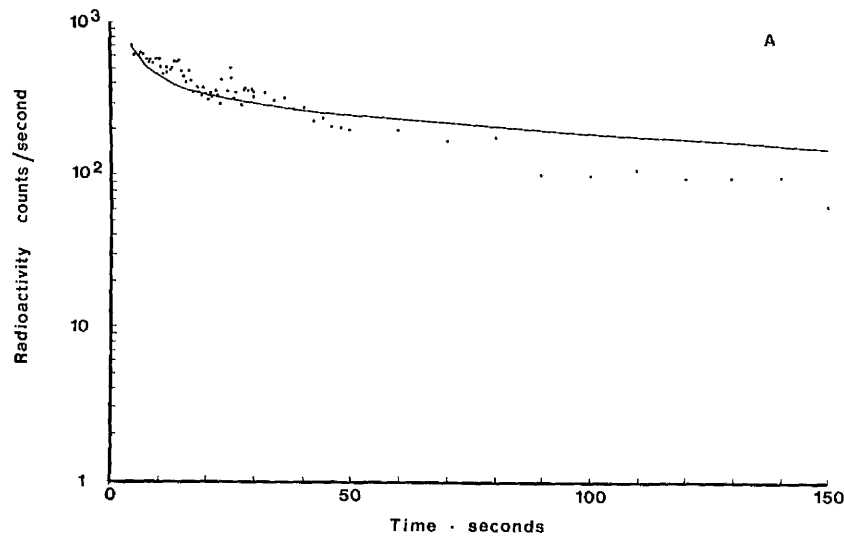


Figure 5.11 Comparison between a predicted washout curve (solid line),  $k = 0.043 \text{ sec}^{-1}$ , and a corresponding experimental washout curve (dots).  
 (A) first 150 seconds      (B) first 15 minutes.

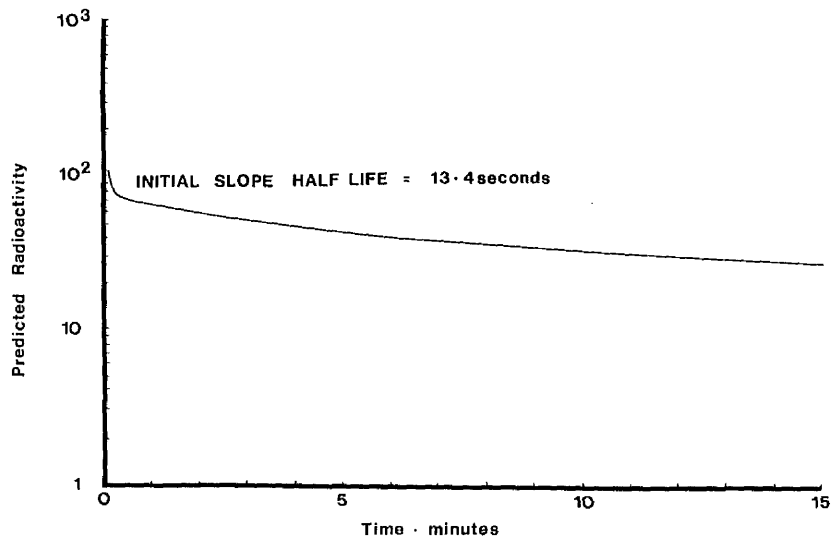


Figure 5.12 Predicted washout curve resulting from diffusion alone, i.e.  $k = 0$ .

next section the effect of prolonged arrival of krypton on the predicted curve will be discussed.

### 5.5 Prolonged Arrival of Krypton

In order to study the effect of prolonged arrival of krypton at the choriocapillaris the input characteristics of the partial pressure were modified. The prolonged arrival of krypton was simulated in the model by maintaining the uniform distribution of partial pressure over the three flow points in the choroid for a fixed time,  $t$ . The effect of prolonged arrival of krypton on the washout curve was studied at values of  $k =$  zero, 0.046, 0.083, 0.17, 0.28, 0.42 and 0.83  $\text{sec}^{-1}$ . For each value of  $k$ , predicted curves were obtained for values of  $t$  between zero (as in previous studies) and five seconds.

In the situation where only diffusion is occurring ( $k$  equal to zero), the effect of increasing  $t$  is to decrease the value of the exponential rate constant (and hence increase the half life) of the initial decline of the predicted curve. At  $t$  equal to zero, corresponding to an instantaneous arrival of krypton, the value of the exponential rate constant was 0.047  $\text{sec}^{-1}$  ( $T_{1/2}^1 = 14.7$  seconds). For  $t = 5$  seconds the value of the exponential rate constant has been reduced to 0.027  $\text{sec}^{-1}$  ( $T_{1/2}^1 = 25.4$  seconds). The first 30 seconds of a log/linear plot, with  $k$  equal to zero, are shown in figure 5.13 for values of  $t =$  zero, 1 second, 3 seconds and 5 seconds. It can be seen from this figure that the prolonged arrival of krypton also has the effect of delaying the peak of the predicted curve.

For  $k = 0.046 \text{ sec}^{-1}$  and  $t = 0$  the situation exists (section 5.4) where the exponential rate constant (equal to 0.03  $\text{sec}^{-1}$ ) of the initial decline is significantly different from  $k$ . As  $t$  increases

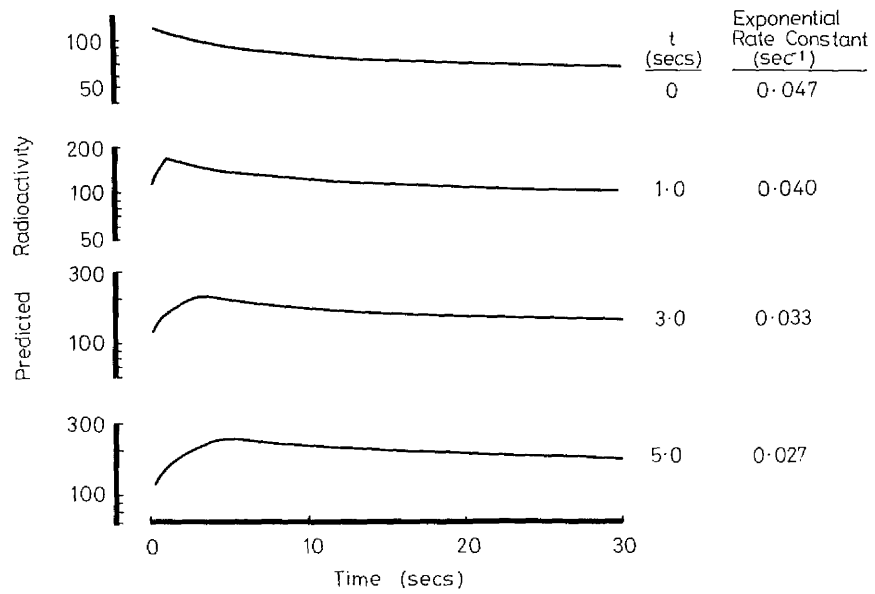


Figure 5.13 The effect of prolonged arrival of krypton at the eye on the predicted washout curve.  $k = 0$

(figure 5.14) the value of the exponential rate constant decreases and for  $t = 4$  seconds the value of the exponential rate constant ( $0.048 \text{ sec}^{-1}$ ) is only slightly greater than  $k$ . At  $t = 5$  seconds the value of the exponential rate constant ( $0.044 \text{ sec}^{-1}$ ) is slightly less than  $k$ .

In the previous study ( $t$  equal to zero) the exponential rate constant of the initial decline of the predicted curve was equal to  $k$  for  $k \geq 0.083 \text{ sec}^{-1}$ . As  $t$  increases the duration of the initial decline decreases. For  $k = 0.083$  and  $0.167 \text{ sec}^{-1}$  (figures 5.15 and 5.16 respectively) the exponential rate constant is equal to  $k$  for  $t \leq 0.5$  second. For  $t > 0.5$  second there is a steady decrease in the values of the exponential rate constants. At  $t = 5$  seconds the values of the rate constants were  $0.055$  and  $0.084 \text{ sec}^{-1}$  respectively.

For  $k = 0.28 \text{ sec}^{-1}$  the exponential rate constant is equal to  $k$  for  $t \leq 0.25$  second. At higher values of  $t$  there is again a steady decrease in the value of the exponential rate constant (figure 5.17).

At very high choroidal blood flows ( $k = 0.417$  and  $k = 0.83 \text{ sec}^{-1}$ ) the exponential rate constant is only equal to  $k$  for  $t$  equal to zero (figures 5.18 and 5.19 respectively).

It is obvious from this study that the prolonged arrival of krypton at the choriocapillaris can affect the relation between the initial slope and the blood flow. An estimate of the duration of the arrival of krypton at the choriocapillaris in the experimental situation was obtained by measuring the time interval,  $T_p$ , between the onset of radioactivity and the peak in radioactivity. This interval was determined in experimental curves with exponential rate constants equal to the blood flow terms used in this study. The values of  $T_p$  are shown in table 5.1. Also shown in this table, for each value of  $k$ , is the maximum time,  $T_e$ , of the peak of the predicted curves for which the exponential rate

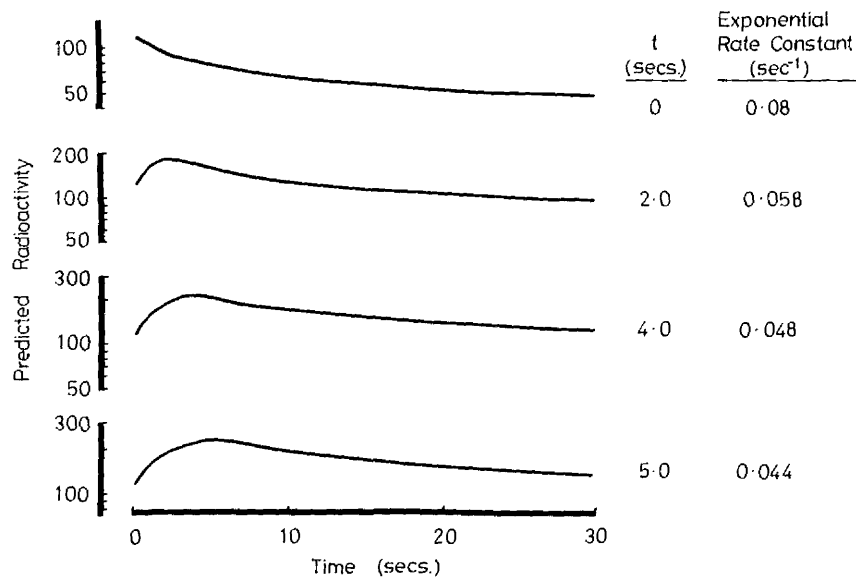


Figure 5.14 The effect of prolonged arrival of krypton at the eye on the predicted washout curve.  $k = 0.046 \text{ sec}^{-1}$ .

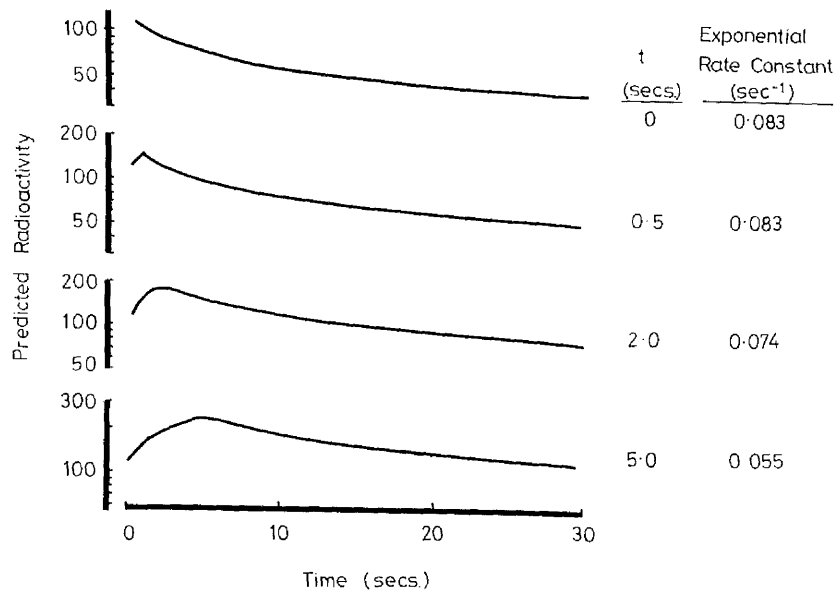


Figure 5.15 The effect of prolonged arrival of krypton at the eye on the predicted washout curve.  $k = 0.083 \text{ sec}^{-1}$ .

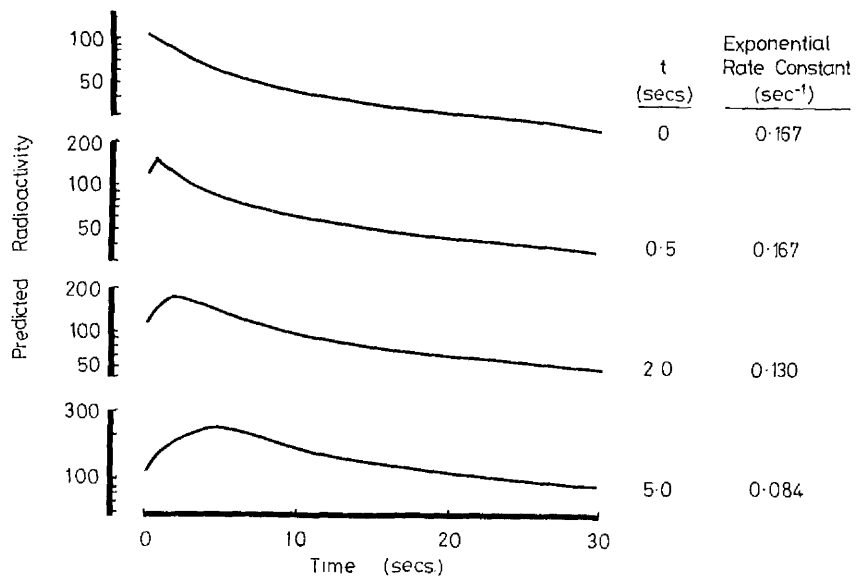


Figure 5.16 The effect of prolonged arrival of krypton at the eye on the predicted washout curve.  $k = 0.167 \text{ sec}^{-1}$ .

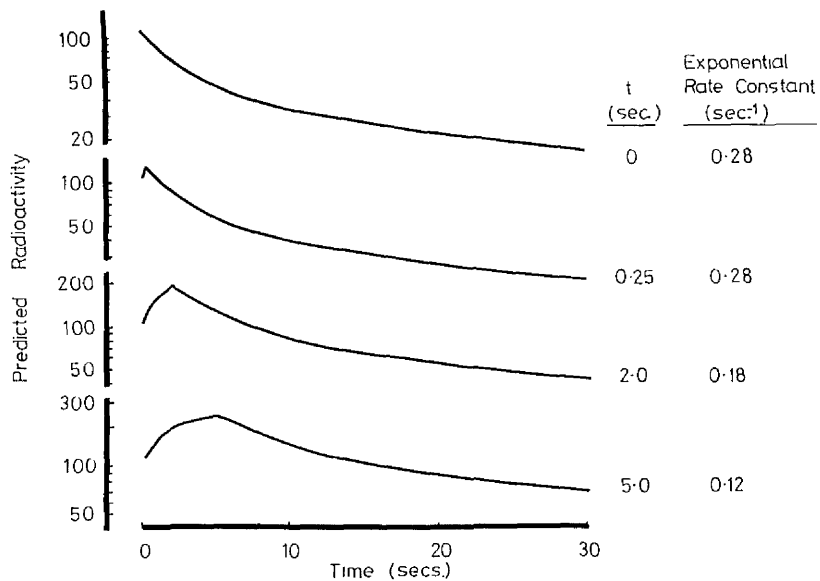


Figure 5.17 The effect of prolonged arrival of krypton at the eye on the predicted washout curve.  $k = 0.28 \text{ sec}^{-1}$ .

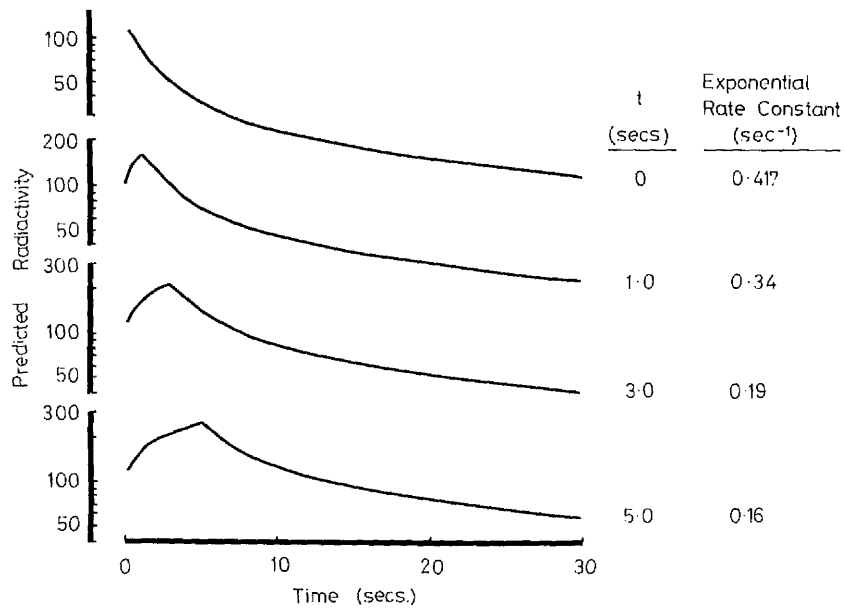


Figure 5.18 The effect of prolonged arrival of krypton at the eye on the predicted washout curve,  $k = 0.417 \text{ sec}^{-1}$ .

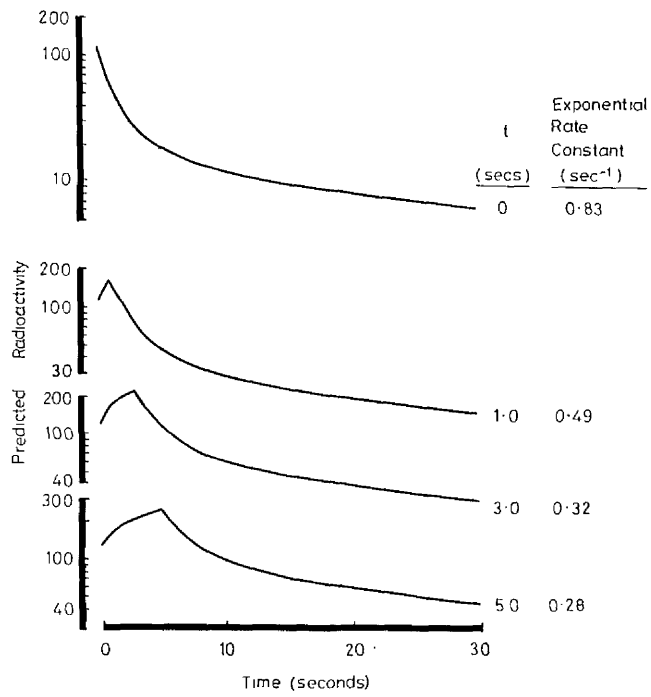


Figure 5.19 The effect of prolonged arrival of krypton at the eye on the predicted washout curve.  $k = 0.83 \text{ sec}^{-1}$ .

Table 5.1 Values of  $T_E$  (mean  $\pm$  I S.D.) and  $T_P$  for various values of the exponential rate constant

EXPONENTIAL RATE CONSTANT (sec. <sup>-1</sup> )	$T_E$ (secs.)	$T_P$ (secs.)
0.0464	3.2 <sup>+</sup> <sub>-</sub> 2.4	-
0.083	2.4 <sup>+</sup> <sub>-</sub> 1.3	0.75
0.17	1.7 <sup>+</sup> <sub>-</sub> 1.0	0.75
0.28	1.2 <sup>+</sup> <sub>-</sub> 0.5	0.5
0.42	1.0 <sup>+</sup> <sub>-</sub> 0.4	0.25
0.83	0.8 <sup>±</sup> 0.4	0.25

constant equals  $k$ .

At all values of the exponential rate constant  $T_E$  is greater than  $T_p$ . This suggests that the relation between the initial slope and the choroidal blood flow may be influenced by the prolonged arrival of krypton at the eye. However, two further factors have to be considered. Firstly, the time constant (0.4 second) of the recording system may give rise to an overestimation of  $T_E$ . Secondly, the fact that a step function, and not a normal distribution, was used in the model for the input characteristic of the arrival of krypton at the choriocapillaris would lead to an underestimation of  $T_p$ . These two factors tend to equalise  $T_E$  and  $T_p$ .

Thus, due to these considerations, within a choroidal blood flow range of 500 - 5000 ml/100g/min ( $0.083 \leq k \leq 0.83$ ), the error in the measured value of the choroidal blood flow will be significantly less than 20%. At choroidal blood flows less than 500 ml/100g/min it is difficult to correlate the exponential rate constant of the initial decline in measured activity with the choroidal blood flow.

The results of this study have explained the existence of experimental washout curves having exponential rate constants smaller than 0.052 (see section 5.4).

## 5.6. Retinal Circulation

### 5.6.1. Introduction

The primate retina is sustained by both the choroidal and retinal circulations. In order to determine the effect of the presence of a retinal circulation on the washout curve the diffusion model was modified to accommodate a retinal circulation. The removal of krypton by the retinal circulation was represented in the model by a term,  $R$ ,

similar to that used for the choroid, namely the subtraction of a fraction of the concentration values at a number of flow points within the retina.

Since later in this section comparison will be made between the predicted washout curves and experimental washout curves obtained from baboon eyes, the values of the thickness of baboon sclera (0.3 mm), choroid (0.12 mm) and retina (0.12 mm) were used in the model. These values were obtained experimentally from fresh tissue using a Mercer dial thickness gauge. The diffusion coefficients and solubilities of krypton in the different rabbit tissues were used. Three flow points were used in both the choroid and retina (figure 5.20) since the retinal circulation is limited to the innermost layers of the retina (nodal points 15,16, 17). O'Day et al (1971) using microspheres obtained a value of 0.036 for the ratio of retinal to choroidal blood flow in monkeys. Alm and Bill (1973) also using microspheres obtained a value of 0.041. Although these values pertain to total blood flow and not capillary blood flow, these results indicate that the retinal blood flow is much smaller than the choroidal blood flow. The effect of variations in both the retinal and choroidal blood flow terms on the washout curve will be described in section 5.6.4.

#### 5.6.2 Partial Pressure Profiles

Figure 5.21 illustrates partial pressure profiles of krypton at 5,20, 100 and 500 seconds resulting from diffusion alone, i.e. no blood flow present. The profiles were obtained for an instantaneous ( $t = 0$ ) arrival of krypton at both sets of flow points. The initial partial pressure at the retinal flow points was taken as equal to that at the choroidal flow points. These profiles are similar to those described previously (figure 5.1a), illustrating the tendency of

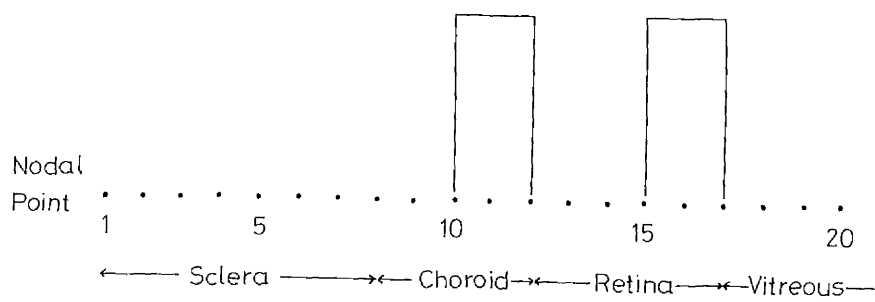


Figure 5.20 Initial uniform distribution of partial pressure of krypton over 3 flow points in the choroid (nodal points 10,11,12) and in the retina (nodal points 15,16,17).

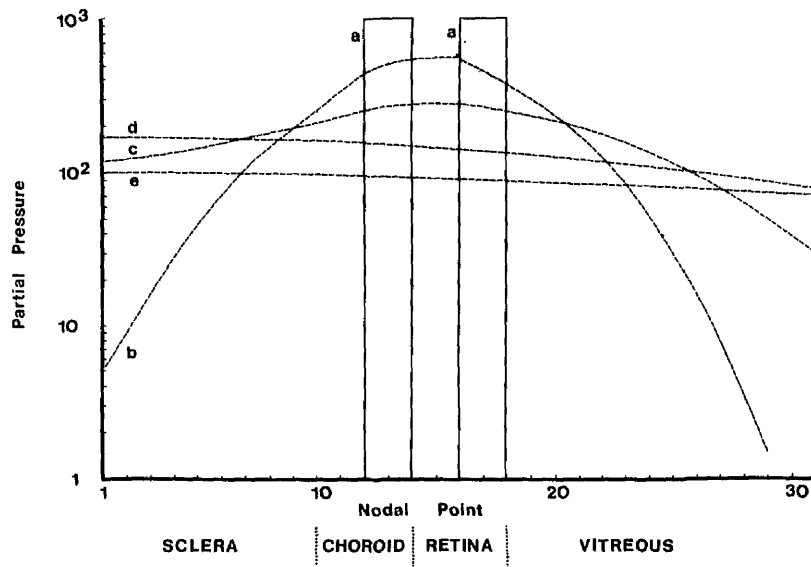


Figure 5.21 Predicted distribution of partial pressure of krypton throughout the ocular tissues resulting from pure diffusion, i.e.  $k_c=0, k_r=0$ , at (a) zero seconds (initial distribution), (b) 5 seconds, (c) 20 seconds, (d) 100 seconds and (e) 500 seconds.

diffusion to equalise the partial pressure throughout the eye.

The effect of removal of krypton by the choroidal and retinal circulations on the partial pressure curves is shown in figure 5.22. These profiles were obtained with a choroidal blood flow term ( $k_c$ ) of  $0.2 \text{ sec}^{-1}$  and a retinal blood flow term ( $k_r$ ) of  $0.02 \text{ sec}^{-1}$ , corresponding to flows of 1200 and 120 ml/100g/min. respectively. These curves illustrate the diffusion of krypton from the high partial pressure areas in the choroid and retina into the other tissues. As was the case with the choroidal circulation present alone, the removal of krypton by the choroidal blood flow results in a trough in the partial pressure. Thus again there will be diffusion at later times from the sclera and retina towards the choroid. The removal of krypton by the retinal blood flow does not result in a second trough in partial pressure and would seem from these results to be overshadowed by (a) diffusion of krypton and (b) the removal of krypton by the choroidal blood flow.

Figure 5.23 shows partial pressure profiles for  $k_c = 0.077 \text{ sec}^{-1}$  and  $k_r = 0.0077 \text{ sec}^{-1}$  (choroidal blood flow = 460 ml/100g/min, retinal blood flow = 46 ml/100g/min). The partial pressure profiles have a similar appearance to those in the previous example with the exception that the trough in the partial pressure curve is much shallower.

### 5.6.3. Predicted Washout Curves

Predicted washout curves were obtained in a similar manner to that described previously. The curves presented in this section were obtained with an initial uniform distribution of partial pressure over both sets of flow points. The affect of different values of initial partial pressure in the choroid and retina and the effect of

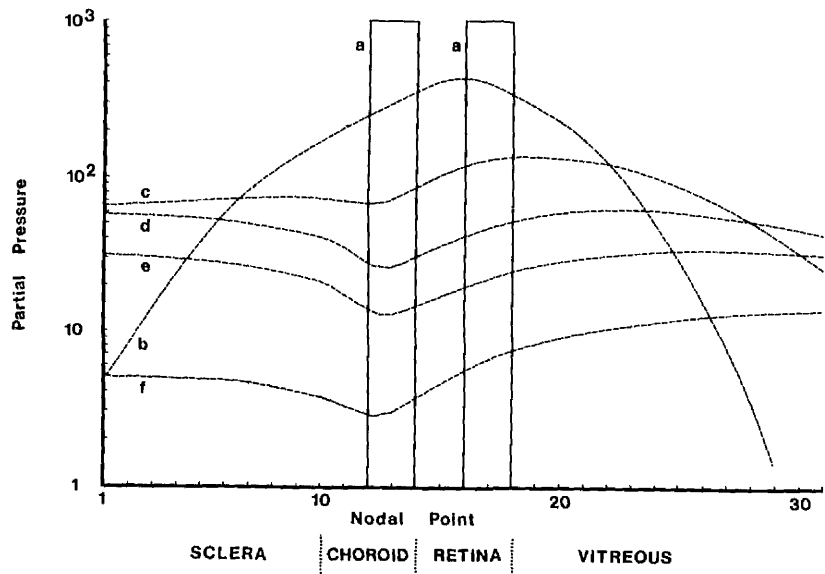


Figure 5.22 Predicted distribution of partial pressure of krypton throughout the ocular tissues for  $k_c = 0.2 \text{ sec}^{-1}$ ,  $k_r = 0.02 \text{ sec}^{-1}$  at (a) zero seconds (initial distribution), (b) 5 seconds, (c) 20 seconds, (d) 50 seconds, (e) 100 seconds and (f) 250 seconds.

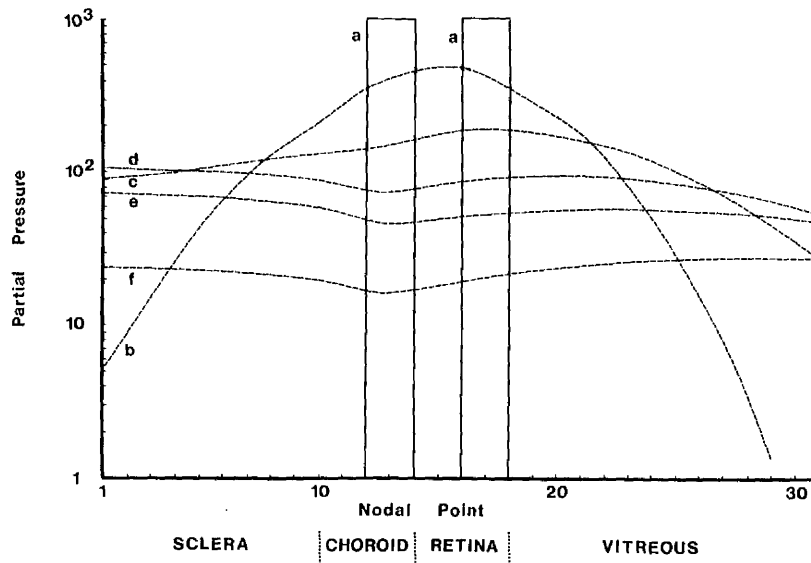


Figure 5.23 Predicted distribution of partial pressure of krypton throughout the ocular tissues for  $k_c = 0.077 \text{ sec}^{-1}$ ,  $k_r = 0.0077 \text{ sec}^{-1}$  at (a) zero seconds (initial distribution), (b) 5 seconds, (c) 20 seconds, (d) 50 seconds, (e) 100 seconds and (f) 250 seconds.

prolonged arrival of krypton at the eye will be discussed in subsequent sections.

Figure 5.24 a,b illustrates a comparison between a predicted curve ( $k_c = 0.077 \text{ sec}^{-1}$ ,  $k_r = 0.0077 \text{ sec}^{-1}$ ) and an experimental washout curve obtained from a baboon's eye (see Chapter 7). The exponential rate constant of the initial decline of the predicted curve is equal to  $k_c$  indicating that, as in the previous study, the initial exponential decline of the washout curve is a measure of choroidal blood flow. The analysis of the subsequent decline of the predicted curve into a second exponential component to correspond to the removal of krypton by the retinal circulation is difficult and results in large errors for any value of the second exponential rate constant. No correlation was obtained between this exponential rate constant and  $k_r$ .

The results of this model imply (at these values of  $k_c$  and  $k_r$ ) that the initial decline of the washout curve for primate eyes is a measure of choroidal blood flow, whereas the subsequent decline is diffusion dependent.

#### 5.6.4. Variation in Blood Flow Terms

In order to determine the effects of variations in choroidal and retinal blood flows on the washout curve, predicted curves were obtained (with similar initial conditions as before) for  $k_c =$  zero, 0.0168, 0.0332, 0.0416, 0.05, 0.0584, 0.0663, 0.085, 0.1, 0.115, 0.133, 0.168 and  $0.2 \text{ sec}^{-1}$ . At each of these values of  $k_c$  a series of predicted curves were obtained for values of  $k_r \leq k_c$ .

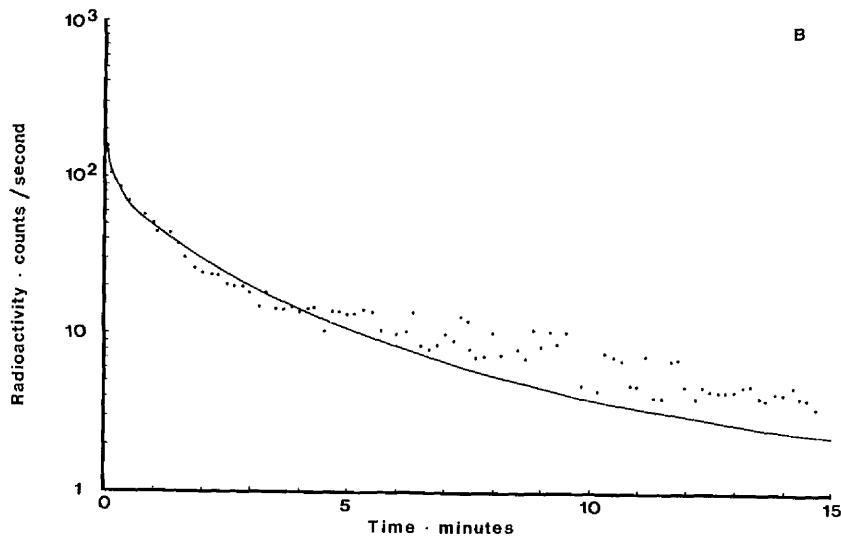
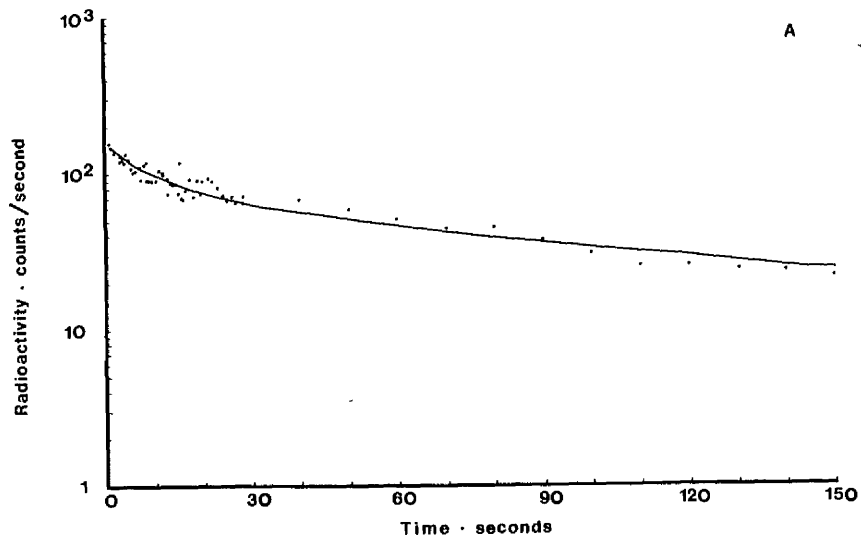


Figure 5.24 Comparison between a predicted washout curve,  $k_c = 0.077 \text{ sec}^{-1}$ ,  $k_r = 0.0077 \text{ sec}^{-1}$ , and a corresponding experimental washout curve.  
 (A) first 150 seconds (B) first 15 minutes

The variation of the exponential rate constant of the initial decline of the predicted curve with the retinal blood flow term,  $k_r$  is shown in figure 5.25 a,b for various values of  $k_c$ . For  $k_c < 0.066 \text{ sec}^{-1}$  the exponential rate constant overestimates  $k_c$  and increases as  $k_r$  increases. For  $0.066 \leq k_c \leq 0.133$  (corresponding to choroidal blood flows between 400 and 800 ml/100g/min) the exponential rate constant is equal to  $k_c$  and within limits is independent of  $k_r$ . At values of  $k_c$  greater than 0.133 the exponential rate constant is again, within limits, independent of  $k_r$ . However, it now underestimates  $k_c$ .

The increase in the exponential rate constant at relatively high values of  $k_r$  can obviously be explained by the increased importance of the retinal circulation. For  $0.066 \leq k_c \leq 0.133$  the ratio  $k_c/k_r$  at the point at which the exponential rate constant no longer equals  $k_c$  varies between 0.09 and 0.4. These values are much greater than the value of 0.04 obtained by O'Day et al (1971) and by Alm and Bill (1973) for the ratio of retinal to choroidal blood flow. Thus for choroidal blood flow values between 400 and 800 ml/100g/min the model suggests that within physiological limits of retinal blood flow the initial slope of the washout curve is dependent solely on the choroidal blood flow.

The relation between the exponential rate constant and  $k_c$  is shown more clearly in figures 5.26 and 5.27. In figure 5.26  $k_c$  is compared with the exponential rate constant. The horizontal bars indicate the range of values of the exponential rate constant at a given value of  $k_c$  obtained by varying  $k_r$  within the range  $0 \leq k_r \leq k_c$ . Figure 5.27 is a similar graph of  $k_c$  against exponential rate constant. The points on this graph were obtained with  $k_r = 0.1 \times k_c$ .

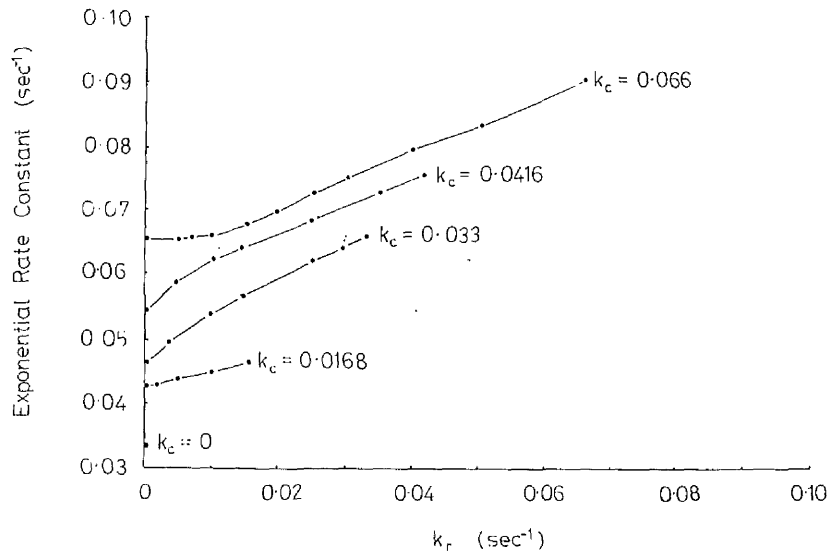
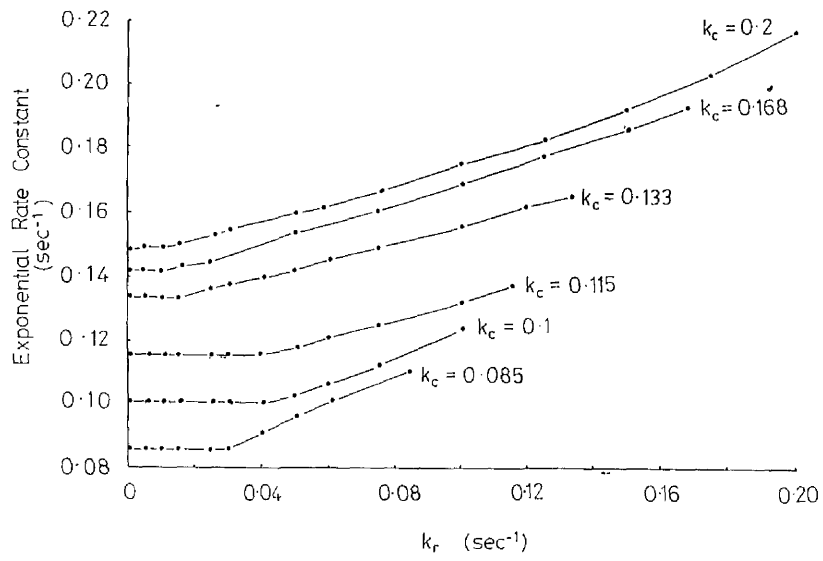


Figure 5.25 Exponential rate constant of the initial decline of the predicted curve versus retinal blood flow term,  $k_r$ , at various values of the choroidal blood flow term,  $k_c$ .

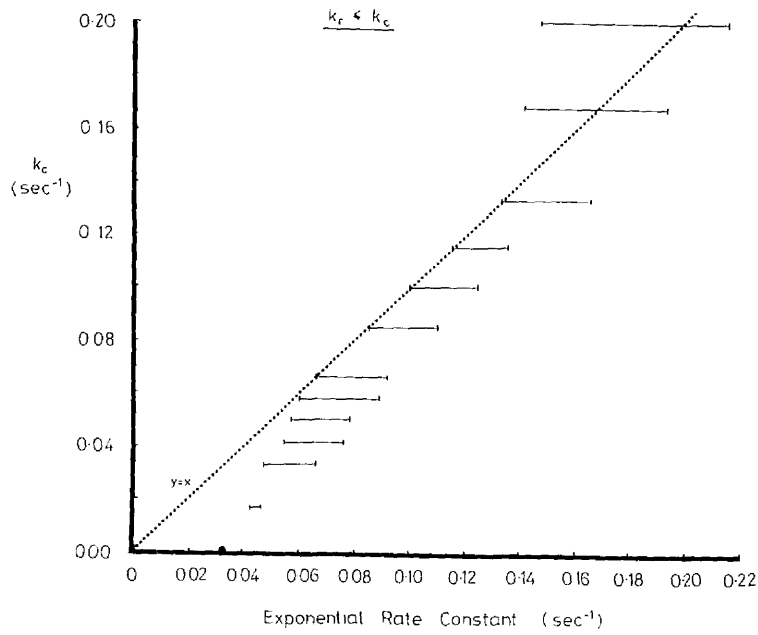


Figure 5.26 Exponential rate constant of the initial decline of the predicted curve versus choroidal blood flow term,  $k_r < k_c$

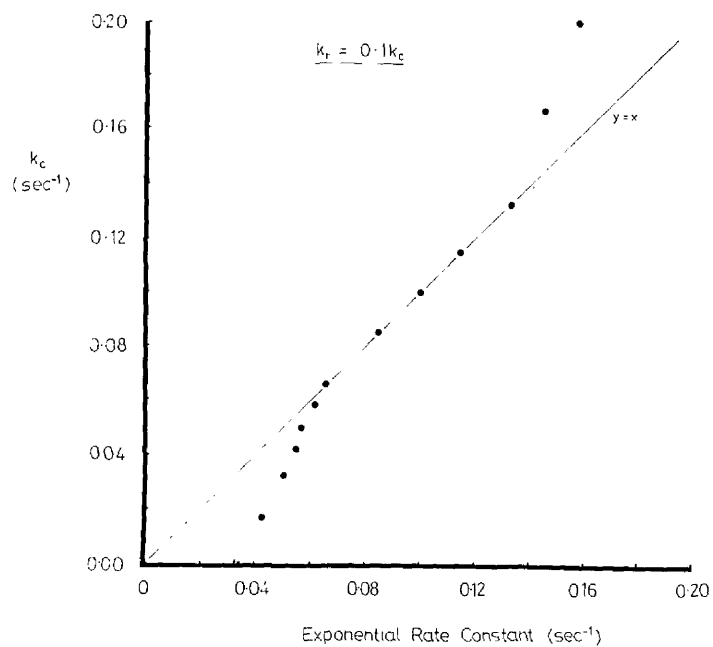


Figure 5.27 Exponential rate constant of the initial decline of the predicted curve versus choroidal blood flow term,  $k_c$ .  $k_r = 0.1k_c$

There are two differences between this graph and the corresponding one for the rabbit model (figure 5.7). At low levels of  $k_c$  the exponential rate constant no longer equals  $k_c$ . In the previous case in which only choroidal circulation was included this lower limit occurred at  $k = 0.083 \text{ sec}^{-1}$  (choroidal blood flow = 500 ml/100g/min). In the situation with the dual circulation, this lower limit occurred at  $k_c = 0.066 \text{ sec}^{-1}$  (choroidal blood flow = 400 ml/100g/min).

The fact that the exponential rate constant is greater than  $k_c$  at low levels of  $k_c$  is attributable to the increased contribution from the diffusion of krypton from the choroid into the retina. Where circulation is assumed in both the choroid and the retina the initial partial pressure gradient between the two is reduced and diffusion effects are small initially.

The other major difference between the two models occurs at high values of  $k_c$ . Whereas in the purely choroidal circulation model there was no upper limit, in the case of the dual circulation model when  $k_c$  is greater than  $0.133 \text{ sec}^{-1}$  the exponential rate constant underestimates  $k_c$ . This was thought to be due to diffusion of krypton from the retina into the choroid. Initially the partial pressures at the choroidal and retinal flow points are equal. After the first removal of krypton by the circulations the partial pressure will be lower in the choroid than in the retina. Thus at high choroidal blood flows there will be a significant partial pressure difference between the choroid and retina resulting in the diffusion of krypton from the retina into the choroid. This effect will tend to increase the count rate and hence reduce the slope of the washout curve.

### 5.6.5. Partial Pressure Variation

In order to determine whether or not the differences between the two models was due to the existence of a region of high partial pressure in the retina predicted curves were obtained for  $k_c = 0.033 \text{ sec}^{-1}$ , ( $k_r = 0.0033 \text{ sec}^{-1}$ ),  $k_c = 0.1 \text{ sec}^{-1}$ , ( $k_r = 0.01 \text{ sec}^{-1}$ ), and  $k_c = 0.2 \text{ sec}^{-1}$ , ( $k_r = 0.02 \text{ sec}^{-1}$ ) at partial pressure ratios (retina/choroid) of 1, 0.75, 0.5, 0.25, 0.1 and 0.05. For all three values of  $k_c$  reduction of the partial pressure ratio resulted in an increase in the exponential rate constant (figure 5-28) confirming the previous explanation for the difference between the two models.

### 5.6.6. Prolonged Arrival of Krypton

The effect of prolonged arrival of krypton at the eye was studied for three sets of blood flow terms in a similar manner to that described in section 5.5.

The prolonged arrival of krypton (i.e. increasing  $t$ ) had a similar effect in the dual circulation model as that in the purely choroidal circulation model. For  $k_c = 0.033 \text{ sec}^{-1}$  ( $k_r = 0.0033 \text{ sec}^{-1}$ ) there was a steady decrease in the value of the exponential rate constant from  $0.0485 \text{ sec}^{-1}$  at  $t = 0$  to  $0.0208 \text{ sec}^{-1}$  at  $t = 5$  seconds (figure 5.29).

For  $k_c = 0.1 \text{ sec}^{-1}$  ( $k_r = 0.01 \text{ sec}^{-1}$ ) the exponential rate constant equalled  $k_c$  for  $t \leq 0.25$  second. Above this value there was a steady decrease in the exponential rate constant.

At high values of  $k_c$  ( $k_c = 0.2 \text{ sec}^{-1}$ ,  $k_r = 0.02 \text{ sec}^{-1}$ ) there was also a steady decrease in the value of the exponential rate

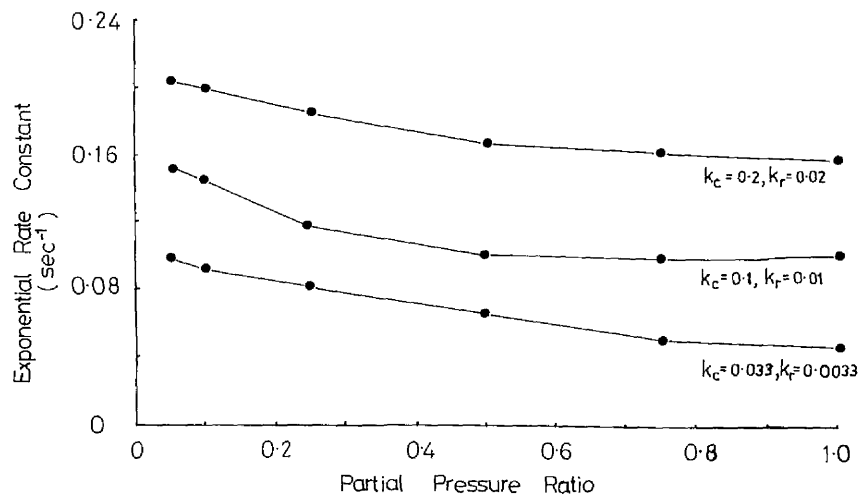


Figure 5.28 Exponential rate constant of the initial decline of the predicted curve versus the initial partial pressure ratio of krypton in the retina and choroid.

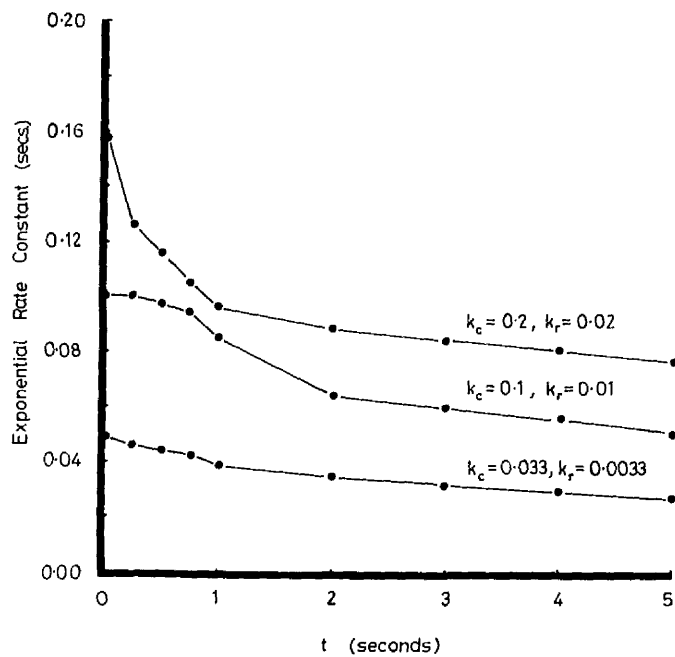


Figure 5.29 The effect of prolonged arrival of krypton at the eye. Exponential rate constant of the initial decline of the predicted curve versus 't'.

constant as  $t$  increases.

The results of this study, as before, indicate that the prolonged arrival of krypton at the eye could affect the relation between the initial decline in radioactivity and the choroidal blood flow. However, as was the case in the rabbit model, the assumption of a step function for the arrival of krypton at the eye is unrealistic. Thus, in practice, the error in the choroidal blood flow measurement is difficult to estimate but will be of the same order as in the rabbit model, i.e.  $< 20\%$ .

## 5.7 Discussion

The four major limitations of the diffusion model are:

- (1) diffusion was only considered in one dimension,
- (2) the boundary between the sclera and the detector was assumed to be impervious,
- (3) the values of the solubility and diffusion coefficients were obtained by in vitro methods,
- (4) the approximation method of obtaining solutions of the partial differential diffusion equations.

The errors resulting from the use of the finite-difference method has been shown to be much smaller than the statistical accuracy of the data points of the washout curve (section 4.4) and can therefore be ignored.

The first two limitations are inherent in the simplification of the anatomy of the eye into a practical model for the solution of the differential diffusion equation. The eye with its specialised anatomy is more amenable to this treatment than any other organ. The assumption of an impervious boundary between the sclera and the detector arose from the difficulty in deciding the physical nature of

the junction. Since the concentration of krypton at this junction is relatively small (figure 5.2b) any error arising from the assumption will be small.

The details of the experimental determinations of the solubility and diffusion coefficients are described in Chapter 6. In the present study only bulk diffusion of krypton in tissue has been considered. No attempt has been made to account for intra and extracellular diffusion. There have been widely conflicting reports concerning the magnitude of the diffusion coefficient of substances within cells. Several studies have yielded values of the order of  $10^{-5} \text{ cm}^2 \text{ sec}^{-1}$  (Ling, Ochensfeld and Karreman, 1967; Bunch and Kallsen, 1969; Kushmerick and Podolsky, 1969) whereas other studies have yielded values of  $10^{-7}$  to  $10^{-10} \text{ cm}^2 \text{ sec}^{-1}$  (Dick, 1959, Fenichel and Horowitz, 1963; Hills, 1967). If Hills' results are true then intracellular diffusion rates would be several orders of magnitude less than extracellular rates. Evans, Busuttill, Gillespie and Unsworth (1974) have reviewed these studies and from their own investigations have concluded that the diffusion coefficient of xenon in cytoplasm must be greater than  $2.2 \times 10^{-8} \text{ cm}^2 \text{ sec}^{-1}$ , several orders of magnitude greater than that obtained by Hills.

Despite these limitations this study of diffusion of krypton in ocular tissue has provided an explanation for the complex nature of the washout curve. The detailed results of the model have shown that for choroidal blood flow values above 500 ml/100g/min in the rabbit the initial slope of the washout curve is a measure of choroidal blood flow. In the case of the baboon it has been shown that, within a physiological range of retinal blood flow, the initial slope of the washout curve is related to the choroidal blood flow for blood flow values within the range 400 to 600 ml/100g/min. No correlation was evident between any

later slope and retinal blood flow.

In both the rabbit and baboon the lower limit to the relation between the initial slope and the choroidal blood flow arises from the increased contribution to the clearance from diffusion of krypton away from the detector. In the rabbit no upper limit is indicated by the model. In practice the upper limit arises when the initial exponential slope is of the same order as that observed during the passage of a non-diffusible indicator. This sets an upper limit of about 6000 ml/100g/min. In the baboon the model indicated that the presence of a retinal circulation gives rise to an upper limit at 800 ml/100g/min.

The results of the studies on the effect of prolonged arrival of krypton at the eye indicate that this factor does have an effect on the relation between initial slope and choroidal blood flow. In the experimental situation it is difficult to measure the duration of the arrival of krypton at the eye. Thus the error arising from this effect is difficult to estimate but will be significantly less than 20%.

The thickness of the various tissues in the human eyewall are different from those of the baboon. As a preliminary investigation into the effect of tissue thickness on the washout curve, predicted washout curves were obtained for  $k_0 = 0.033, 0.1$  and  $0.2 \text{ sec}^{-1}$  for different thicknesses of the ocular tissues. Three sets of values of thickness of the sclera, choroid and retina were used corresponding to anterior, equatorial and posterior regions of the human eye. These values were taken from Logan, Alvarado and Weddell (1971) and are shown in table 5.2. The values of the exponential rate constants obtained

Table 5.2 Variation in thickness of the sclera, choroid and retina of the human eye

Region	Thickness (cm)		
	Sclera	Choroid	Retina
Anterior	0.06	0.015	0.010
Equatorial	0.05	0.010	0.018
Posterior	0.10	0.022	0.056

from these predicted curves are shown in table 5.3.

For  $k_c = 0.1 \text{ sec}^{-1}$  the exponential rate constant for the initial slope of the predicted curve equals  $k_c$  for each of the three regions. For  $k_c = 0.033 \text{ sec}^{-1}$  the exponential rate constants differ slightly and all overestimate  $k_c$ . For  $k_c = 0.2 \text{ sec}^{-1}$  all three values again differ, each underestimating  $k_c$ . These results indicate that the inert gas clearance method will give an estimate of choroidal blood flow through the human eye. However, the range of blood flow over which the method gives a true measure of blood flow will depend on the region of the eye under study. Similar studies as those described in this chapter will be undertaken to investigate this in detail, the results of which are outwith the scope of this thesis.

Table 5.3 The effect of changes in eyewall thickness on the exponential rate constant of the initial decline of predicted curve for three values of the choroidal blood flow term,  $k_c$ .

Region	Exponential Rate Constant ( $\text{sec}^{-1}$ )		
	$k_c = 0.033$	$k_c = 0.1$	$k_c = 0.2$
Anterior	0.050	0.1	0.144
Equatorial	0.049	0.1	0.133
Posterior	0.062	0.1	0.151

## Chapter 6

### Measurement of Linear Absorption Coefficient, Solubility and Diffusion Coefficients

#### 6.1 Introduction

This chapter presents the experimental procedures and results of measurements of the constants used in the model described earlier. These are:-

- (1) the correction term for the absorption of the krypton beta particles in tissue (the linear absorption coefficient),
- (2) the solubility of krypton in ocular tissue and in blood, and
- (3) the diffusion coefficient of krypton in ocular tissue.

#### 6.2 Measurement of Linear Absorption Coefficient

##### 6.2.1 Introduction

The count rate measured by a detector from a source of beta particles declines exponentially as the thickness of absorbing material between the detector and source is increased, provided the thickness of the absorber is less than the maximum range of the beta particles (Hine and Brownell, 1958). For a given thickness of absorber, the count rate,  $I$ , is given by:

$$I = I_0 \cdot e^{-\mu \cdot x} \quad (6-1)$$

$$\text{or } I = I_0 \cdot e^{-\mu_m \cdot m_x} \quad (6-2)$$

where  $I_0$  = the count rate with absorber absent,

$x$  = the thickness of absorber in cm.,

$m_x$  = the thickness of absorber in mg/cm<sup>2</sup>,

$\mu$  = the linear absorption coefficient (cm<sup>-1</sup>), and

$\mu_m$  = the mass absorption coefficient (cm<sup>2</sup> mg<sup>-1</sup>).

The linear absorption coefficient is related to the mass absorption coefficient by the expression:

$$\mu = p \cdot \mu_m \quad (6-3)$$

where  $p$  = the density of the material ( $\text{mg}/\text{cm}^3$ ).

For a given beta energy the mass absorption coefficient is to a good approximation independent of the absorber material. Thus the linear absorption coefficient of tissue can be calculated from the mass absorption coefficient in other materials e.g. aluminium ( $p = 2620 \text{ mg}/\text{cm}^3$ ) and melinex ( $p = 1510 \text{ mg}/\text{cm}^3$ ).

Since,

$$\mu_m(\text{tissue}) = \mu_m(\text{aluminium}) = \mu_m(\text{melinex})$$

$$\mu(\text{tissue}) = p(\text{tissue}) \cdot \mu_m(\text{aluminium})$$

(6-4)

$$= p(\text{tissue}) \cdot \mu_m(\text{melinex})$$

The density of tissue was assumed to be  $1000 \text{ mg}/\text{cm}^3$ .

### 6.2.2 Method

The mass absorption coefficient of aluminium and melinex were obtained by placing known thicknesses of the material between the Geiger - Muller tube and a krypton source (figure 6.1) and noting the change in count rate. The thickness of material (in  $\mu\text{m}$ ) was determined using a Mercer dial thickness gauge. This was converted to  $\text{mg}/\text{cm}^2$  by the relation

$$m_x = p \cdot x$$

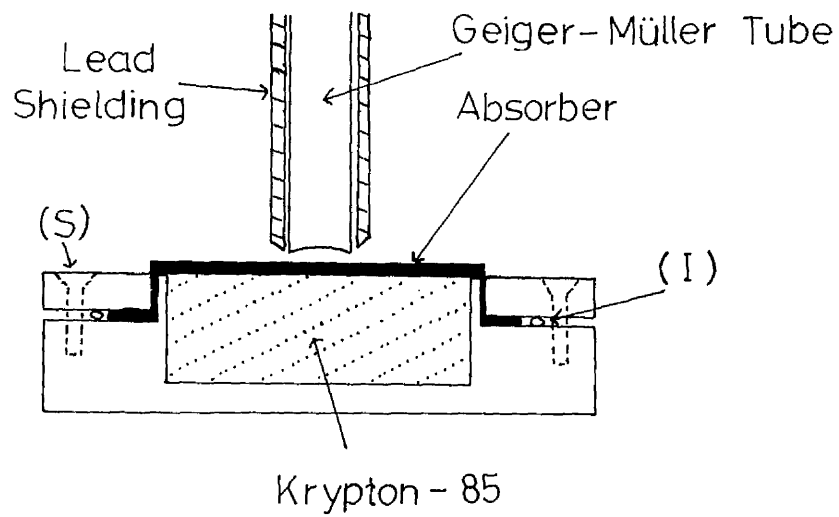


Figure 6.1 Apparatus for measurement of absorption coefficient.  
(I) Indium seal (S) Clamping screw

### 6.2.3 Results

The decline in detected radioactivity with increasing thickness of aluminium and of melinex is shown in figures 6.2 and 6.3 respectively. The graph of count rate on a logarithmic scale against absorber thickness on a linear scale (figure 6.4) was linear for both aluminium and melinex ( $r = 0.999$  and  $r = 0.998$  respectively). The mass absorption coefficients obtained from the graphs were

$$\begin{aligned} \mu_m (\text{aluminium}) &= 0.0206 \text{ cm}^2/\text{mg} \\ \text{and } \mu_m (\text{melinex}) &= 0.0191 \text{ cm}^2/\text{mg}. \end{aligned}$$

Application of equation (6-4) to these values results in values of 20.6 and 19.1  $\text{cm}^{-1}$  for the linear absorption coefficient in tissue.

Substitution of the mean value ( $19.9 \text{ cm}^{-1}$ ) for the linear absorption coefficient into equation (6-1), with  $I_0 = 1$ , gives the correction factor for absorption of the beta particles in tissue to be applied to the concentration values at the nodal points.

$$\text{i.e. correction factor} = e^{-19.9 x} \quad (6-5)$$

where  $x$  = distance (cm) from the detector.

## 6.3 Measurement of solubility of krypton

### 6.3.1 Introduction

The solubility of a gas in a liquid can be expressed in several ways (Kety, 1951).

- (1) The Huenen solubility coefficient, defined as the amount of gas ( $\text{cm}^3$ ) at STPD, taken up by 1 gm of liquid.

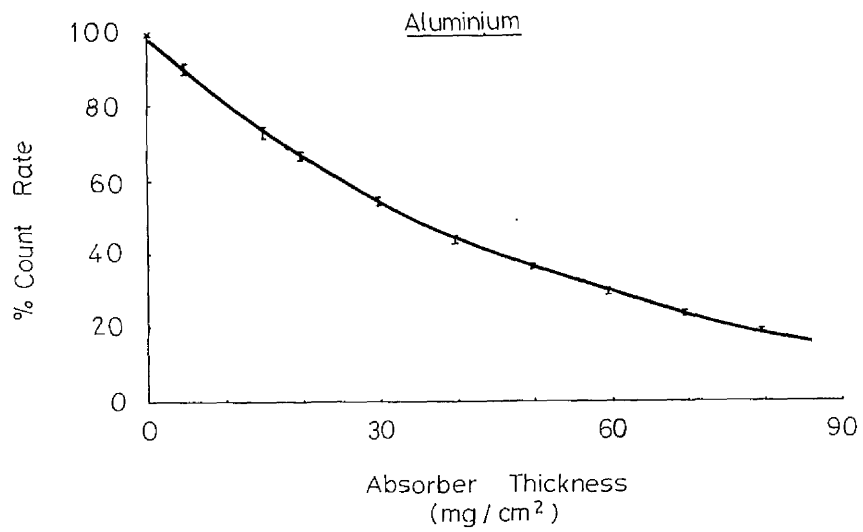


Figure 6.2 Radioactivity versus absorber thickness.  
Aluminium.

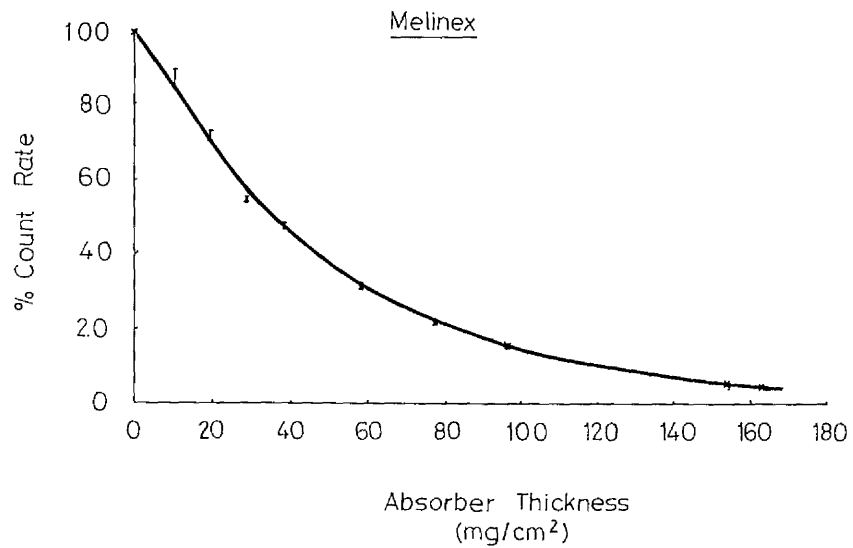


Figure 6.3 Radioactivity versus absorber thickness.  
Melinex.

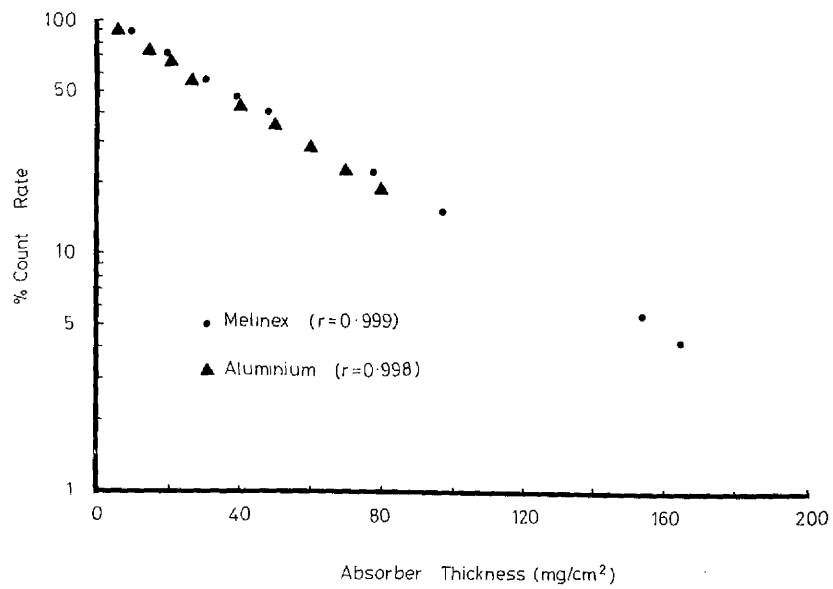


Figure 6.4 Radioactivity (logarithmic scale) versus absorber thickness (linear scale).

- (2) The Bunsen solubility coefficient, defined as the amount of gas ( $\text{cm}^3$ ) at STPD taken up by 1 ml of the liquid at the temperature observed.
- (3) The Ostwald solubility coefficient, defined as the amount of gas ( $\text{cm}^3$ ) at ambient conditions taken up by 1 ml of the liquid at the temperature observed.

The solubility coefficients are related by the equation

$$\lambda = \beta \cdot (1 + \alpha \cdot t) \delta_t = \beta_1 \cdot (1 + \alpha \cdot t)$$

where  $\lambda$  = Ostwald solubility coefficient,

$\beta$  = Kuenen solubility coefficient,

$\beta_1$  = Bunsen solubility coefficient,

$\alpha$  = expansion coefficient for gas =  $1/273$ , and

$\delta_t$  = density of solution at  $t^\circ\text{C}$ .

### 6.3.2 Method (liquid samples)

The Ostwald solubility coefficient was determined for water, rabbit vitreous, whole blood, plasma and erythrocytes. Approximately 1 ml of the liquid sample was placed in a glass vial (volume 3.6ml) and equilibrated at  $37^\circ\text{C}$  with approximately  $3\mu\text{Ci}$  of krypton - 85. Measurements were made at various equilibration periods between 0.5 and 24 hours.

Heparinized arterial blood samples were obtained from rabbits prior to death. This blood was used for the measurements on whole blood, erythrocytes and plasma. The plasma was separated by spinning the blood in a centrifuge at 3000 rpm for 20 minutes.

The total radioactivity,  $A_1$ , in the vial was determined by counting the 0.51 Mev  $\gamma$ -emission (see Table 3.1) in a well scintillation counter (NE 5502/8622). At the end of the equilibration period a fraction of the sample (approximately 0.4ml) was pipetted into a second vial and the radioactivity,  $A_2$ , determined as before.

The transfer of only a fraction of the sample avoided the transfer of radioactive gas. The time taken for the transfer of the sample between the vials varied between 10 and 30 seconds. The volumes of liquid equilibrated and transferred were obtained by weighing; the volumes being obtained from previously determined graphs of weight of sample versus volume of sample (figure 6.5).

The Ostwald solubility coefficient,  $\lambda$ , is equivalent to

$$\lambda = \frac{\text{radioactivity/ml of liquid}}{\text{radioactivity/ml of air}}$$

In terms of the measured quantities:

$$\lambda = \frac{A_2 / V_c}{(A_1 - (A_2 \cdot V_e / V_c)) / (V_v - V_e)}$$

$$\lambda = \frac{A_2 (V_v - V_e)}{A_1 \cdot V_c - A_2 \cdot V_e}$$

where  $\lambda$  = solubility coefficient,

$A_1$  = radioactivity in first vial (gas + sample),

$A_2$  = radioactivity in second vial (sample),

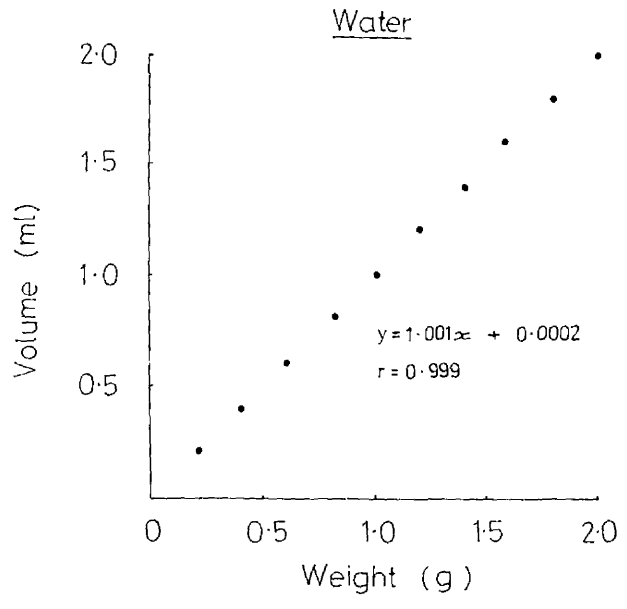
$V_v$  = volume of first vial (ml),

$V_e$  = volume of liquid equilibrated (ml), and

$V_c$  = volume of liquid transferred (ml).

This method is similar in many respects to that employed by Ladefoged and Anderson (1967). One difference is that Ladefoged and Anderson used rubber-capped vials and transferred the liquid sample by connecting the two vials with a needle. In this study the glass vials were sealed by heat.

(a)



(b)

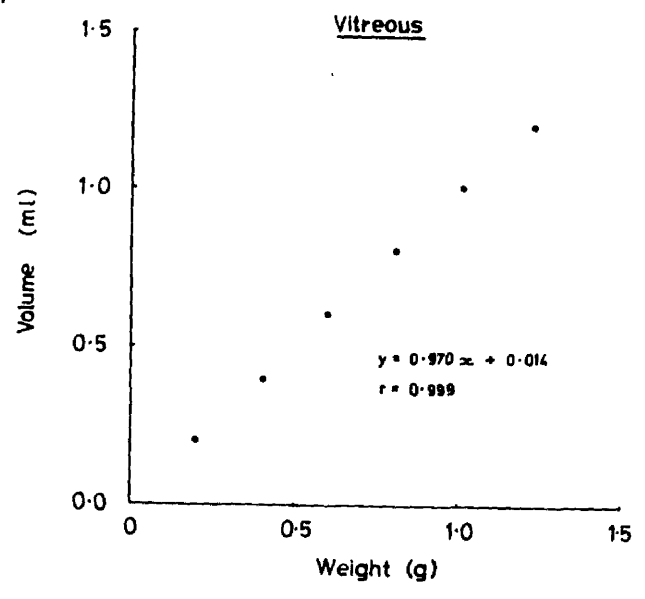
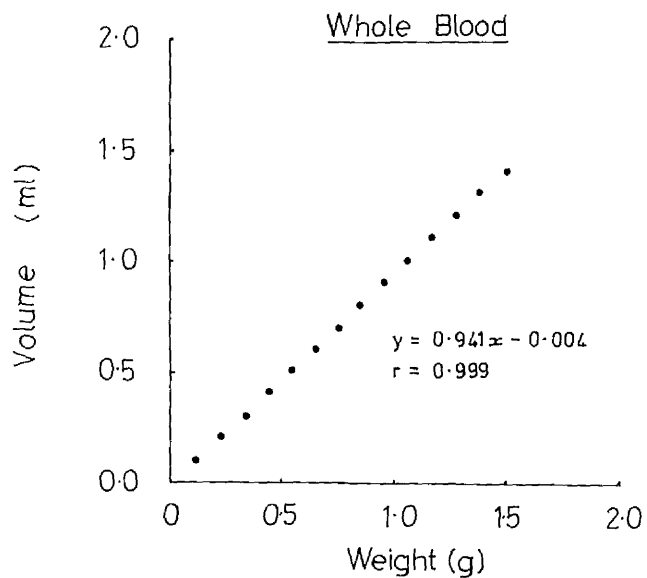


Figure 6.5 Volume of sample versus weight of sample.  
(a) water (b) vitreous

(c)



(d)

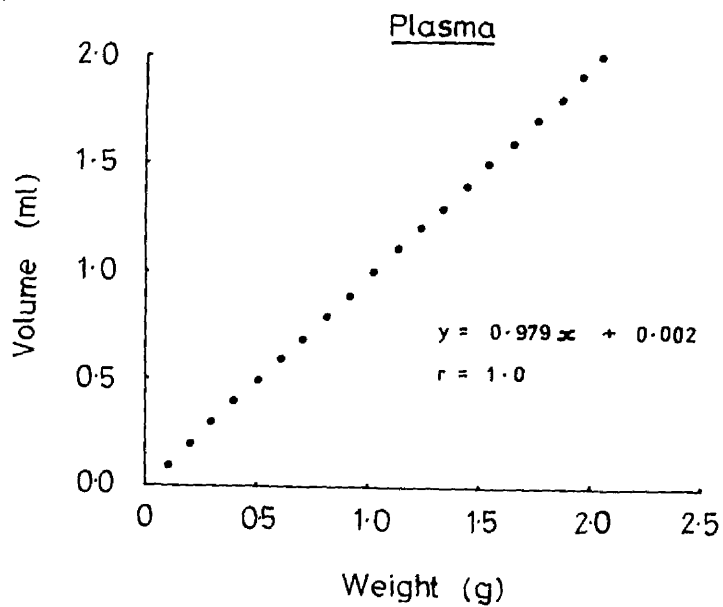


Figure 6.5 Volume of sample versus weight of sample.  
(c) whole blood (d) plasma

(e)

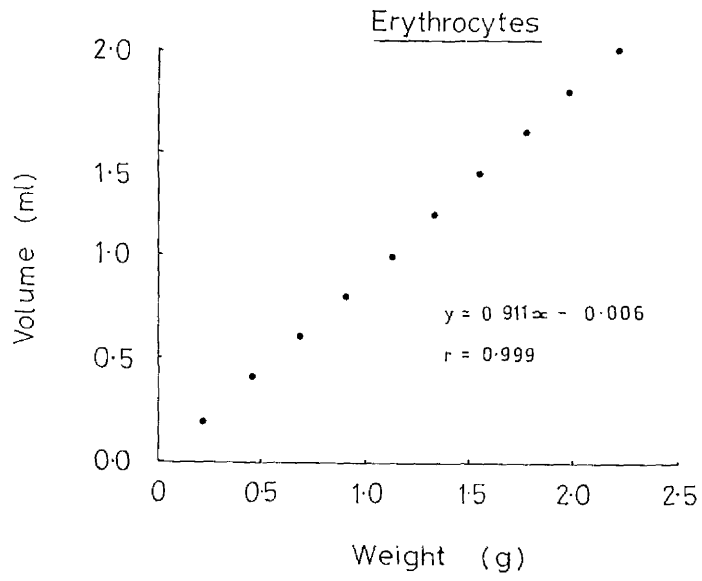


Figure 6.5 Volume of sample versus weight of sample.  
(e) erythrocytes.

This method overcomes any difficulties arising from absorption of krypton by the rubber caps of the vials.

### 6.3.3 Method (tissue samples)

Tissue samples were obtained from freshly enucleated rabbits' eyes which were dissected under saline to give samples of sclera, choroid and retina weighing between 0.015g and 0.05g. The solubility coefficient was determined by a method similar to that employed in the liquid samples. The transfer of the tissue between the two vials at the end of the equilibration period was achieved by introducing approximately 1 ml of saline into the first vial displacing the gas above the tissue. The tissue and a fraction of the saline were then pipetted into the second vial. This avoided transfer of the radioactive gas.

For the tissue samples the solubility coefficient,  $\lambda$ , was taken as:-

$$\lambda = \frac{\text{radioactivity/g of tissue}}{\text{radioactivity/ml of air}} \quad (6-9)$$

In terms of the measured quantities:

$$\lambda = \frac{A_2/m}{(A_1 - A_2)/(V_v - V_T)}$$

$$\lambda = \frac{A_2 (V_v - V_T)}{m (A_1 - A_2)} \quad (6-10)$$

where  $\lambda$  = solubility coefficient,

$A_1$  = radioactivity in first vial (gas + sample),

$A_2$  = radioactivity in second vial (sample),

$m$  = mass of the tissue sample (g),

$V_v$  = volume of the vial (ml), and

$V_T$  = volume of the tissue sample (ml).

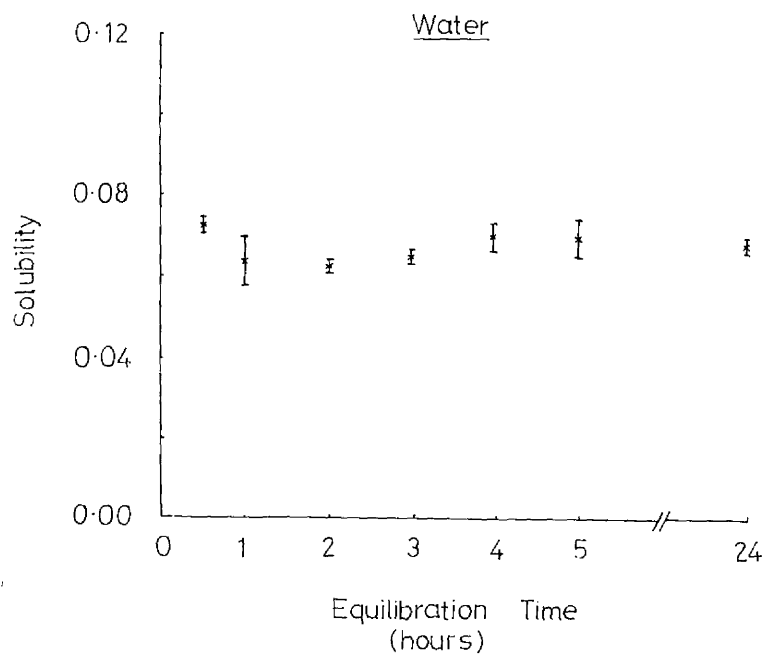


Figure 6.6 Solubility of krypton in water versus equilibration time.

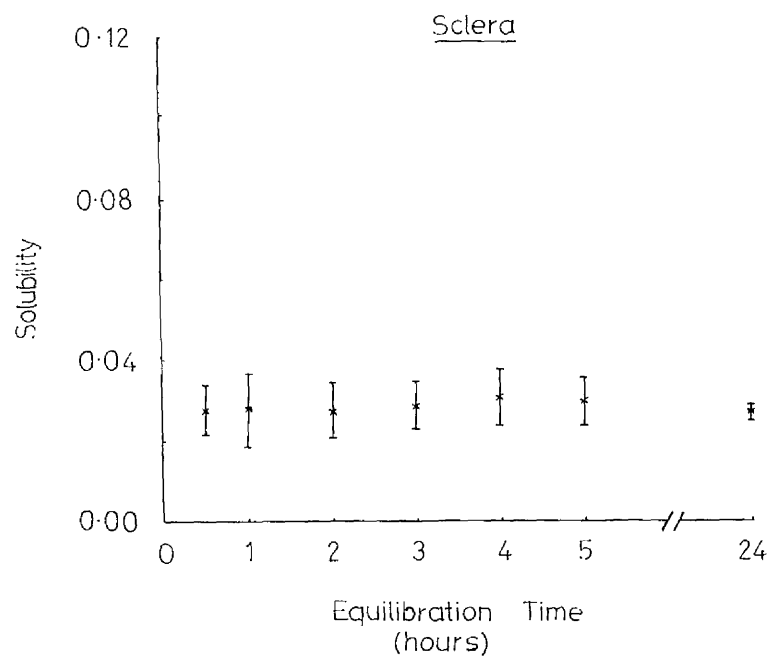


Figure 6.7 Solubility of krypton in sclera versus equilibration time.

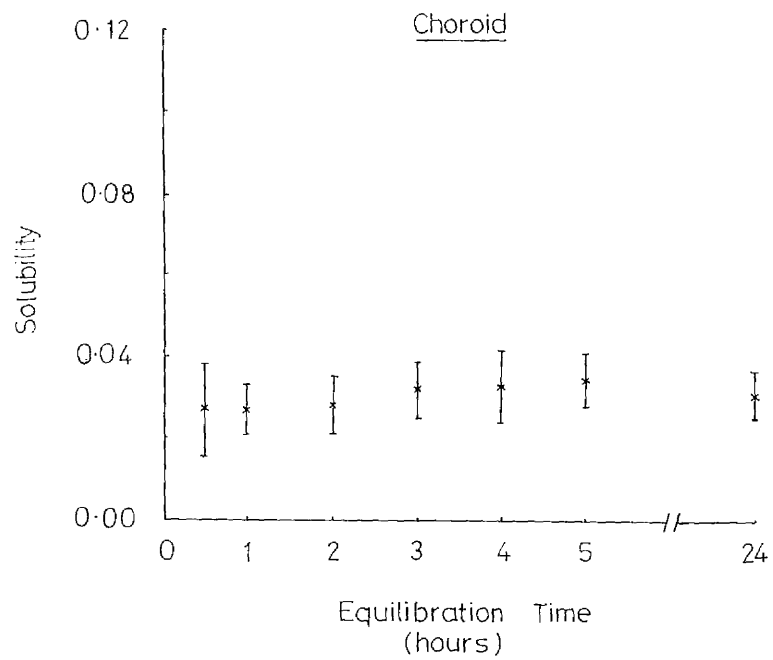


Figure 6.8 Solubility of krypton in choroid versus equilibration time.

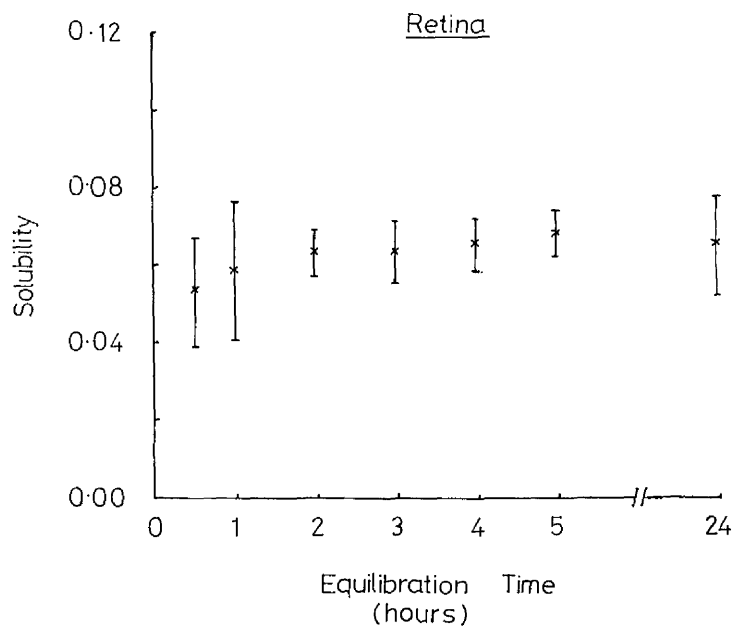


Figure 6.9 Solubility of krypton in retina versus equilibration time.

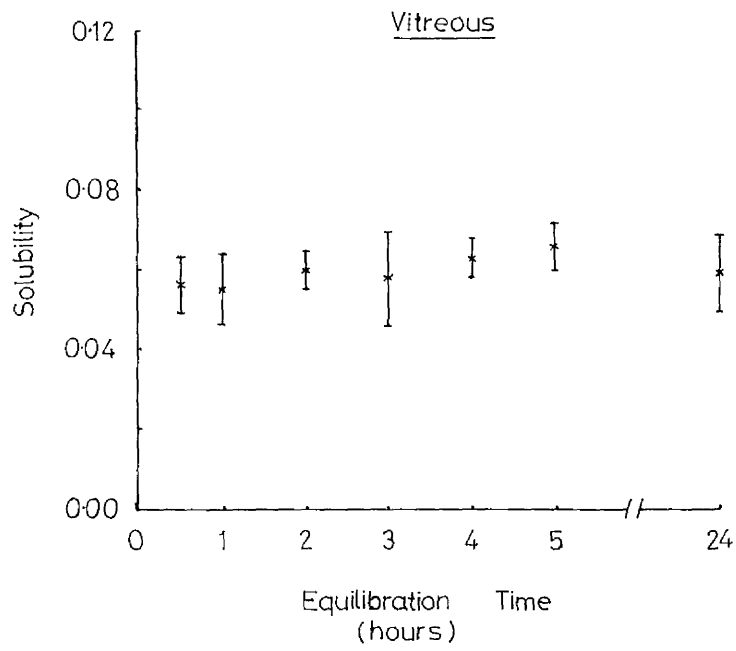


Figure 6.10 Solubility of krypton in vitreous versus equilibration time.

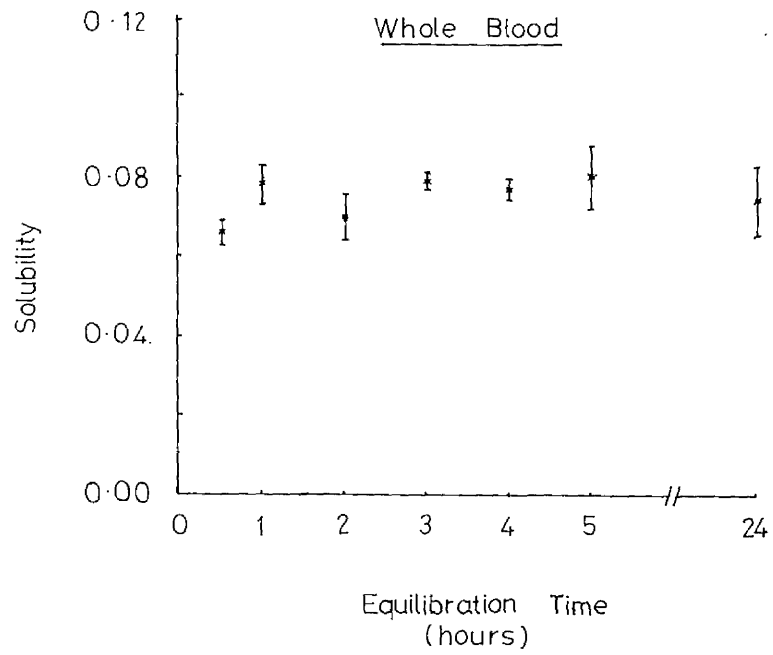


Figure 6.11 Solubility of krypton in whole blood versus equilibration time.

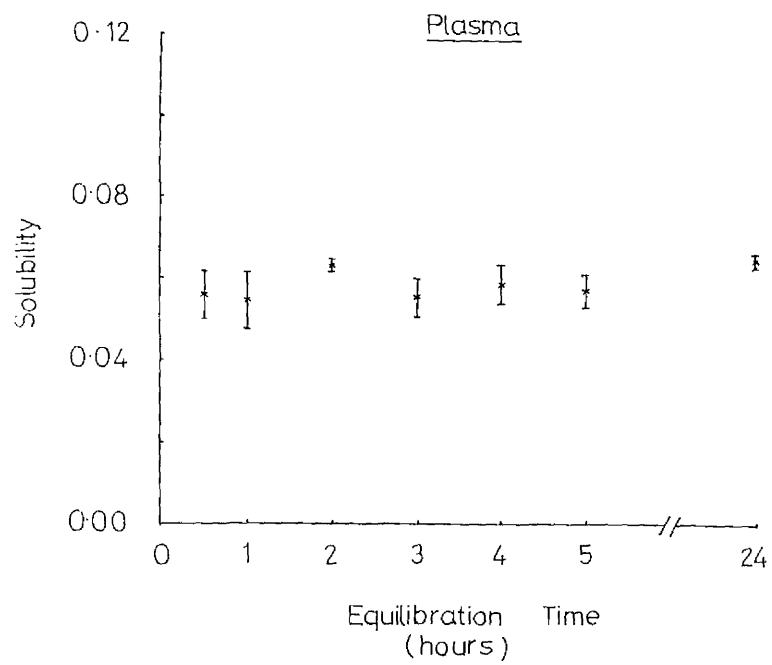


Figure 6.12 Solubility of krypton in plasma versus equilibration time.

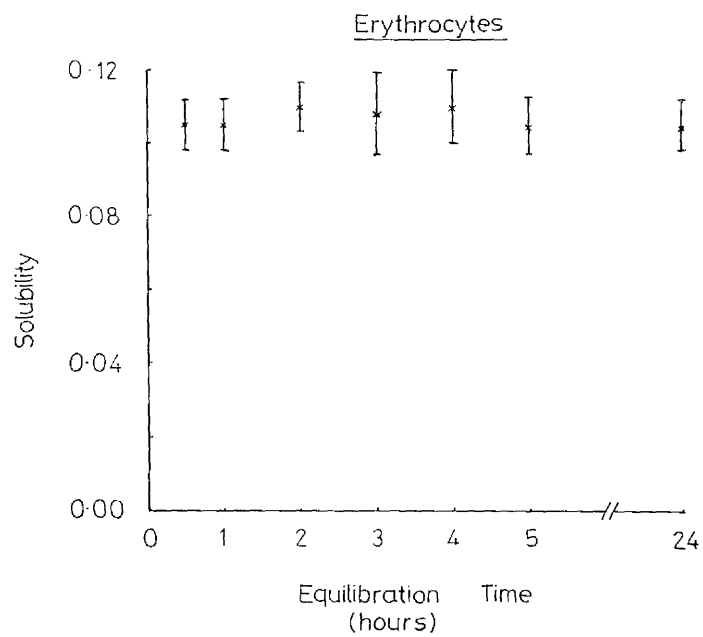


Figure 6.13 Solubility of krypton in erythrocytes versus equilibration time.

Table 6.1 Ostwald solubility coefficient for krypton at 37°C (mean  $\pm$  1 S.D.)

SAMPLE	NUMBER OF MEASUREMENTS	SOLUBILITY COEFFICIENT
Water	32	0.067 $\pm$ 0.005
Whole Blood (Hct. 38)	32	0.076 $\pm$ 0.007
Plasma	32	0.059 $\pm$ 0.005
Erythrocytes	32	0.107 $\pm$ 0.009
Sclera	46	0.028 $\pm$ 0.006
Choroid	44	0.030 $\pm$ 0.008
Retina	35	0.062 $\pm$ 0.011
Vitreous	28	0.059 $\pm$ 0.008

#### 6.3.4 Results

At least four determinations of solubility for each sample were made for equilibration periods of  $\frac{1}{2}$  hr., 1 hr., 2 hrs., 3 hrs., 4 hrs., 5 hrs., and 24 hrs. The results for each sample are shown in figures 6.6 to 6.13 as a graph of solubility against equilibration time. The mean result for each sample over all equilibration times is shown in table 6.1.

#### 6.3.5 Discussion

The extrapolation of the in vitro solubility measurements to living tissue depends on the validity of several assumptions. Firstly, essentially complete equilibrium of krypton with the sample must have been achieved by the end of the equilibration period. The fact that the solubility coefficients were not significantly different after periods of equilibration varying between 0.5 and 24 hours, would suggest that equilibration had occurred in all cases.

Secondly it has to be assumed that tissue unmaintained for the duration of the experiment has a krypton uptake similar to that of living tissue. In a similar investigation Conn (1961) found similar xenon uptake by whole blood, skeletal muscle and by liver in vivo and in vitro.

The magnitude of the error resulting from the loss of krypton from the sample during the transfer between the two vials was estimated by considering the rate of diffusion of krypton out of the sample. When one face of an extended sample containing krypton at uniform partial pressure is suddenly maintained at zero partial pressure, the mean partial pressure of krypton within the sample will decline exponentially. The half life,  $T_{\frac{1}{2}}$ , to a first approximation is given by (Gillespie and Unsworth, 1968):

$$\overline{t_{1/2}} = \frac{0.282 \times L^2}{D}$$

6.8

where L = thickness of the sample (cm), and

D = diffusion coefficient ( $\text{cm}^2 \text{sec}^{-1}$ ).

(see section 6.4.2).

During the period between opening the vial and the start of pipetting (approximately 3 seconds) the mean partial pressure will decline with a half life of the order of 20 seconds. This corresponds to a 10% loss of krypton. This estimate assumes zero partial pressure of krypton in the vial above the sample, which is not the case. Thus, the true loss will be less than 10%. During the period the sample is within the pipette ( $\leq 15$  seconds) the half life for the liquid samples will be of the order of  $10^4$  seconds ( $L \approx 1$  cm). Thus there will be negligible loss of krypton during this phase of the transfer. For the tissue samples any loss of krypton will be into the surrounding saline. Most of this saline is pipetted into the second vial. Any further loss of krypton from either the liquid or tissue samples will be contained within the second vial. Thus the loss of krypton from the sample during transfer will be less than 10%.

The solubility values obtained in this study are in agreement with those found by other workers (table 6.2). Friedman, Kopald and Smith (1964) obtained a value of "slightly greater than one" for the ratio of the solubility of krypton in the cat retina to the solubility in whole blood (i.e. the partition coefficient). The value obtained in this study was  $0.62 \pm 0.2$ . Since the solubility of krypton in erythrocytes is significantly different from that in plasma (table 6.2), the magnitude of this ratio is dependent on the haematocrit. Figure 6.14 shows the variation in the partition coefficient of the retina with haematocrit for the limited data available from this study.

Table 6.2 Ostwald solubility coefficient for krypton  
at 37°C in various solvents - literature values

SOLVENT	OSTWALD COEFFICIENT	REFERENCE
Water	0.052 * 0.052 * 0.0499  0.048 * 0.067	Von Antropoff (1919) Valentiner (1930) Hardewig, Rochester and Brocoe (1960)  Yeh and Peterson (1964) Present study
Plasma	0.051 0.053 *  0.059	Hardewig et al (1960) Muehlbaecher, DeBon and Featherstone (1966) Present study
Erythrocytes	0.120 0.107	Muehlbaecher et al (1966) Present study
Whole blood	0.045 0.085 * 0.076	Yeh and Peterson (1965) Muehlbaecher et al (1966) Present study
<u>Lipids:</u> olive oil  human fat	0.49 *  0.458 0.462	Lawrence, Loomis, Tobias and Tunpin (1946) Yeh and Peterson (1963) Yeh and Peterson (1963)
<u>Tissues:</u> Brain homogenate muscle sclera Choroid retina vitreous	0.0454 0.0439 0.028 0.030 0.062 0.059	Yeh and Peterson (1965)  Present study

\* Values are calculated from Bunsen coefficient

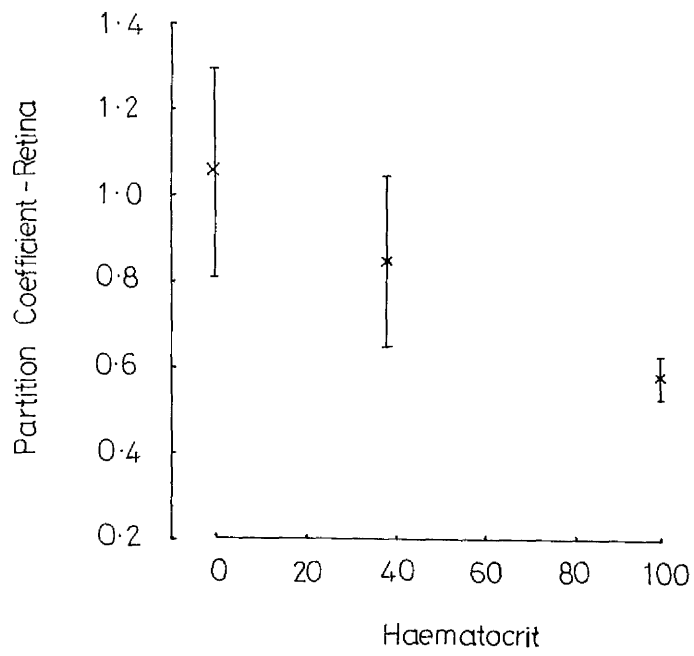


Figure 6.14 Partition coefficient (retina) versus haematocrit.

These workers also obtained a value of "slightly less than one" for the partition coefficient of the choroid. In vivo, the choroid comprises approximately 95% blood by volume. Unlike Friedman, Kopald and Smith (1964) the value of the solubility of krypton in the choroid (0.030) obtained in this study was for exsanguated choroid. This value is smaller by a factor of two than the solubility of krypton in whole blood and is significantly lower than that obtained by Lawrence, Loomis, Tobias and Turpin (1946) and by Yeh and Peterson (1963) for the solubility of krypton in lipids (table 6.2).

The true value of the solubility of krypton in the choroid (including its contained blood) is

$$0.95 \lambda_{wb} + 0.05 \lambda_{ex.ch.}$$

where  $\lambda_{wb}$  = the solubility of krypton in whole blood, and

$\lambda_{ex.ch.}$  = the solubility of krypton in exsanguated choroid.

The percentage error involved in using in the model the solubility of krypton in whole blood as the solubility of krypton in the choroid (including its contained blood) is thus:

$$\left( \frac{0.95 \lambda_{wb} + 0.05 \lambda_{ex.ch.} - 1.0 \lambda_{wb}}{0.95 \lambda_{wb} + 0.05 \lambda_{ex.ch.}} \right) \times 100$$

This is of the order of 3%.

## 6.4 Measurement of the Diffusion Coefficient of krypton

### 6.4.1 Introduction

The measurement of the diffusion coefficients of krypton in rabbit sclera, choroid, retina and vitreous were obtained using the radioisotope technique developed by Unsworth and Gillespie (1971).

These workers have shown that the ratio of the diffusion coefficients in water of xenon and krypton is equal to the inverse

ratio of their molecular weights. This relation is the same as that given by Graham's Law. In this method it is necessary to detect the  $\gamma$ -radiation from the dissolved gas (see section 6.4.2). Unfortunately only 0.7% of the total emissions from krypton -85 are  $\gamma$ -rays as compared to 35%  $\gamma$  emission from xenon -133. In order to obtain sufficient statistical accuracy the diffusion coefficient of krypton in the samples were obtained by first determining the diffusion coefficients of xenon and applying the relation observed by Unsworth and Gillespie.

#### 6.4.2 Theory

It has been shown (Carslaw and Jaeger, 1959; Gillespie and Unsworth, 1968) that when one face of an extended slice of homogeneous material initially containing a dissolved gas at uniform partial pressure is suddenly maintained at zero partial pressure the mean partial pressure of the gas within the material will initially decrease rapidly owing to the very steep partial pressure gradients at the surface. At times greater than  $0.1L^2/D$ , where  $L(\text{cm})$  is the thickness of the material and  $D(\text{cm}^2/\text{sec.})$  is the diffusion coefficient of the gas in the material, the mean partial pressure decreases at a less rapid monoexponential rate. The diffusion coefficient is related to the halving time,  $T_{\frac{1}{2}}^1$  (secs), of the exponential by the formula

$$T_{\frac{1}{2}}^1 = \frac{0.282 \cdot L^2}{D} \quad (6-11)$$

If the dissolved gas is radioactive and emits  $\gamma$  radiation, then a narrowly collimated scintillation detector will have a uniform detection efficiency for plane sources at various depths in the material,

providing absorption is negligible. The count rate will therefore be proportional to the mean partial pressure of the gas within the material. At later times the radioactivity will thus decline at a monoexponential rate with a halving time given by equation (6-11).

This technique has the advantages, (a) that high sensitivity can be achieved thereby allowing thin layers of tissue to be studied, and (b) that tissue uptake is measured directly rather than indirectly as in other methods by deducing it from the loss of gas from the surrounding media (Evans, Busuttill, Gillespie and Unsworth, 1974).

#### 6.4.3 Method

The apparatus used is shown in figure 6-15. Approximately 0.5 ml of gas containing approximately  $100 \mu\text{Ci}$  of xenon  $^{133}$  was introduced into the sample vessel. Measurements were made on freshly taken samples of rabbit sclera, choroid and retina which were placed on a glass microscopy slide within the sample vessel. Measurements were also obtained from vitreous samples with thicknesses between 0.6 mm and 1.3 mm, care being taken to level the vessel before each measurement to ensure constancy of thickness within the vessel. The depth of the vitreous samples was determined from the volume of vitreous introduced into the vessel and the cross sectional area of the vessel. Thicknesses of the tissue samples were determined from the sample area and the weight of the sample. A specific gravity of 1.04 was assumed for all tissue samples in this calculation.

The samples were allowed to equilibrate with the xenon at atmospheric pressure for at least four times the expected halving time. At the end of the equilibration period the space above the sample was continuously flushed with air at a rate of 20 ml/sec. The

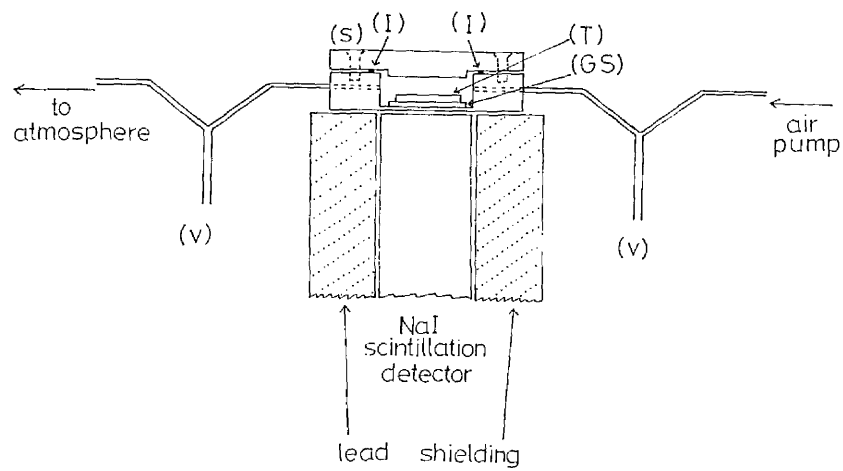


Figure 6.15 Apparatus for measuring diffusion coefficient.

- |                   |                    |
|-------------------|--------------------|
| (I) Indium seal   | (S) Clamping screw |
| (T) Tissue sample | (GS) Glass slide   |
| (V) Mercury valve |                    |

80 keV xenon  $^{133}\text{X}$  radiation from the sample was counted using a collimated sodium iodide scintillation detector, coupled via a pulse height analyser to a digital ratemeter and printer.

The system was tested for xenon retention by observing the clearance of xenon from the vessel with no sample present. An equilibration period of 30 minutes was used in this test.

#### 6.4.4 Results

Two sets of apparatus were used. Figure 6-16 shows the clearance of xenon from the empty sample vessel of the first apparatus used for the tissue studies. The initial count rate was approximately 200000 counts per second. The clearance halving time was of the order of 1.0 second. However, the residual count rate, although varying very slowly, was significantly above room background levels. This was thought to be due to absorption of xenon into the araldite joins between the glass 'Y'-tubes of the mercury valves and the metal (brass) sample vessel.

It was possible to allow for this in the measurements on the tissue samples. Figure 6-17 shows the clearance of xenon from a retinal sample of thickness 0.025 cm. The radioactivity declines at a monoexponential rate for approximately two halving times before declining at a much slower rate. Approximately three minutes after the start of the clearance the sample was removed from the vessel and the radioactivity monitored for a further ten minutes. The residual radioactivity variation was extrapolated and subtracted from the sample clearance curve. The result of this subtraction is shown in figure 6-18. The halving time was obtained from this graph.

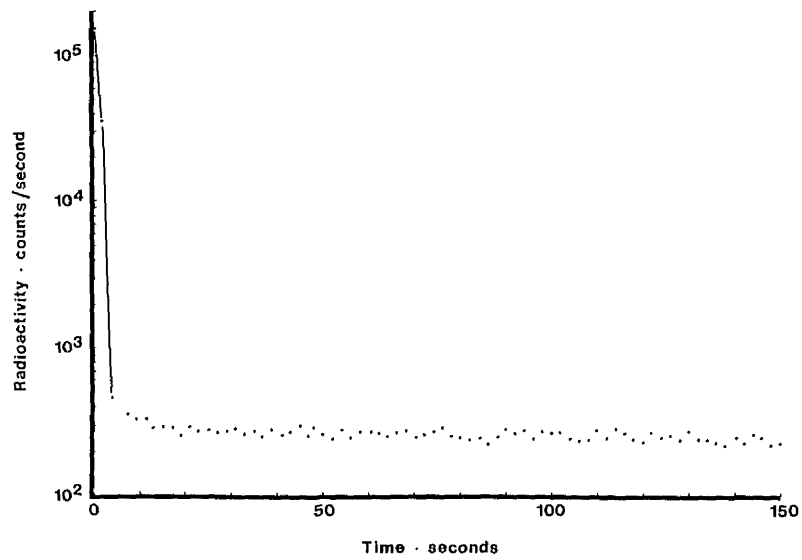


Figure 6.16 Clearance of xenon from empty sample vessel.  
(1st apparatus).

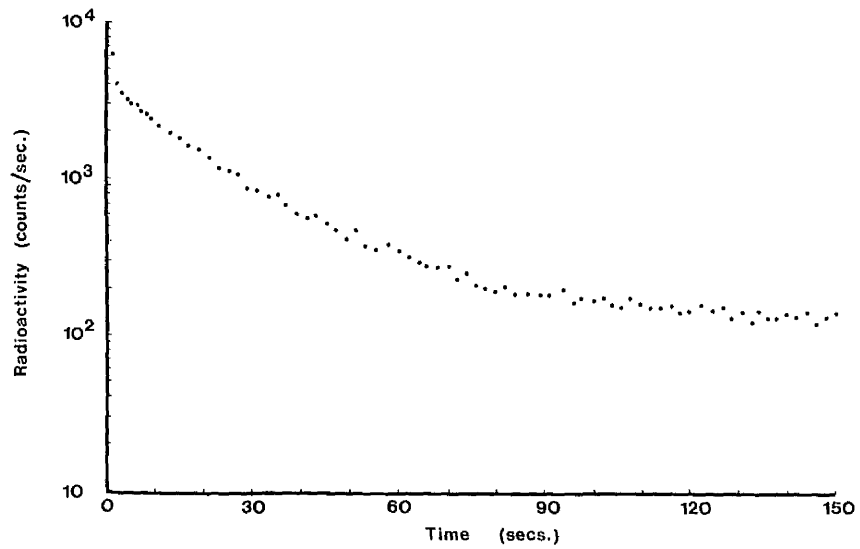


Figure 6.17 Clearance of xenon from a retinal sample.

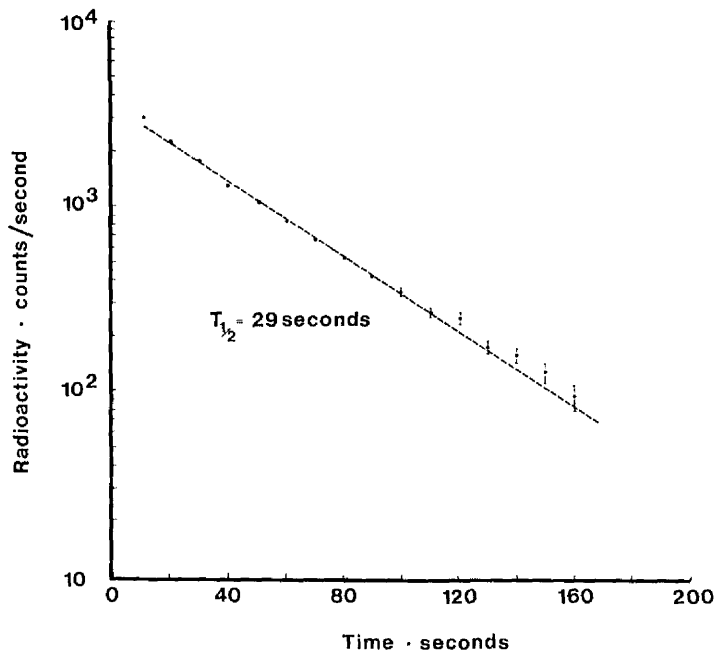


Figure 6.18 Result of subtraction of residual radioactivity.

In the vitreous measurements it was not possible to remove the sample during the clearance because of the liquid nature of the sample. A new apparatus was constructed. The glass 'Y'-tubes of the mercury valves were replaced by metal tubes, soldered to the sample vessel. This avoided the use of araldite. The clearance of xenon from the empty sample vessel of the second apparatus is shown in figure 6-19. As before, the clearance halving time was of the order of one second. However, the residual count rate was only marginally greater than the room background, showing that incorporation of xenon in the various parts of the sample vessel and in valves was negligible.

Two measurements of the diffusion coefficient in vitreous were made at thicknesses of 0.075, 0.088, 0.063 and 0.125 cm. The clearance of xenon from a vitreous sample of thickness 0.083 cm is shown in figure 6-20. The halving times corresponding to the various thicknesses are shown in table 6.3. Figure 6.21 is a graph of the square of the sample thickness ( $L^2$ ) against the halving time ( $T_{1/2}^1$ ). The diffusion coefficient of xenon in rabbit vitreous was calculated, using equation (6-11), from the slope of this graph. The diffusion coefficients of xenon in rabbit sclera, choroid and retina were calculated by substituting the halving times into equation (6-11). The mean diffusion coefficients so determined are shown in table 6.4. The calculated values of the diffusion coefficient of krypton in the various samples are also shown in this table.

#### 6.4.5 Discussion

It was evident from the results of clearance studies with the sample vessel empty that the lower limit to the measurement of clearance halving time was of the order of one second. In the various experiments the clearance halving time varied between 14 seconds

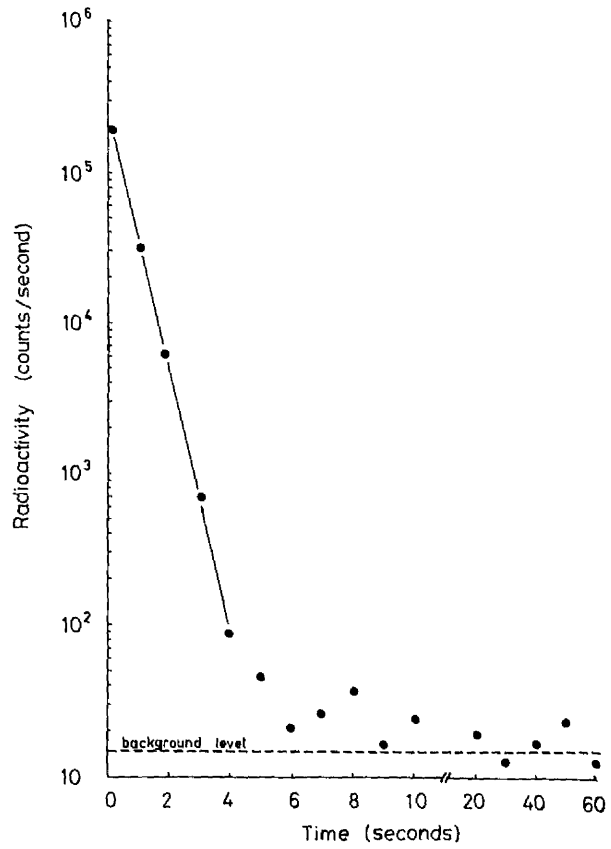


Figure 6.19 Clearance of xenon from empty sample vessel.  
(2nd apparatus).

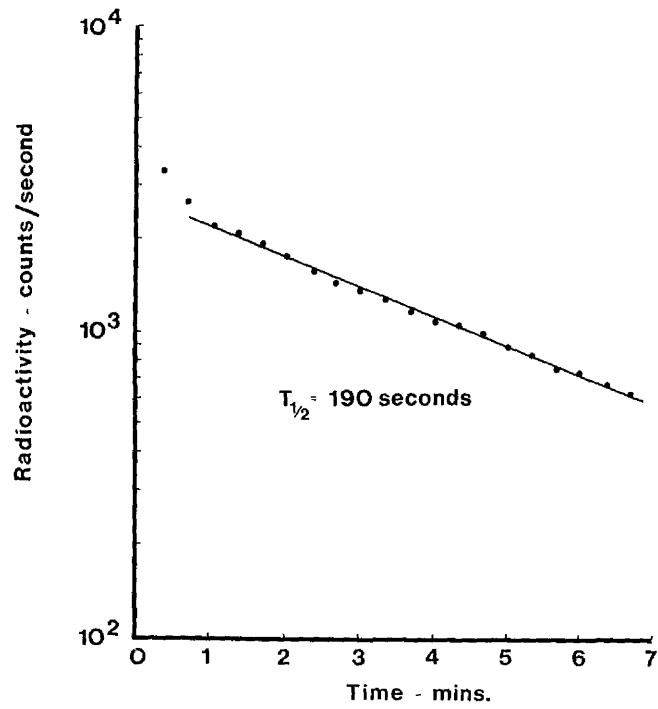


Figure 6.20 Clearance of xenon from a vitreous sample.

Table 6.3

Final exponential clearance half-lives  
for various thicknesses of vitreous

Thickness L (cm)	0.063	0.075	0.088	0.125
Half life 1	80	150	190	415
$T_{\frac{1}{2}}$ (sec) 2	105	140	175	440

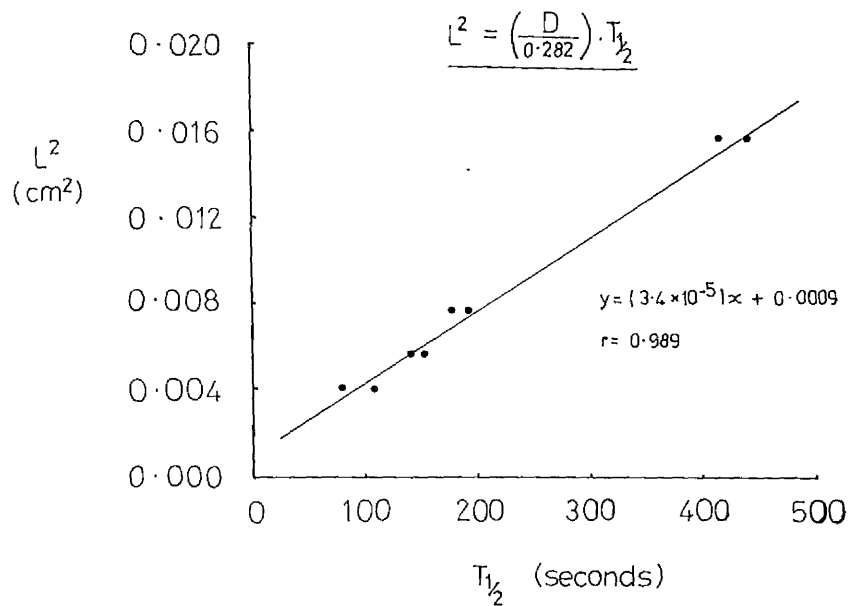


Figure 6.21 (vitreous thickness,  $L$ )<sup>2</sup> versus clearance halving time,  $T_{1/2}$ .

Table 6.4 Diffusion Coefficients (mean  $\pm$  S.D.)

Tissue	Number of Measurements	Diffusion Coefficient XENON ( $\times 10^{-5} \text{cm}^2 \text{sec}^{-1}$ )	Calculated Diffusion Coefficient KRYPTON ( $\times 10^{-5} \text{cm}^2 \text{sec}^{-1}$ )
Sclera	6	$1.3 \pm 0.3$	$1.6 \pm 0.3$
Choroid	5	$0.61 \pm 0.14$	$0.76 \pm 0.14$
Retina	5	$0.64 \pm 0.05$	$0.80 \pm 0.05$
Vitreous	8	$0.96 \pm 0.12$	$1.2 \pm 0.12$

(choroid) and 440 seconds (vitreous). These values are at least one order of magnitude greater than those obtained with the vessel empty.

In this study the diffusion coefficient was calculated from an expression (equation 6-11) relating the diffusion coefficient to the clearance halving time. This relation involves the assumption that the clearance of xenon is from a tissue sample of infinite area. The error resulting from diffusion out of the edges of a tissue sample of finite area was investigated. At later times the clearance halving time from a cuboid tissue sample is given by

$$T_{1/2} = \frac{0.282}{D \left( \frac{1}{L_1^2} + \frac{1}{L_2^2} + \frac{1}{L_3^2} \right)} \quad (6-12)$$

(Unsworth, 1974 - private communication)

where  $L_1$  = thickness of sample (cm),  
 $L_2$  = length of sample (cm),  
 $L_3$  = breadth of sample (cm), and  
 $D$  = diffusion coefficient ( $\text{cm}^2 \text{sec}^{-1}$ ).

The percentage error resulting from neglecting edge diffusion from a cuboid tissue sample was taken as

$$\% \text{ error} = \left( \frac{(T_{1/2})_{\tau} - (T_{1/2})_{\infty}}{(T_{1/2})_{\tau}} \right) \times 100$$

where  $(T_{1/2})_{\tau}$  = true clearance halving time obtained from equation (6-12), and  
 $(T_{1/2})_{\infty}$  = clearance halving time assuming an infinite tissue sample (equation (6-11)).

Thus, substituting from equations (6-11) and (6-12)

$$\text{Percentage error} = L_1^2 \left( \frac{1}{L_3^2} + \frac{1}{L_2^2} \right) \times 100 \quad (6-13)$$

Substituting typical values of  $L_1$ ,  $L_2$  and  $L_3$  (table 6.5) into equation (6-13) gives error values of 0.2%, 0.1% and 0.3% for the choroid, retina and sclera respectively. These errors are negligible. No edge diffusion could occur with the vitreous samples.

Table 6.5 Typical dimensions of the tissue samplea employed in the determination of the diffusion coefficient.

Sample	Thickness $L_1$ (cm)	Length $L_2$ (cm)	Breadth $L_3$ (cm)
Sclera	0.048	1.8	1.0
Choroid	0.020	1.4	1.0
Retina	0.022	1.7	1.5

Chapter 7Carbon Dioxide Response7.1 Introduction

In the previous chapters the viability of the inert gas clearance method for measuring choroidal blood flow in rabbits and primates was demonstrated. In this chapter the results of a study to determine the response of the choroidal blood flow in rabbits and baboons to changes in arterial carbon dioxide tension will be presented.

It is well known that the cerebral circulation increases with increasing arterial carbon dioxide tension, and vice versa. (Kety and Schmidt, 1948; Reivich, 1964).

Much less is known about the ocular circulation. Spatler, Ten Eick and Nahas (1964) observed retinal vessel dilatation in dogs by one-third when the  $P_a CO_2$  was increased to 70 mmHg. Tsacopoulos and David (1973), using a dye dilution technique in monkeys, demonstrated an increase in retinal blood flow with increasing  $P_a CO_2$ . Bettman and Fellows (1956) using labelled erythrocytes found a marked and consistent increase in choroidal blood volume in cats on administration of 8-10% carbon dioxide into the inhalation mixture. Trokel (1965) reported that the administration of carbon dioxide in albino rabbits increased both the choroidal blood volume and blood flow. Friedman and Chandra (1972), using cats, also noted an increase in choroidal blood flow with administration of carbon dioxide. The purpose of this present study was to investigate the relation between choroidal blood flow and arterial carbon dioxide tension in the rabbit and primate.

## 7.2 Rabbit Experiments

### 7.2.1 Experimental Method

Twelve albino rabbits weighing between 2-4 kg were used. The experimental arrangement was similar to that described in Chapter 3. The only difference was that the tracheostomy tube was connected to a Harvard small animal respirator. This allowed greater control of the arterial blood gas tensions. Muscle relaxation was maintained throughout each experiment with half-hourly injections of pancuronium bromide (0.03 - 0.04 mg/kg). Respiration was adjusted so that initial blood flow determinations were made at low levels of  $P_a\text{CO}_2$ . The concentration of carbon dioxide in the inspired air was increased in a stepwise manner and choroidal blood flow,  $P_a\text{CO}_2$ ,  $P_a\text{O}_2$  and pH were measured 15 minutes after each step increase.

### 7.2.2 Results

In 8 out of the 12 animals an increase in the arterial carbon dioxide tension was followed by an increase of up to 15mmHg in the systemic arterial blood pressure. The direct effect of changes in  $P_a\text{CO}_2$  on the choroidal blood flow was separated from the effect of increased arterial blood pressure by dividing the choroidal blood flow by the perfusion pressure. Perfusion pressure was taken as the mean systemic arterial blood pressure minus the intraocular pressure. This correction is valid if a linear relation exists between choroidal blood flow and perfusion pressure. Friedman (1970) in anaesthetised cats, and Alm and Bill (1972b; 1973) in cats and monkeys, have shown that such a relation exists.

The response of the choroidal blood flow to increased arterial carbon dioxide tension seemed to fall into three groups. Figure 7.1 shows the results for two animals from each group. The error bars at the low flow values in group 1 represent an estimate of the uncertainty of the measurement at such low flow values.

All the five animals of the first group had very low levels of flow at low  $P_a\text{CO}_2$ . A rapid increase in flow occurred with increasing  $P_a\text{CO}_2$ . This was followed by a rapid decrease in flow at high  $P_a\text{CO}_2$ . The  $P_a\text{CO}_2$  level at which flow decreased varied with each animal but occurred at a partial pressure of about 60 mmHg.

The two animals of the second group had higher flow values at low  $P_a\text{CO}_2$  than the first group. An increase in flow occurred with increasing  $P_a\text{CO}_2$  up to levels over 100 mmHg. No decrease in flow was observed in these two animals at these very high levels of  $P_a\text{CO}_2$ .

The third group of five animals had very high flow values at low levels of  $P_a\text{CO}_2$ . Increasing  $P_a\text{CO}_2$  resulted in a decrease in flow in three animals and no change in flow in the other two.

Wilcoxin rank sum tests were applied to the values of systemic arterial blood pressure and  $P_a\text{O}_2$  for each pair of groups in turn. No significant differences were found between any of the three groups ( $p > 0.1$ ).

### 7.3 Baboon Experiments

#### 7.3.1 Experimental Method

Experiments were performed on 6 baboons (papio hamadrius), each weighing approximately 12 kg. In this study both cerebral and choroidal blood flow were measured. The cerebral

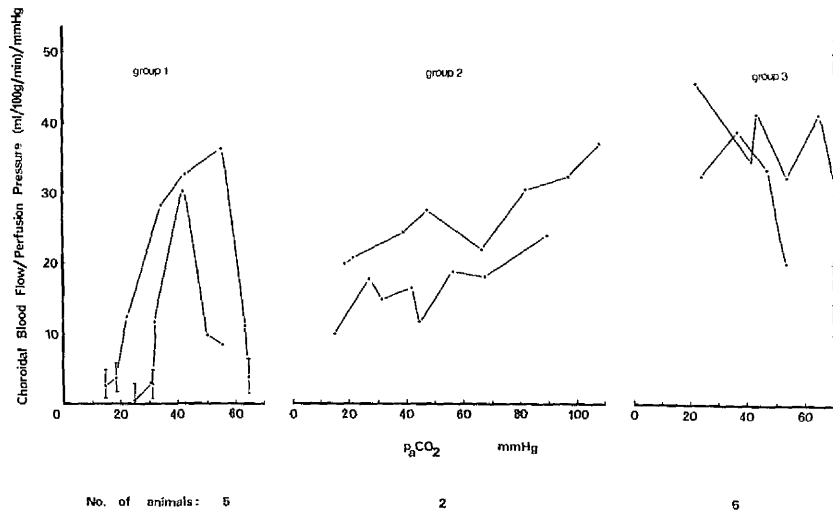


Figure 7.1 Choroidal blood flow / perfusion pressure versus  $P_aCO_2$  in the rabbit.

blood flow was measured by monitoring the clearance of xenon-133 from the brain. This was achieved by placing a collimated sodium iodide scintillation detector over the parietal region. The height over area method of analysis of the clearance curve was employed. (Høedt-Rasmussen, Sveingottir, and Lassen, 1966). The choroidal blood flow was determined using krypton -85.

The animals were sedated with phencyclidine (12 mg. i.m.) and anaesthetised with sodium thiopentone (75mg/kg. i.v.). Following endotracheal intubation anaesthesia was maintained with 75% nitrous oxide and 25% oxygen on open circuit. Supplementary doses of phencyclidine (2-4 mg) and suxamethonium (50 mg) were given every half hour. All animals were artificially respired. Catheters were inserted into a femoral artery and vein for the measurement of mean arterial blood pressure, the withdrawal of arterial blood samples for the measurement of blood gases, and the infusion of saline. A further catheter was inserted into the lingual facial trunk. The remaining branches of the external carotid artery were ligated. Bolus injections of xenon-133 and krypton -85, dissolved in saline, were made via this catheter into the internal carotid artery. The ipsilateral temporalis muscle and scalp were reflected to avoid extracranial sources of radiation.

Respiration was adjusted so that initial flow values were obtained at a  $P_aCO_2$  of around 40mmHg. Step increases in arterial carbon dioxide tension were produced by introducing carbon dioxide into the inspired gas mixture. Choroidal and cerebral blood flow were measured sequentially at each level of  $P_aCO_2$ .

### 7.3.2 Results

In this study a total of 6 measurements of choroidal blood flow were obtained within limits of  $P_a\text{CO}_2$  ( $39 \pm 1.3$  mmHg, mean  $\pm$  1 s.d.),  $P_a\text{O}_2$  ( $92 \pm 7$  mmHg), and mean systemic arterial blood pressure ( $94 \pm 12$  mmHg). The mean control value of the choroidal blood flow in the baboon from this limited data was  $463 \pm 44$  ml/100g /min. (mean  $\pm$  1 s.d.). The corresponding value for the cerebral blood flow was  $46 \pm 5$  ml/100g/min.

A total of 36 measurements of cerebral blood flow and 25 measurements of choroidal blood flow were made at various levels of  $P_a\text{CO}_2$ . Within the range of  $P_a\text{CO}_2$  investigated both circulations increased linearly with increasing arterial carbon dioxide tension (figure 7.2a,b). The percentage increases in blood flow per mmHg rise in  $P_a\text{CO}_2$  were  $3.63$  (mmHg) $^{-1}$  and  $3.52$  (mmHg) $^{-1}$  for the cerebral and choroidal circulations respectively. The blood flow at a  $P_a\text{CO}_2$  of 40 mmHg was taken as the control value.

### 7.4 Discussion

The explanation of the variable response of the rabbit choroidal circulation to increasing arterial carbon dioxide tension is not clear. The very high flow values occurring at low levels of  $P_a\text{CO}_2$  in the third group lie outwith the previously determined control values (Chapter 3). These high flow values and the variable response of the choroidal circulation may be the result of a number of different factors such as individual variations in the response to surgical trauma or anaesthetic agents. However, it is of interest that the maximum flow values of the first two groups do not exceed the initial high values in the third group. This suggests that these values may represent a state of maximal dilatation of the choroidal vessels. If this is true no further increase in flow is possible.

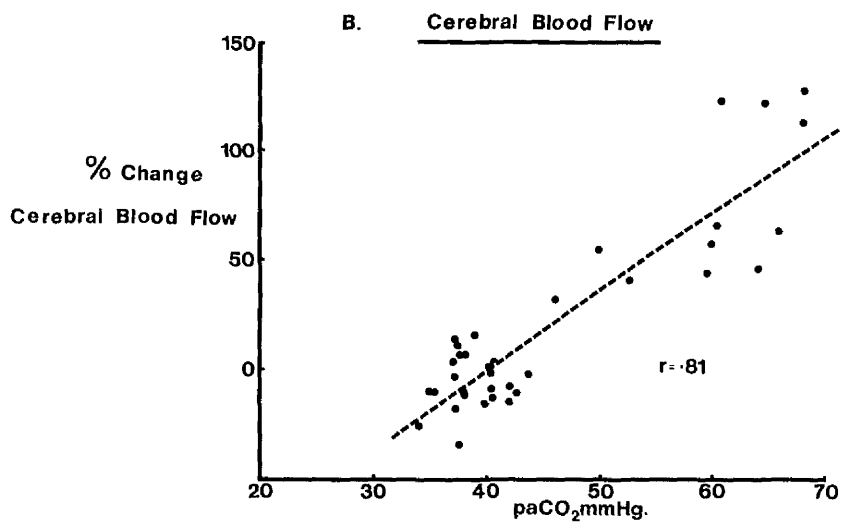
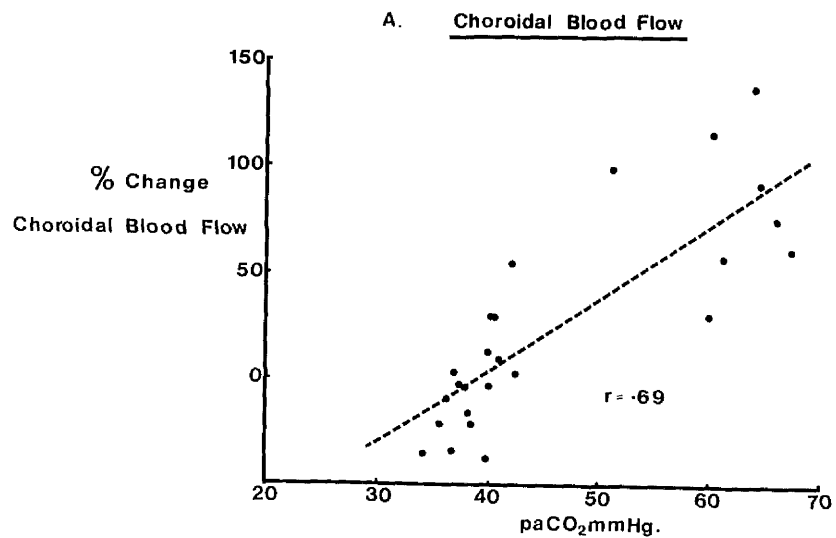


Figure 7.2 Percentage change in blood flow versus P<sub>a</sub>CO<sub>2</sub> in the baboon.  
 (A) Choroidal blood flow  
 (B) Cerebral blood flow  
 Blood flow at P<sub>a</sub>CO<sub>2</sub> = 40mmHg taken as control value.

The decrease in flow at high levels of  $P_a\text{CO}_2$  in group 1 did not occur in group 2. In group 1 the  $P_a\text{CO}_2$  was raised slowly to very high levels. In group 2 only one determination of flow was made at each level of  $P_a\text{CO}_2$  as compared with two determinations in groups one and three. This resulted in a relatively more rapid rise in  $P_a\text{CO}_2$  levels in group 2. The decrease in flow occurring in groups 1 and 3 may therefore be due to the effect of prolonged, severe hypercapnia.

The response of the choroidal blood flow to increasing arterial carbon dioxide tension was uniform in the 6 baboons studied. The very similar responses of the choroidal and cerebral circulations is further evidence that the two circulations behave in a similar manner (Porsaa, 1941).

The physiological mechanism by which changes in arterial carbon dioxide tension affect the various circulations is not fully understood. It has been suggested that the response is the results of the conversion of carbon dioxide by the enzyme carbonic anhydrase into hydrogen ions which acts directly on the arteriolar smooth muscle, producing a change in vascular volume (Wahl, Deetjen, Thurau, Ingvar and Lassen, 1970).

Chapter 8Conclusions

The purpose of this project was to investigate the feasibility of applying the radioactive inert gas clearance method to the measurement of choroidal blood flow in experimental animals. In a homogeneously perfused organ the clearance of a radioactive inert gas is monoexponential and the blood flow is related to the exponential rate constant. However, the eye is not a homogeneously perfused organ. It is therefore unrealistic to expect the simple theory and method of analysis described in Chapter 2 to be applicable. Experiments described in Chapter 3 showed that the clearance of radioactive krypton from rabbit ocular tissue is not monoexponential.

The main aim of this thesis was thus to find an explanation for the complex nature of the washout curve and to determine which component of the curve, if any, was a measure of choroidal blood flow.

Theoretical washout curves were predicted by studying the diffusion of krypton in ocular tissue for comparison with the experimental data. Initially a model of diffusion based on the anatomy of the rabbit eye was developed (Chapter 4). The results from this model showed good agreement with experimental data and showed that the experimental washout curves can be explained in terms of simple diffusion. In particular it was shown that for choroidal blood flows greater than 500ml/100g/min. the exponential rate constant of the initial decline of the washout curve is an accurate measurement of choroidal blood flow. The subsequent decline in radioactivity was shown to be dependent on diffusion within the ocular tissue. At low flow values (i.e.  $< 500\text{ml}/100\text{g}/\text{min}$ ) the

initial slope of the washout curve is partially dependent on diffusion.

The results of a model whose structure was based on the anatomy of the baboon eye which has both retinal and choroidal circulations, indicated that the initial slope of the clearance of krypton accurately measures choroidal blood flow within the range 400 to 800 ml/100g/min. No relation was evident between the retinal blood flow and any component of the washout curve.

It has also been shown (section 5.6.7) that the initial slope of predicted curves derived from a model based on the anatomy of the human eye is a measure of choroidal blood flow. However, this is only valid for a bolus arrival of krypton at the eye (sections 5.5 and 5.6.6). This requires arterial injection of the radioisotope close to the eye, e.g. the carotid artery. This would not normally be feasible in the clinical situation for ethical reasons. Thus, the use of the inert gas clearance method will be restricted to experimental animals.

The mean control values of choroidal blood flow obtained in the studies described in this thesis were 920 and 460 ml/100g/min. for the rabbit and baboon respectively. Two points of interest are apparent from these values. Firstly, they represent just about the highest blood flow found in any organ in either animals. Secondly, the choroidal blood flow in the rabbit (which has only a choroidal circulation) is approximately twice that in the baboon.

If the assumption is made that the difference in blood flows is not due to specialised retinal function, it is interesting to speculate on the reason for the high blood flow.

Light falling on the retina is converted into a neural signal in the photoreceptors. These are in close proximity to the choroidal circulation. If the high choroidal blood flow exists to dispel heat

generated or remove waste products arising from the light conversion, this does not explain the difference in choroidal blood flow in the rabbit and baboon. Further information could be obtained by investigating what happens, if anything, to the choroidal blood flow on changing from light to dark adaptation. It would also be interesting to compare the choroidal blood flow in eyes which have a pecten with those which do not, since it is thought that the pecten regulates the temperature in the eye (Bacsich, Chisholm and Gellert, 1966).

On the other hand if the high blood flow is necessary to supply the relatively avascular retina with nutrients, this would explain the difference between the rabbit and baboon. The choroidal circulation in the rabbit has to supply the whole retina, whereas in the baboon it has to supply only the outer  $\frac{2}{3}$  rds of the retina. In both animals the choroidal circulation nourishes the highly metabolic photoreceptors. It would be interesting to know whether or not the choroidal blood flow responds to changes in intensity of light falling on the retina.

Obviously, the assumption regarding the choroidal blood flow in the rabbit and baboon can be only tentative.

However, the radioactive inert gas clearance method, despite being limited in application to experimental animals, should be a useful tool in answering some of these questions. Although there is difficulty in extrapolating from animals to man, this method should also be useful in studying the effects of changes in physiological parameters, e.g. the effect of increased intraocular pressure, on the choroidal blood flow and in evaluating the response of the choroidal circulation to various drugs. For example, the affect of acetazolamide (Diamox) on choroidal blood flow is currently being investigated.

APPENDIX I

```

C *****
C ***** PROGRAM SOLVES DIFFUSION EQUATIONS FOR OCULAR MODEL *****
C ***** WITH BLOOD FLOW TERM *** SEMI INFINITE VITREOUS *****
C ***** N=1, M IS SIZE OF ARRAY ALONG X AXIS *****
C ***** TSTEP = TIME INTERVAL, DSTEP = DISTANCE INTERVAL *****
C ***** DO = DIFFUSION COEFFICIENT OF MEDIUM 0 *****
C ***** D1 = DIFFUSION COEFFICIENT OF MEDIUM 1 *****
C ***** D2 = DIFFUSION COEFFICIENT OF MEDIUM 2 *****
C ***** D3 = DIFFUSION COEFFICIENT OF MEDIUM 3 *****
C ***** MM IS BOUNDARY BETWEEN MEDIUM 0 AND MEDIUM 1 *****
C ***** II IS BOUNDARY BETWEEN MEDIUM 1 AND MEDIUM 2 *****
C ***** III IS BOUNDARY BETWEEN MEDIUM 2 AND MEDIUM 3 *****
C ***** F1 IS THE BLOOD FLOW TERM FOR THE CHOROID *****
C ***** F2 IS THE BLOOD FLOW TERM FOR THE RETINA *****
C ***** ABS IS THE LINEAR ABSORPTION COEFFICIENT *****
C *****
      DIMENSION CON1(999),CON2(999)
      READ (5,3) N,M
      READ (5,4) TSTEP,DSTEP,DO,D1,D2,D3
      READ (5,5) MM,II,III
      READ (5,14) ABS
      READ (5,42) SOLO,SOL1,SOL2,SOL3
      READ (5,6) F1,F2
3     FORMAT (I1,I3)
6     FORMAT (2F6.4)
4     FORMAT (2F5.3,4E9.3)
5     FORMAT (3I2)
14    FORMAT (F6.3)
42    FORMAT (4F6.4)
C ***** INITIAL VALUES OF PARTIAL PRESSURE *****
      DO 29 I=1,11
29    CON1(I) = 0.0
      DO 27 I=12,14
27    CON1(I) = 1000.0
      DO 28 I=15,999
28    CON1(I) = 0.0
      DO 30 I=16,18
30    CON1(I) = 1000.0
C *****
      FF1 = F1/TSTEP
      FF2 = F2/TSTEP
      WRITE (6,7) N,M
      WRITE (6,8) TSTEP,DSTEP,DO,D1,D2,D3
      WRITE (6,43) SOLO,SOL1,SOL2,SOL3
      WRITE (6,9) MM,II,III
      WRITE (6,12) FF1,FF2
      WRITE (6,19) ABS
7     FORMAT (5H N = ,I1,5X,5H M = ,I3)
8     FORMAT (9H TSTEP = ,F6.3,5H(SEC),/,9H DSTEP = ,F6.3,4H(CM),
1/ ,6H DO = ,E9.3,11H(CM**2/SEC),/,6H D1 = ,E9.3,11H(CM**2/SEC
2),/,6H D2 = ,E9.3,11H(CM**2/SEC),/,6H D3 = ,E9.3,11H(CM**2/S
3EC))
43    FORMAT (22H SOLUBILITY MEDIA 0 = ,F6.3,/,18X,4H1 = ,F6.3,/,1
18X,4H2 = ,F6.3,/,18X,4H3 = ,F6.3)

```

```

9   FORMAT (6H MM = ,I2,3X,6H II = ,I2,3X,7H III = ,I2)
12  FORMAT (6H F1 = ,F6.4,6H F2 = ,F6.4)
19  FORMAT (7H ABS = ,F6.3,6H(CM-1))
    PO = DSTEP**2/(TSTEP*DO)
    P1 = DSTEP**2/(TSTEP*D1)
    P2 = DSTEP**2/(TSTEP*D2)
    P3 = DSTEP**2/(TSTEP*D3)
    RO = TSTEP*DO/DSTEP**2
    R1 = TSTEP*D1/DSTEP**2
    R2 = TSTEP*D2/DSTEP**2
    R3 = TSTEP*D3/DSTEP**2
    J = M - 1
    JJ = II - 1
    JJJ = III - 1
    JJJJ = MM - 1
    L = N + 1
C *****
C ***** XDIST = DISTANCE (CM) OF PT. IN NETWORK FROM DETECTOR ***
C ***** XDISO = DIST. OF BOUNDARY BETWEEN MEDIA 0 & MEDIA 1 *****
C ***** XDIS1 = DIST. OF BOUNDARY BETWEEN MEDIA 1 & MEDIA 2 *****
C ***** XDIS2 = DIST. OF BOUNDARY BETWEEN MEDIA 2 & MEDIA 3 *****
C ***** XDISE = DIST. OF END POINT OF NETWORK *****
C ***** CORR = CORRECTION FOR DETECTOR EFFICIENCY *****
C ***** CORO = CORR FOR BOUNDARY 0 & 1 *****
C ***** COR1 = CORR FOR BOUNDARY 1 & 2 *****
C ***** COR2 = CORR FOR BOUNDARY 2 & 3 *****
C ***** CORE = CORR FOR END POINT *****
C ***** CCN = CORRECTED CONCENTRATION *****
C ***** TCON = SUMMATION OF CONC. OVER ALL PTS. OF NETWORK *****
C ***** TCCN = TCON WITH DETECTOR EFFICIENCY TERM *****
C *****
    XDISO = DSTEP*(MM-1)
    XDIS1 = DSTEP*(II-1)
    XDIS2 = DSTEP*(III-1)
    XDISE = DSTEP*(M-1)
    CORO = EXP(-(ABS*XDISO))
    COR1 = EXP(-(ABS*XDIS1))
    COR2 = EXP(-(ABS*XDIS2))
    CORE = EXP(-(ABS*XDISE))
    TT = 0.0
    KK = 0
    NN = 0
    NNN = 0
40  TCON = 0.0
    TCCN = 0.0
    NN = NN + 1
    NNN = NNN + 1
C ***** MEDIA 0 CALCULATIONS *****
    DO 77 I=L,JJJJ
    CON2(I) = ((1.0-(2.0*RO))*CON1(I)+RO*(CON1(I+1)+CON1(I-1)))
1)  CON2(I) = SOLO*CON2(I)
    TCON = TCON + CON2(I)
    XDIST = DSTEP*(I-1)
    CORR = EXP(-(ABS*XDIST))

```

```

      CCN = CORR*CON2(I)
      TCCN = TCCN + CCN
      CON2(I) = CON2(I)/SOLO
77  CONTINUE
C ***** MEDIA 1 CALCULATIONS *****
      LLLL = MM + 1
      DO 17 I=LLLL, JJ
      CON2(I) = (1.0-(2.0*R1))*CON1(I)+R1*(CON1(I+1)+CON1(I-1))
      CON2(I) = SOL1*CON2(I)
      TCON = TCON + CON2(I)
      XDIST = DSTEP*(I-1)
      CORR = EXP(-(ABS*XDIST))
      CCN = CORR*CON2(I)
      TCCN = TCCN + CCN
      CON2(I) = CON2(I)/SOL1
17  CONTINUE
C ***** MEDIA 2 CALCULATIONS *****
      LL = II + 1
      DO 20 I=LL, JJJ
      CON2(I) = (1.0-(2.0*R2))*CON1(I)+R2*(CON1(I+1)+CON1(I-1))
      CON2(I) = SOL2*CON2(I)
      TCON = TCON + CON2(I)
      XDIST = DSTEP*(I-1)
      CORR = EXP(-(ABS*XDIST))
      CCN = CORR*CON2(I)
      TCCN = TCCN + CCN
      CON2(I) = CON2(I)/SOL2
20  CONTINUE
C ***** MEDIA 3 CALCULATIONS *****
      LLL = III + 1
      DO 60 I=LLL, J
      CON2(I) = (1.0-(2.0*R3))*CON1(I)+R3*(CON1(I+1)+CON1(I-1))
      CON2(I) = SOL3*CON2(I)
      TCON = TCON + CON2(I)
      XDIST = DSTEP*(I-1)
      CORR = EXP(-(ABS*XDIST))
      CCN = CORR*CON2(I)
      TCCN = TCCN + CCN
      CON2(I) = CON2(I)/SOL3
60  CONTINUE
C ***** CALC. OF BOUNDARY VALUE BETWEEN MEDIA 1 & MEDIA 0 *****
      CON2(MM) = (D1*CON2(MM+1)+D0*CON2(MM-1))/(D0+D1)
      CON2(MM) = SOLO*CON2(MM)
C ***** CALC. OF BOUNDARY VALUE BETWEEN MEDIA 1 & MEDIA 2 *****
      CON2(II) = (D2*CON2(II+1)+D1*CON2(II-1))/(D1+D2)
      CON2(II) = SOL1*CON2(II)
C ***** CALC. OF BOUNDARY VALUE BETWEEN MEDIA 2 & MEDIA 3 *****
      CON2(III) = (D3*CON2(III+1)+D2*CON2(III-1))/(D2+D3)
      CON2(III) = SOL2*CON2(III)
C ***** CALC. (EXTRAPOLATION) OF FIRST POINT OF NETWORK *****
      CON2(J) = (CON2(2)*SOLO)+((CON2(2)*SOLO)-CON2(3)*SOLO)/2.0
C ***** CONDITION - 1ST POINT CANNOT BE NEGATIVE *****
      IF (CON2(1)-0.0) 38,48,48
38  CON2(1) = 0.0
C ***** CALC. (EXTRAPOLATION) OF END POINT OF NETWORK *****
48  CON2(999) = (CON2(998)*SOL3)+((CON2(998)*SOL3)-CON2(997)*
      1SOL3)/2.0
C ***** CONDITION - END POINT CANNOT BE NEGATIVE *****
      IF (CON2(999)-0.0) 58,57,57
58  CON2(999) = 0.0

```

```

57   TCON = TCON+CON2(1)+CON2(II)+CON2(III)+CON2(MM)+CON2(999)
      CCNO = CORO*CON2(MM)
      CCNI = COR1*CON2(II)
      CCN2 = COR2*CON2(III)
      CCNE = CORE*CON2(999)
      TCCN = TCCN + CON2(1) + CCNO + CCNI + CCN2 + CCNE
      CON2(1) = CON2(1)/SOLO
      CON2(MM) = CON2(MM)/SOLO
      CON2(II) = CON2(II)/SOL1
      CON2(III) = CON2(III)/SOL2
      CON2(999) = CON2(999)/SOL3
      KK = KK + 1
      TT = TT + TSTEP
C ***** PARTIAL PRESSURE OUTPUT CONDITIONS *****
      IF (NN-500) 61,59,61
59   WRITE (6,15) (CON2(I),I=1,J)
15   FORMAT (143(3X,7E14.6,/))
61   CONTINUE
      IF (TT-5.0) 89,89,85
85   IF (KK-4) 88,84,84
84   IF (TT-100.0) 89,89,83
83   IF (NNN-200) 88,89,89
89   WRITE (6,13) TT,TCON
13   FORMAT (8H TIME = ,F8.3,6H(SECS),/,8H TCON = ,E14.6)
      WRITE (6,24) TCCN
24   FORMAT (8H TCCN = ,E14.6,/)
      KK = 0
      NNN = 0
88   CONTINUE
C ***** REMOVAL OF KRYPTON BY CHOROIDAL BLOOD FLOW *****
      DO 70 I=12,14
70   CON2(I) = CON2(I) - F1*CON2(I)
C ***** REMOVAL OF KRYPTON BY RETINAL BLOOD FLOW *****
      DO 71 I=16,18
71   CON2(I) = CON2(I) - F2*CON2(I)
      DO 50 I=1,M
50   CON1(I) = CON2(I)
C ***** INJECTION FUNCTION *****
      IF (TT-0.0) 91,91,90
91   DO 92 I=10,12
92   CON1(I) = 1000.0
90   IF (TT-900.0) 40,33,33
33   WRITE (6,21) PO,P1,P2,P3
21   FORMAT (1H ,/,6H PO = ,E12.5,/,6H P1 = ,E12.5,/,6H P2 = ,E1
12.5,/,6H P3 = ,E12.5)
      STOP
      END

```

REFERENCES.

- ABSON, W., ALLSWORTH, F.L., and SALMON, P.G. (1968).  
Semiconductor radiation detection probes for medical applications.  
Phys. Med. Biol. 13:668
- AIM, A. (1972).  
Effects of norepinephrine, angiotensin, dihydroergotamine,  
papaverine, isoproterenol, histamine, nicotinic acid and xanthinol  
nicotinate on retinal oxygen tension in cats.  
Acta Ophthalmol. (Kbh) 50:707
- AIM, A., and BILL, A. (1972a).  
The oxygen supply to the retina. I. Effects of changes in  
intraocular and arterial blood pressures and in arterial PO<sub>2</sub> and  
PCO<sub>2</sub> on the oxygen tension in the vitreous body of the cat,  
Acta Physiol. Scand. 84:261
- AIM, A., and BILL, A. (1972b).  
The oxygen supply to the retina. II. Effects of high intraocular  
pressure and of increased arterial carbon dioxide tension on  
uveal and retinal blood flow in cats.  
Acta Physiol. Scand. 84:306
- AIM, A., and BILL, A. (1973).  
Ocular and optic nerve blood flow at normal and increased  
intraocular pressure in monkeys. A study with radioactively  
labelled microspheres including flow determinations in brain and  
some other tissues.  
Exp. Eye Res. 15:15
- AIM, A., BILL, A., and YOUNG, F.A. (1973).  
The effects of pilocarpine and neostigmine on the blood flow  
through the anterior uvea in monkeys. A study with radioactively  
labelled microspheres.  
Exp. Eye Res. 15:31
- ANDERSON, B., SALTZMANN, H.A., and FRAYSER, R. (1967).  
Changes in arterial PCO<sub>2</sub> and retinal vessel size with oxygen  
breathing.  
Invest. Ophthalmol. 6:416
- ARONSON, S.B., HOWES, E.L., FISH, M.B., POLLCOVE, M., and O'DAY, D.N.  
(1974).  
Ocular blood flow in experimentally induced immunogenic uveitis.  
Arch. Ophthalmol. 91:60
- ASATANI, H. (1970).  
Studies on the ocular circulation by the method of reflexion  
ocular photoelectric plethysmogram.  
Acta Soc. Ophthalmol. Jap. 71:64
- BACSICH, P., CHISHOLM, I.A., and GELLERT, A. (1966).  
The riddle of the pecten in the bird's eye and the probable  
usefulness of the laser in the analysis of its function.  
In: Aspects of Comparative Ophthalmology. (Pergamon Press,  
Oxford), p299.
- BEN-SIRA, I., and RIVA, C.E. (1973).  
Fluorophotometric recording of fluorescein dilution curves in  
human retinal vessels.  
Invest. Ophthalmol. 12:310

- BETTMAN, J.W., and FELLOWS, V.G. (1956).  
Factors influencing the blood volume of the choroid and retina.  
Trans. Am. Acad. Ophthalmol. and Otolaryng. 60:791
- BILL, A. (1960).  
A calorimetric method for continuous quantitative determinations  
of uveal blood flow in rabbits.  
Acta Soc. Med. Upsal. 65:181
- BILL, A. (1962a).  
Quantitative determination of uveal blood flow in rabbits.  
Acta Physiol. Scand. 55:101
- BILL, A. (1962b).  
A method for quantitative determination of the blood flow through  
the cat uvea.  
Arch. Ophthalmol. 67:62
- BILL, A. (1962c).  
Aspects of physiological and pharmacological regulation of uveal  
blood flow.  
Acta Soc. Med. Upsal. 67:122
- BILL, A. (1962d).  
Calorimetric procedures for the study of the blood flow through  
the ciliary region and the choroid in rabbits.  
Acta Ophthalmol. (Kbh) 40:131
- BILL, A. (1963).  
Effects of cervical sympathetic tone on the blood pressure and  
the uveal blood flow after carotid occlusion.  
Exp. Eye Res. 2:203
- BING, R.J., HAMMOND, M.M., HANDELSMAN, J.C., POWERS, S.R., SPENCER, F.C.,  
ECKENHOFF, J.E., GOODALE, W.T., HAFKENSCHIEL, J.H., and KETY, S.S.  
(1949).  
Measurement of coronary blood flow, oxygen consumption, and  
efficiency of the left ventricle in man.  
Am. Heart J. 38:1
- BISHOP, S., and NYBOER, J. (1962).  
Electrical impedance plethysmography of canine and human eyes.  
Harper Hosp. Bull. 20:142
- BROADFOOT, K.D., GLOSTER, J., and GREAVES, D.P. (1961).  
Photoelectric method of investigating the amount and oxygenation  
of blood in the fundus oculi.  
Br. J. Ophthalmol. 45:161
- BUNCH, W.H., and KALLSEN, G. (1969).  
Rate of intracellular diffusion as measured in barnacle muscle.  
Science, N.Y. 164:1178
- BYNKE, H.G. (1968).  
Influence of intraocular pressure on the amplitude of the corneal  
pulse.  
Acta Ophthalmol. (Kbh) 46:1135
- CARSLAW, H.S., and JAEGER, J.C. (1959).  
Conduction of Heat in Solids. (Oxford University Press)

- CHAO, P., and BETTMAN, J.W. (1957).  
Relative volume of blood in the choroid and retina.  
Am. J. Ophthalmol. 43:294
- CHIDSEY, C.A., FRITTS, H.W., HARDEWIG, A., RICHARDS, D.W., and  
COURNAND, A. (1959).  
Fate of radioactive krypton (Kr-85) introduced intravenously  
in man.  
J. Appl. Physiol. 14:63
- CHRISTENSEN, R.E., POSALSKI, I., WONG, R., and WEISMAN, H. (1971).  
Photoelectric plethysmography.  
Invest. Ophthalmol. 10:247
- COHAN, B.E., and COHAN, S.B. (1963a).  
Flow and oxygen saturation of blood in the anterior ciliary  
vein of the dog eye.  
Am. J. Physiol. 205:60
- COHAN, B.E., and COHAN, S.B. (1963b).  
Anterior ciliary venous blood flow and oxygen saturation at  
reduced arterial pressure.  
Am. J. Physiol. 205:67
- COLE, D.F., and RUMBLE, R. (1970a).  
Effects of catecholamines on circulation in the rabbit iris.  
Exp. Eye Res. 9:219
- COLE, D.F., and RUMBLE, R. (1970b).  
Response of iris blood flow to stimulation of the cervical in  
the rabbit.  
Exp. Eye Res. 10:183
- COLEMAN, D.J. (1971).  
Measurements of choroidal pulsations in M-scan ultrasound.  
Am. J. Ophthalmol. 71:363
- CONN, H.L. (1961).  
Equilibrium distribution of radioxenon in tissue: xenon -  
hemoglobin association curve.  
J. Appl. Physiol. 16:1065
- CONN, H.L., WOOD, J.C., and SCHMIDT, C.F. (1953).  
Comparison of renal blood flow results obtained in the intact  
animal by the nitrous oxide (derived Fick) method and by the  
para-aminohippurate (direct Fick) method.  
J. Clin. Invest. 32:1180
- DAVIS, F.A. (1929).  
The anatomy and histology of the eye and orbit of the rabbit.  
Trans. Am. Ophthalmol. Soc. 24:401
- DICK, D.A.T. (1959).  
The rate of diffusion of water in the protoplasm of living cells.  
Expl. Cell. Res. 17:5
- DOBREE, J.H. (1956).  
Calibre changes in retinal vessels occurring in raised ocular  
tension.  
Br. J. Ophthalmol. 40:1

DOLLERY, C.T., HENKIND, P., KOHLER, E.M., and PATERSON, J.W. (1968).  
Effect of raised intraocular pressure on the retinal and  
choroidal circulations.  
Invest. Ophthalmol. 7:191

DOLLERY, C.T., HENKIND, P., PATERSON, J.W., RAMALHO, P.S. and  
HILL, D.W. (1966).  
Ophthalmoscopic and circulatory changes in focal retinal ischemia.  
Br. J. Ophthalmol. 50:285

DOLLERY, C.T., HODGE, J.V., and ENGEL, M. (1962).  
Studies of the retinal circulation with fluorescein.  
Br. Med. J. 2:1210

ELGIN, S.S. (1964).  
Arterio-venous oxygen difference across the uveal tract of the  
dog eye.  
Invest. Ophthalmol. 3:417

EVANS, A.L., BUSUTTIL, A., GILLESPIE, F.C., and UNSWORTH, J. (1974).  
The rate of clearance of xenon from rat liver sections in vitro  
and its significance in relation to intracellular diffusion rates.  
Phys. Med. Biol. 19:303

FENICHEL, I.R., and HOROWITZ, S.B. (1963).  
The transport of nonelectrolytes in muscle as a diffusional  
process in cytoplasm.  
Acta Physiol. Scand. Suppl. 221

FICK, A. (1855).  
Ueber Diffusion.  
Pogg. Ann. 94:59

FICK, A. (1870).  
Uber die Messung des Blutquantums in den Herzventrikeln.  
Verhandl. d. Phys. Med. Gesellschaft. 2:16

FISCHER, F.P. (1930).  
Ein Versuch, den Energiewechsel des Auges zu bestimmen.  
Ber Dtsch. Ophthalmol. Ges. 48:95

FITCH, W. (1975).  
Autoregulation of cerebral blood flow during controlled  
hypotension.  
In: The Third MacKenzie Symposium on Vision and Circulation.  
Ed. Cant, J.S. (Kimpton, London)

FLOCKS, M., MILLER, J., and CHAO, P. (1959).  
Retinal circulation time with the aid of fundus cinephotography.  
Am. J. Ophthalmol. 48:3

FLOHR, H. (1968).  
Methode zur Messung regionaler Durchblutungsgrossen mit  
radioaktiv markierten Partikeln.  
Pfluegers Arch. Ges. Physiol. 302:268

FLOHR, H., and KAUFMANN, H. (1971).  
Ocular blood flow determined by the particle distribution method  
in anaesthsed cats.  
Ophthal. Res. 2:304

FLOWER, R.W. (1972).

Infrared absorption angiography of the choroid and some observations on the effects of high intraocular pressures.  
Am. J. Ophthalmol. 74:600

FLOWER, R.W., and HOCHHEIMER, B.F. (1973).

A clinical technique and apparatus for simultaneous angiography of the separate retinal and choroidal circulations.  
Invest. Ophthalmol. 12:248

FRAYSER, R., and HICKAM, J.R. (1964).

Retinal vascular response to breathing increased carbon dioxide and oxygen concentrations.  
Invest. Ophthalmol. 3:427

FRAYSER, R., and HICKAM, J.B. (1965).

Effect of vasodilator drugs on the retinal blood flow in man.  
Arch. Ophthalmol. 73:640

FRAYSER, R., SALTZMANN, H.A., ANDERSON, B., HICKAM, J.E., and SIEKKE, H.O. (1967).

The effect of hyperbaric oxygenation on the retinal circulation.  
Arch. Ophthalmol. 77:265

FRIEDMAN, E. (1970).

Choroidal blood flow. Pressure - flow relationships.  
Arch. Ophthalmol. 83:95

FRIEDMAN, E., and CHANDRA, S.R. (1972).

Choroidal blood flow. III. Effects of oxygen and carbon dioxide.  
Arch. Ophthalmol. 87:70

FRIEDMAN, E., KOPALD, H.H., and SMITH, T.R. (1964).

Retinal and choroidal blood flow determined in anaesthetised animals.  
Invest. Ophthalmol. 3:539

FRIEDMAN, E., and SMITH, T.R. (1965).

Estimation of retinal blood flow in animals.  
Invest. Ophthalmol. 4:1122

GIBBS, F.A. (1933).

A thermoelectric blood flow recorder in the form of a needle.  
Proc. Soc. Exp. Biol. 31:141

GILLESPIE, F.C. (1968).

Some factors influencing the interpretation of regional blood flow measurements using inert gas clearance techniques.  
In: Blood Flow through Organs and Tissues. Eds. Bain and Harper. (Livingstone, Edinburgh)

GILLESPIE, F.C., and UNSWORTH, J. (1968).

Anoxia in radiobiology.  
Br. J. Radiol. 41:640

GLASS, H.I., and DE GARREPA, A.C. (1971).

The quantitative limitations of exponential curve fitting.  
Phys. Med. Biol. 16:119

GLOSTER, J. (1969).  
Studies of the ocular circulation by fundus reflectometry.  
In: The William MacKenzie Centenary Symposium on the Ocular  
Circulation in Health and Disease. Ed. Cant, J.S. (Kimpton, London)

GOLBERG, R.B., and SARIN, L.K. (1967).  
The Doppler transcutaneous flow indicator.  
In: Ultrasonics in Ophthalmology -- Diagnostic and Therapeutic  
Applications. (W.B. Saunders, Philadelphia)

GRANGSJO, G., ULFENDAHL, H.R., and WOLGAST, M. (1966).  
Determination of regional blood flow by means of small semiconductor  
detectors and red cells tagged with phosphorus-32.  
Nature 211:1411

GREEN, I.D. (1961).  
Response of the human retinal vessels to positive pressure breathing.  
Aerosp. Med. 32:407

HARDEWIG, A., ROCHESTER, D.F., and BRISCOE, W.A. (1960).  
Measurement of solubility coefficients of krypton in water, plasma  
and human blood using radioactive Kr-85.  
J. Appl. Physiol. 15:723

HICKAM, J.B., and FRAYSER, R. (1965).  
A photographic method for measuring the mean retinal circulation  
time using fluorescein.  
Invest. Ophthalmol. 4:876

HILL, L., and FLACK, M. (1912).  
The relation between capillary pressure and secretion. II. The  
secretion of aqueous and the intraocular pressure.  
Proc. Roy. Soc. B. 85:439

HILLS, B.A. (1967).  
Diffusion versus perfusion in limiting the rate of uptake of inert  
non-polar gases by skeletal rabbit muscle.  
Clin. Sci. 33:67

HINE, G.J., and BROWNELL, G.L. (1958).  
Radiation Dosimetry. (Academic Press, New York)

HØEDT-RASMUSSEN, K., SVEINSDOTTIR, E., and LASSEN, N. (1966).  
Regional cerebral blood flow in man determined by intra-arterial  
injection of radioactive inert gas.  
Circ. Res. 18:237

HOGAN, M.J., ALVARADO, J.A., and WEDDELL, J.E. (1971).  
Histology of the Human Eye. (W.B. Saunders, Philadelphia)

JOHNSON, N.F., STRANG, R., and WILSON, T.M. (1973).  
Further observations on the retinal fine structure after long-term  
anaesthesia.  
Exp. Eye Res. 17:73

JOHNSON, N.F., WILSON, T.M., and STRANG, R. (1973).  
Retinal fine structure after long-term anaesthesia.  
Exp. Eye Res. 15:127

- JONES, H.B. (1951).  
Respiratory system: nitrogen elimination.  
In: Medical Physics, Vol. II. (Year Book Publishers, Chicago), p855.
- KETY, S.S. (1951).  
The theory and applications of the exchange of inert gas at the lungs and tissues.  
Pharmacol. Rev. 3:1
- KETY, S.S., and SCHMIDT, C.F. (1945).  
The determination of cerebral blood flow in man by the use of nitrous oxide in low concentrations.  
Am. J. Physiol. 143:53
- KETY, S.S., and SCHMIDT, C.F. (1948).  
Effects of altered arterial tensions of carbon dioxide and oxygen on cerebral blood flow and oxygen consumption of normal young men.  
J. Clin. Invest. 27:484
- KOGURE, F., ASATANI, H., TOGASHI, M., and YAGIHASHI, T. (1971).  
Studies on ocular photoelectric plethysmogram. The changes of dog's ocular and auricular blood flow by occlusion and releasing of v. cava superior.  
Jap. J. Ophthalmol. 15:109
- KOGURE, G., DAVID, N.J., YAMANOUCI, U., and CHOROMOKOS, F. (1970).  
Infrared absorption angiography of the fundus circulation.  
Arch. Ophthalmol. 83:209
- KOHNER, E.M. (1969).  
The effect of raised intraocular tension on the retinal circulation.  
In: The William MacKenzie Centenary Symposium on the Ocular Circulation in Health and Disease, Ed. Cant, J.S. (Kimpton, London)
- KUSHMERICK, M.J., and PODOLSKY, R.J. (1969).  
Ionic mobility in muscle cells.  
Science, N.Y. 166:1297
- LADEFEGED, J., and ANDERSON, A.M. (1967).  
Solubility of xenon-133 at 37C in water, saline, olive oil, liquid paraffin, solutions of albumin, and blood.  
Phys. Med. Biol. 12:353
- LANGHOLM, M.E., and ROSENTHAL, A.R. (1960).  
Role of sympathetic nerve in regulating intraocular pressure and circulation.  
Am. J. Physiol. 210:786
- LASSEN, N.A. (1959).  
Cerebral blood flow and oxygen consumption.  
Physiol. Rev. 39:183
- LASSEN, N.A., and INGVAR, D.H. (1961).  
The blood flow of the cerebral cortex determined by radioactive krypton.  
Experientia (Basel) 17:42

- LASSEN, N.A., and MUNCK, O. (1955).  
The cerebral blood flow in man determined by the use of  
radioactive krypton.  
Acta Physiol. Scand. 33:30
- LAUBER, A., and WOLGAST, M. (1972).  
Needle type solid state detectors for in vivo measurement of  
tracer activity.  
Phys. Med. Biol. 17:525
- LAWRENCE, J.H., LOOMIS, N.F., TOBIAS, C.A., and TURPIN, F.H. (1946).  
Preliminary observations of the narcotic effect of xenon with a  
review of values for solubilities of gases in water and oils.  
J. Physiol. 105:197
- LAWRENCE, C., and SCHLEGEL, W.A. (1966).  
Ophthalmic pulse studies. I. Influence of intraocular pressure.  
Invest. Ophthalmol. 5:515
- LEVIENE, R.Z. (1957).  
Studies on ocular blood flow in the rabbit.  
Arch. Ophthalmol. 58:19
- LING, G.N., OCHSENFELD, M.M., and KARREMAN, G. (1967).  
Is the cell membrane a universal rate-limiting barrier to the  
movement of water between the living cell and its surrounding  
medium?  
J. Gen. Physiol. 50:1807
- LINNER, E. (1952).  
Ascorbic acid as a test substance for measuring relative changes  
in the rate of plasma flow through the ciliary process.  
Acta Physiol. Scand. 26:57
- LUIKOV, A.V. (1968).  
Analytical Heat Diffusion Theory. (Academic Press, London), p72
- MAROON, J.C., PIERONI, D.W., and CAMPBELL, R.L. (1969).  
Ophthalmosonometry - an ultrasonic method for assessing carotid  
blood flow.  
J. Neurosurg. 30:238
- MATSUO, H., KOGURE, F., and TAKAHASHI, Y. (1966).  
Studies on the photoelectric plethysmogram of the eye.  
Acta Soc. Ophthalmol. Jap. 69:1741
- MEESMAN, A. (1930).  
Blutgasanalysen am Kaninchenauge.  
Ber Dtsch. Ophthalmol. Ges. 48:99
- MUEHLBAECHER, C.A., DEBON, F.L., and FEATHERSTONE, R.M. (1966).  
Further studies on the solubilities of xenon and cyclopropane in  
blood and protein solutions.  
Mol. Pharmacol. 2:86
- NAKAMURA, Y., and GOULSTINE, D. (1973).  
The effect of intraocular pressure on the vortex vein blood flow.  
Exp. Eye Res. 15:461

NIESEL, P. (1962).

Messungen von experimentellerzeugten Änderungen der  
Aderhautdurchblutung bei Kaninchen.  
Ophthalmologica Suppl. 1

NOVOINY, H.R., and ALVIS, D.L. (1961).

A method of photographing fluorescence in circulating blood in  
the human retina.  
Circulation 24:82

O'DAY, D.M., FISH, M.B., ARONSON, S.B., POLLYCOVE, M., and  
COON, A. (1971).

Ocular blood flow measurement by nuclide labelled microspheres.  
Arch. Ophthalmol. 86:205

OOSTERHUIS, J.A., BAKKER, R.B., and VAN DEN BERGE, K.M. (1970).

Binnocular fundus reflectometry.  
Ophthalm. Res. 1:109

OOSTERHUIS, J.A., and GORTZAK-MOORSTEIN, N. (1970).

Fluorescein angiography of the optic disc in glaucoma.  
Ophthalmologica 160:331

OWEN, D.A.A. (1971).

Responses to pressor substances in conscious and anaesthetised  
cats.  
Br. J. Pharmacol. 43:668

PILKERTON, R., BULLE, P.H., and O'ROURKE, J. (1964).

Uveal blood flow determined by the nitrous oxide method.  
Invest. Ophthalmol. 3:227

PORSAA, K. (1941).

Experimental studies on the vasomotor innervation of the retinal  
arteries.  
Acta Ophthalmol. (Kbh) Suppl. 18

PRINCE, J.H. (Ed.) (1964).

The Rabbit in Eye Research. (Charles C. Thomas, Illinois)

REIVICH, M. (1964).

Arterial PCO<sub>2</sub> and cerebral hemodynamics.  
Am. J. Physiol. 206:25

RIVA, C., ROSS, B., and BENEDEK, G.B. (1972).

Laser Doppler measurements of blood flow in capillary tubes and  
retinal arteries.  
Invest. Ophthalmol. 11:936

RODENHAUSER, J.H. (1960).

Eine methode zur fortlaufenden registrierung der Aderhautdurch-  
blutung beim Menschen, Heidelberg.  
Ber Dtsch. Ophthalmol. Ges. 63:505

RODENHAUSER, J.H. (1963).

Uveadurchblutung und Augeninnendruck.  
Klin. Mbl. Augerhkl. Suppl. 42

- RODENHAUSER, J.H. (1969).  
Continuous registration of uveal circulation.  
Arch. Ophthalmol. 82:15
- SAPIRSTEIN, L.A. (1956).  
Fractionation of the cardiac output of rats with isotopic potassium.  
Circ. Res. 4:689
- SAPIRSTEIN, L.A. (1958).  
Regional blood flow by fractional distribution of indicators.  
Am. J. Physiol. 193:161
- SCHACHAR, R.A., WEITZER, J.J., and ERNEST, J.T. (1973).  
Control of intraocular blood flow. III. Effect of chemical sympathectomy.  
Invest. Ophthalmol. 12:848
- SCHLEGEL, W.A., and LAWRENCE, C. (1969).  
Doppler measurement of vortex vein blood flow animals.  
Invest. Ophthalmol. 8:201
- SEIDEL, W., RODENHAUSER, J.H., HAGIHARA, Y., and HENSEL, H. (1960).  
Fortlaufende registrierung der Aderhautdurchblutung des Auges.  
Pfluegers Arch. Ges. Physiol. 272:70
- SONDERMANN, R. (1932).  
Experimentelle Untersuchungen uber die Durchblutungsgrosse des Auges bei normalen und abnormalen Drucks.  
Arch. Augenheilk 105:698
- SPATLER, H.F., TEN EICK, R.E., AND NAHAS, G.G. (1964).  
Effect of hypercapnia on retinal vessel size at constant intracranial pressure.  
Am. J. Ophthalmol. 57:741
- SUZUKI, I., and SATOMURA, S. (1959).  
Studies on circulatory dynamics of peripheral arteries of the head, eye and limb by an ultrasonic method.  
Acta. Soc. Ophthalmol. Jap. 63:3163
- TAYLOR, B., and ALLISON, R. (1964).  
Simultaneous impedance oculogram and electroretinogram. Preliminary report.  
In: Clinical Electroretinography. Eds. Burian and Jacobson. (pergamon Press, Edinburgh), p23.
- TOKORO, T. (1972).  
Relationship between the blood flow velocity in the ciliary body and the intraocular pressure of rabbit eyes.  
Invest. Ophthalmol. 11:945
- TROKEL, S. (1964a).  
Measurement of ocular blood flow and volume by reflective densitometry.  
Arch. Ophthalmol. 71:88
- TROKEL, S. (1964b).  
Photometric study of ocular blood flow in man.  
Arch. Ophthalmol. 71:528

- TROKEL, S. (1965a).  
Quantitative studies of choroidal blood flow by reflected densitometry.  
Invest. Ophthalmol. 4:1129
- TROKEL, S. (1965b).  
Effect of respiratory gases upon choroidal hemodynamics.  
Arch. Ophthalmol. 73:838
- TSACOPOULOS, M., and DAVID, N. J. (1973).  
The effect of arterial PCO<sub>2</sub> on relative retinal blood flow in monkeys.  
Invest. Ophthalmol. 12:335
- UNSWORTH, J. (1974).  
Private communication.
- UNSWORTH, J., and GILLESPIE, F. C. (1971).  
Diffusion Processes. (Gordon and Breach, London), p75.
- VALENTINER, S. (1930).  
Bemerkung zu meiner Arbeit: Uber die Loslichkeit der Edelgase in Wasser.  
Z. Phys. 61:563
- VON ANTROPOFF, A. (1919).  
Experimentelle Untersuchung uber die Loslichkeit der Edelgase in Flussigkeiten.  
Z. Electro-chem. 25:269
- WAHL, M., DEETJEN, P., THURAU, K., INGVAR, D. H., and LASSEN, N. A. (1970).  
Micropuncture evaluation of the importance of perivascular pH for the arteriolar diameter on the brain surface.  
Pflugers Arch. 316:152
- WEITER, J. J., SCHACHAR, R. A., and ERNEST, J. T. (1973a).  
Control of intraocular blood flow. I. Intraocular pressure.  
Invest. Ophthalmol. 12:327
- WEITER, J. J., SCHACHAR, R. A., and ERNEST, J. T. (1973b).  
Control of intraocular blood flow. II. Effects of sympathetic tone.  
Invest. Ophthalmol. 12:332
- WINKELMAN, J. Z., ZAPPIA, R. J., and GAY, J. (1971).  
Human arm to retina circulation time. Determination by simultaneous fluorophotometry.  
Arch. Ophthalmol. 86:626
- WOLGAST, M. (1968).  
Studies on the regional renal blood flow with P-32 labelled red cells and small beta-sensitive semiconductor detectors.  
Acta Physiol. Scand. Suppl. 313
- WOLGAST, M., and LAUBER, A. (1972).  
Some aspects of the use of small needle shaped semiconductor detectors in the determination of regional distribution and transport of labelled compounds.  
Phys. Med. Biol. 17:538

WUDKA, E., and LEOPOLD, I.H. (1956).  
Experimental studies of the choroidal vessels.  
Arch. Ophthalmol. 55:857

YAMAMOTO, Y.L., PHILLIPS, K.M., HODGE, C.P., and FEINDEL, W. (1971).  
Microregional blood flow changes in experimental cerebral ischemia.  
Effects of arterial carbon dioxide studied by fluorescein  
angiography and xenon-133 clearance.  
J. Neurosurg. 35:155

YEH, S.Y., and PETERSON, R.E. (1963).  
Solubility of carbon dioxide, krypton and xenon in lipids.  
J. Pharm. Sci. 52:453

YEH, S.Y., and PETERSON, R.E. (1964).  
Solubility of carbon dioxide, krypton and xenon in aqueous  
solutions.  
J. Pharm. Sci. 53:822

YEH, S.Y., and PETERSON, R.E. (1965).  
Solubility of krypton and xenon in blood, protein solutions,  
and tissue homogenates.  
J. Appl. Physiol. 20:1041

